Spring 2016

PARAGENESIS AND GEOCHEMISTRY OF THE CALVERT TUNGSTEN SKARN DEPOSIT, PIONEER MOUNTAINS, MONTANA

Joshua Messenger
Montana Tech of the University of Montana

PARAGENESIS AND GEOCHEMISTRY OF THE CALVERT TUNGSTEN SKARN DEPOSIT, PIONEER MOUNTAINS, MONTANA

by

Joshua Messenger

A thesis submitted in partial fulfillment of the

requirements for the degree of

Masters of Science in Geosciences

Geology Option

Montana Tech

2016

Abstract

The Calvert tungsten skarn deposit is located in the northern extent of the West Pioneer Mountains, approximately 40 miles southwest of Butte, Montana. The orebody was a significant tungsten producer from 1956-1957 and 1960-1962 during which time the mine produced a total of approximately 113,000 tons of ore averaging 1.10% WO_3. The mine has a measured reserve of 128,000 tons at 1.10% WO_3. The scheelite-bearing deposit occurs within skarn developed in the Pennsylvanian Amsden Formation near or in contact with a satellite pluton of the Late Cretaceous Pioneer Batholith.

Mineral paragenetic studies reveal at least three stages of skarn and ore formation. The first stage represents early prograde metasomatism and is characterized by diopside, forsterite, and trace grossular garnet. The second stage represents main-stage prograde metasomatism and is characterized by grossular, diopside(?), epidote, calcite, and quartz together with scheelite, hematite, zircon, magnetite, apatite and sphene. Retrograde alteration caused local replacement of early mineral assemblages by actinolite, calcite, and quartz together with scheelite, hematite, magnetite, phlogopite, chlorite, and muscovite.

Fluid inclusion microthermometric measurements of the Calvert skarn minerals show that the main prograde mineral assemblage was formed at temperatures between 400°-450°C and pressures between 2-2.5 kbar which correspond to a depth of 7-8.75 km. The salinity of these fluid inclusions increases from 3.2 wt.% to 11.2 wt.% NaCl eq., suggesting either a mixing between a high salinity magmatic fluid and a dilute fluid of meteoric origin, or an increase in salinity due to loss of water to the formation of hydrous skarn minerals.

The protolith marble has $\delta^{13}C$ and $\delta^{18}O$ values that average 0.6‰ (VPDB) and 25.2‰ (VSMOW), respectfully. These isotopic values are depleted relative to unmetamorphosed marine limestone values of 0.0‰ (VPDB) and 30.6‰ (VSMOW). The $\delta^{13}C$ and $\delta^{18}O$ values of the skarn calcite range from -5.0‰ to -9.4‰ for carbon and from 7.7‰ to 14.0‰ for oxygen. The observed depletion towards isotopic magmatic values indicates an interaction between the marble and metasomatic fluids derived from the source igneous body. Mass-balance calculations indicate that the isotopic values of the skarn calcites could have been produced by the interaction between wallrock ($\delta^{13}C_i$ = 0.0‰, $\delta^{18}O_i$ = 30.6‰) and magmatic fluid ($\delta^{13}C_i$ = -5.5‰, $\delta^{18}O_i$ = 7.5‰, X_{CO2} = 0.01) at a minimum fluid/rock ratio of > 40.

Mineral stability relationships combined with fluid inclusion data suggest that during formation of the metasomatic skarn the mole fraction CO_2 was approximately 0.01 and fugacity of oxygen was 10^{-21} bars. Scheelite precipitation most likely resulted from cooling coupled with an increase in the activity of calcium due to fluid/rock interaction with the calcite-marble host rock. During retrograde alteration, temperatures dropped below 400°C but the fugacity of oxygen remained high (~ 10^{-23} bars) allowing minimal sulfides to be precipitated.

Mineral paragenesis, mineral chemistry, fluid inclusion and stable isotope studies are consistent with the hypothesis that the Calvert deposit is a distal skarn. The source of the hydrothermal fluids is not known but could include the Foolhen Mountain Tonalite or the Bryant Creek Granite which outcrop in the study area. An alternative possible source is a buried pluton at greater depth. This could account for the large amounts of water involved with the formation of the Calvert skarn.

Keywords: skarn, scheelite, geochemistry, tungsten, stable isotopes, paragenesis

Acknowledgements

I would like to thank my committee chair and thesis advisor Dr. Christopher Gammons for offering me this project and for his guidance. I also want to thank the other members of my committee, Dr. Diane Wolfgram and Stanley Korzeb for their edits and helpful suggestions. A big thank you to Gary Wyss for all of his help in the SEM and Raman labs, to Simon Poulson of The University of Nevada-Reno for his analyses of stable isotopes, to Ashley Huft of the Montana Bureau of Mines and Geology (MBMG) Analytical Lab for her analysis of leachates with the ICP-AES, and to Christopher Smith of the MBMG GIS department for his technical support.

I would like to thank Mr. Roger Haskins from the Federal Mineral Lands Assistance, LLC, for his early support and advice. I would also like to thank the Tobacco Root Geologic Society and the Rocky Mountain Association of Geologists for their support in scholarships.

Table of contents

List of Tables

List of Figures

1. Introduction

The Calvert tungsten skarn deposit is located in the northern portion of the West Pioneer Mountains in southwestern Montana. The Pioneer Mountains host numerous tungsten skarn prospects as well as other skarn types, carbonate replacement and quartz lode deposits. The largest known skarn is the LenTung tungsten deposit with drill-indicated reserves of 3.3 million tons averaging 0.48% WO_3 (Deboer, 1991). The Calvert deposit was discovered by W.I. Ferguson and George Henderson who located two lode claims which later became the site of the Calvert open pit. The orebody was a significant tungsten producer between 1956-1957 and 1960-1962 during which time the mine produced a total of approximately 113,000 tons of ore averaging 1.10% WO_3 (Walker, 1963). The mine has a measured reserve of 128,000 tons at 1.10% WO_3 (Kemp, 2013). The scheelite-bearing deposit occurs within skarn developed in the Pennsylvanian Amsden Formation near or in contact with a satellite pluton of the Pioneer Batholith.

The purpose of this study is to undertake mineralogical and geochemical investigations to establish a comprehensive paragenetic relation of skarn and ore minerals, characterize the mineralogical and geochemical controls on the skarn and ore-forming processes, determine factors controlling ore deposition, and to suggest a possible source(s) of skarn and ore fluids. Fluid inclusion and stable isotope studies were conducted to determine the conditions and controlling factors of the mineralization. Understanding the nature of this deposit will help assess the potential for other skarn deposits in the Pioneer Mountains. Moreover, these results can be compared to other tungsten skarn deposits around the world to aid in tungsten skarn exploration.

1.1. Location of the Study Area

The Calvert Mine (formerly the Red Button Mine) is located in the northwest Pioneer Mountains, approximately 40 miles southwest of the city of Butte and 11 miles northwest of Wise River in Beaverhead County, Montana (Figure 1). It is situated in the SE 1/4 Sec. 12, T1N, R13W and is centered on 45.854°N latitude and 113.158°W longitude at an elevation of approximately 7,100 feet, with a vertical relief of about 120 feet. The Pioneer Mountains are divided into two, north-south trending mountain ranges (known as the West and East Pioneer Mountains, respectfully), by the Wise River and Grasshopper Creek valleys. Access to the study area can be gained from Butte by travelling south on Interstate 15 to exit 102, then west on Montana HW-43 to the Big Hole River bridge. Take a left onto Bryant Creek Road and continue to Calvert Loop Road, which merges with Forest Service Rd 70648 and leads to the southeast corner of the Calvert mine. Unimproved roads allow access around the entire site.

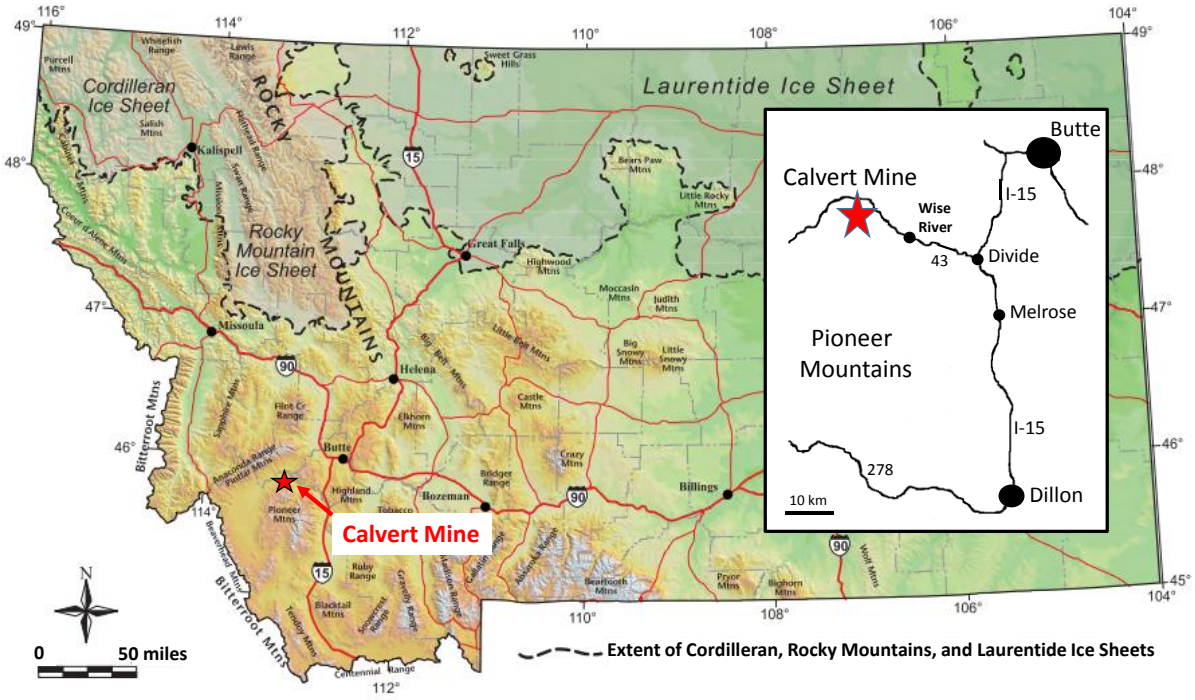

Figure 1. Location of the Calvert mine in the Pioneer Mountains. Montana image adapted from the Montana Bureau of Mines and Geology (MBMG).

The Calvert Hill climate is semi-humid with temperatures ranging from about 78 degrees Fahrenheit in the summer months to about 9 degrees Fahrenheit in the winter. Occasional low temperatures dropping below -30 degrees Fahrenheit are common in winter. The driest months of the year are July, August and September with occasional showers. Most of the region's precipitation falls as snow between September and April and may not fully melt until July. The vegetation is dominated by lodgepole pine forests typical of this altitude in southwestern Montana.

1.2. Previous Studies

Previous investigations of the Pioneer Mountains are ample, primarily due to work conducted by the U.S. Geological Survey, the U.S. Bureau of Mines and the Montana Bureau of Mines and Geology (MBMG). Research on the regional stratigraphy in the Pioneer Mountains was completed by Sloss and Moritz (1951), McMannis (1965), Suttner (1969), Smith and Gilmour (1980), and Sando (1985). A discussion on the tectonics and structures related to the Laramide Orogeny in southwestern Montana was presented by Ruppel and Lopez (1984). Regional structures associated with the Pioneer Mountains have been described by Myers (1952) and Zen (1988). Kalakay et al. (2001) proposed a model for syntectonic ramp-top emplacement of the Pioneer and Boulder Batholiths to explain how space is made for plutons within fold-and-thrust belts.

Extensive petrographic and geochemical work has been conducted on the Pioneer Batholith. Zen et al. (1975) conducted preliminary work on the petrography, chemistry, and age of the Pioneer Batholith. Snee (1978 and 1982) further examined the geology of the Pioneer Batholith and completed an age dating and emplacement model as part of his Masters and Ph.D theses. Hammarstrom (1982) completed an investigation on the chemical and mineralogic

variation of the Pioneer Batholith. Arth et al. (1986) conducted a strontium isotope study for all plutons associated with the Pioneer Batholith and concluded that the high strontium ratios reflect partial melting of portions of Precambrian lower crustal lithosphere. Foster et al. (2012) conducted a Lu-Hf study of magmatic zircons from multiple phases of the Pioneer Batholith and concluded that the East Pioneer Mountains were derived from Mesoarchean and early Paleoproterozoic mafic crust, and that the West Pioneer Mountains, which includes the Calvert deposit, were derived from Paleoproterozoic and possibly Mesoproterozoic mafic crustal sources.

Pattee (1960) summarized the tungsten resources of the Pioneer Batholith. Walker (1963) evaluated the tungsten resources of the western United States, including all known tungsten occurrences in western Montana. Walker described the Calvert main ore body as being 200 feet wide and irregular-shaped, garnet-rich containing epidote, quartz, minor amounts of chlorite and sporadically disseminated scheelite. Geach (1972) investigated past mining in the region and produced a summary of the mines and mineral deposits of Beaverhead County, Montana.

Table I shows known tungsten skarn deposits in the Pioneer Mountains that have been described in a number of theses and reports (Walker, 1963; Geach, 1972; Collins, 1975 and 1977; Crump, 1976; Mellon, 1978; Zimbelman, 1984; Schutz, 1986; Franklin, 1989; Deboer, 1991). Geologic mapping and mineral resource evaluations of Wilderness Study Areas were conducted in the Eastern Pioneer Mountains by Pearson and Zen (1985), and in the Western Pioneer Mountains by Berger and Benham (1984). Ruppel et al. (1993) compiled a geologic map of the Dillon Quadrangle, which includes the Calvert Hill, at a scale of 1:250,000. The geology of the northern portion of the West Pioneer Mountains, which includes the Calvert Hill,

was mapped and described by Truckle (1988). Recent mapping by the Montana Bureau of Mines and Geology is in progress, but no updated maps were available at the time of this writing.

1.3. Exploration and Mining History of Calvert Mine

Prior to 1954, Montana's national contribution of tungsten was minimal. But in 1952, the Defense Minerals Exploration Administration provided purchasing and stockpiling programs which made the mining of low-grade ores economical, greatly increasing exploration for Montana tungsten deposits. The Calvert deposit was discovered by W.I. Ferguson and George Henderson who located two lode claims which later became the site of the Calvert open pit (Figure 2). In August 1956, the property was leased by Minerals Engineering Company of Grand Junction, Colorado, and the production of tungsten ore began by open pit methods and the ore was shipped to concentrator facilities located at Glen, Montana. Operations continued until August 1957 when the government's tungsten-purchasing program was terminated. This short period of operation produced 102,800 tons of ore averaging 1.13% WO_3 (Walker, 1963; Geach, 1972).

Waste stripping operations resumed in September 1959, enlarging the open pit to 250 feet by 300 feet in area and deepened to 85 feet. Open pit mining operations resumed in 1960 and continued to early 1962, producing about 10,000 tons of ore averaging 0.66-1.47% WO_3 (Walker, 1963). During its lifetime, the mine produced a total of approximately 113,000 tons of ore averaging 1.10% WO_3 (Walker, 1963). When mining operations ceased, the open pit flooded with groundwater and snowmelt, creating a 90 foot deep lake of exceptional clarity and chemical purity (Gammons et al., 2013).

Table I. Recorded tungsten skarn deposits and prospects associated with the Pioneer Batholith (modified from Deboer, 1991).

Deposit Name	Deposit Name	Location	Host formation	Production
Brown's Lake	Browns Lake (Ivanhoe)	Sec 3 & 4 T4S R10W	Amsden Fm	(1953-57) 625,107 tons @ 0.35% WO_3 (1928-29) 87 tons - 12,629 lbs Cu, 647 oz Ag, 1 oz Au
	Lentung	Sec 3 T4S R10W	Amsden Fm	Proven & probable reserves 3.3 m.t. of 0.48% WO_3
	Garnet	Sec 33 T3S R10W	Amsden Fm	(1944) >30 tons of unknown grade WO_3
	Mammoth	Sec 33 T3S R10W	Amsden Fm	
Lost Creek	Lost Creek	Sec 11, 14 & 23 T4S R10W	Amsden Fm	(1953-57) 21,150 tons @ 0.18% WO_3
Utopia (Birch Creek)	Greenstone	Sec 2 & 11 T5S R10W	Amsden Fm	1 ton tungsten ore. (1908-09 & 1949) 106 tons-6,684 lbs Cu, 153 oz Ag and 1 oz Au
	Copper Contact	Sec 14 & 15 T5S R10W	Mission Canyon Fm	
	Glowworm/ Greenhorn	Sec 2 & 11 T5S R10W	Amsden Fm	
	Haggerty	Sec 15 T5S R10W	Mission Canyon Fm	
	Stanfield	Sec 22 T5S R10W	Mission Canyon Fm	Mill samples only
Baldy Mountain	Little Hawk	Sec 10, 11, 14 & 15 T6S R12W	Jefferson Dolomite (?)	Mill samples only
	Hazel	Sec 11 T6S R12W	Jefferson Dolomite (?)	
	Agnes/Echo	Sec 11 & 14 T6S R12W	Jefferson Dolomite (?)	
	Virginia	Sec 14 T6S R12W	Jefferson Dolomite (?)	
Other Mines	Calvert (Red Button)	Sec 12 T1N R13W	Amsden Fm	(1956-57) 102,800 tons @ 1.1% WO_3 (1960-62) 10,000 tons @ 0.66-1.47% WO_3
	Foolhen	Sec 19 & 20 T1N R12W	Amsden Fm	

An exploration program was initiated in June 1966 by the Beaverhead Development Ventures and Minerals Engineering Company to evaluate the potential for additional reserves below the existing open pit and to evaluate the surface exposure of medium-grade ore to the northwest of the open pit. This exploration program consisted of 22 diamond drill holes totaling 3,318.5 feet and four excavated surface trenches totaling 132 feet in total length (Kemp, 2013). In 1967, proposals for alternative mining methods and associated costs for the extraction of the ore blocks defined below the bottom of the pit were completed for Minerals Engineering Company. Surface diamond drilling continued in 1967, evaluating extensions to the previously defined ore blocks below the open pit. In 1971, exploration continued by Minerals Engineering Company and consisted of more than 2,500 feet of diamond drilling (Kemp, 2013). Further exploration was delayed because of weather conditions until the spring of 1972, which is the last exploration drill program documented on the property. The measured reserve at Calvert mine is 128,000 tons at 1.10% WO_3 (Kemp, 2013).

The Calvert mine open pit was staked by local prospectors Paul and Ted Antonioli with the claims registered under the name of Paul Antonioli. US Tungsten Corporation entered into an option agreement to acquire all interest in the three claims in 2010, and by October 2012, US Tungsten Corporation staked an additional 65 claims surrounding the original three claims. A field examination of the area by US Tungsten in 2012 concluded that the 1967 reserve estimate is still in place beneath the flooded pit. US Tungsten approached Montana Tech for technical assistance in their exploration and evaluation efforts. A small grant from US Tungsten provided the initial impetus for the current thesis project.

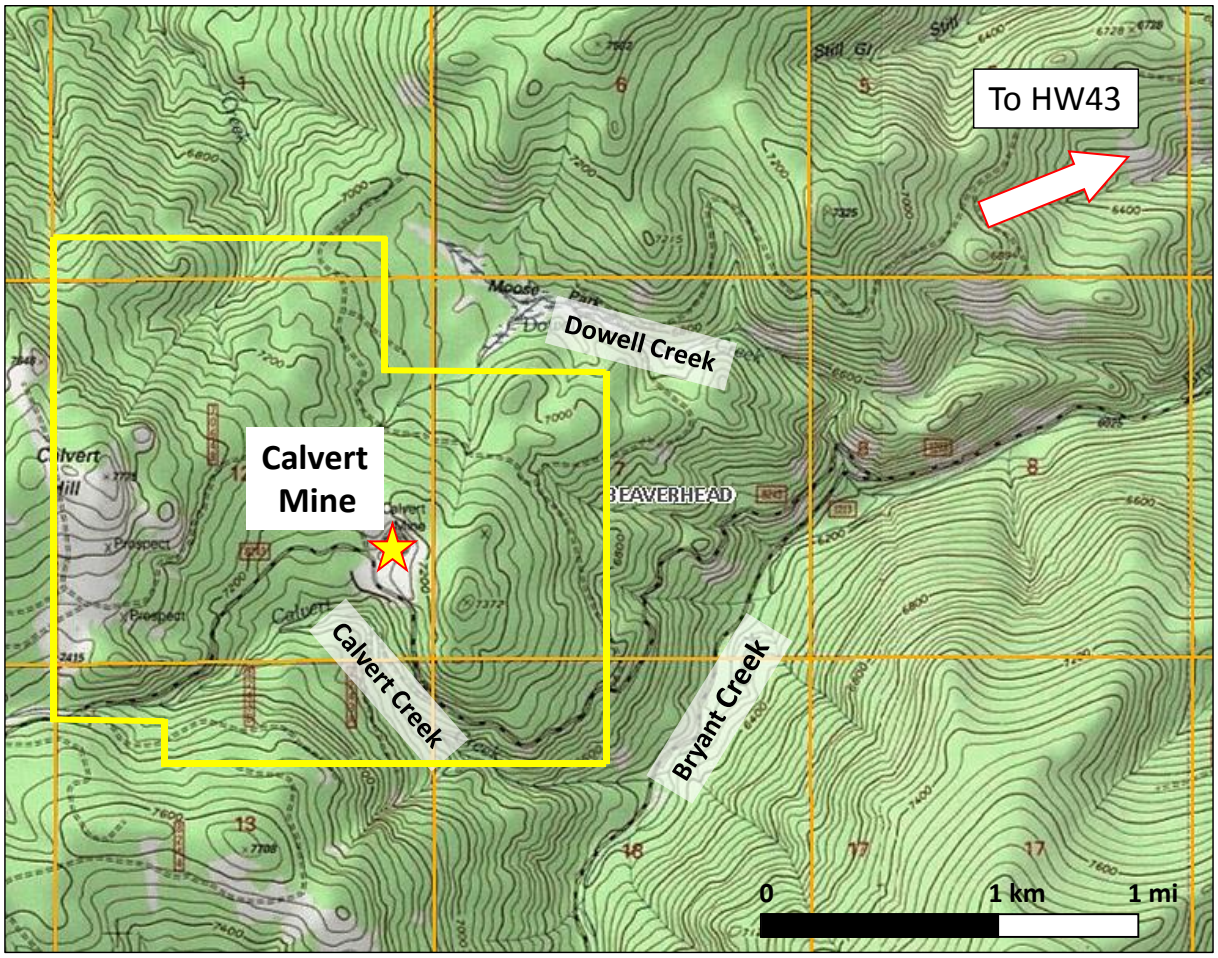

Figure 2. Calvert mine location on Calvert Hill, West Pioneer Mountains. Yellow confined area is the approximate Calvert property boundary.

1.4. General Characteristics of Tungsten Skarns

The term skarn refers to a rock type defined by a specific mineralogy consisting of coarse-grained Ca-Fe-Mg-Mn-silicates of metasomatic origin accompanying regional or contact metamorphism and metasomatism (Einaudi et al., 1981). The term skarn deposit refers to metal deposits that contain skarn minerals as gangue. The type of skarn deposit discussed in this study is interpreted to be related to magmatic-hydrothermal systems. World skarn deposits have been well described and discussed in many major literary works (Einaudi et al., 1981; Einaudi and Burt, 1982; Meinert, 1983 and 1992; Newberry, 1998; Meinert et al., 2005), and the reader is

encouraged to review these works for a thorough discussion on skarn terminology and evolution, and for a description of world skarn deposits.

The general characteristics of tungsten skarns have been compiled by Einaudi et al. (1981) and are shown in Table II. Tungsten skarns are associated with coarse-grained, generally unaltered, equigranular calc-alkaline plutons in deep environments along continental margin subduction zones (Meinert et al., 2005). Aplite and pegmatite pods and dikes are common features of intrusive masses associated with tungsten skarns. Newberry and Einaudi (1981) and Meinert (1992) concluded that tungsten deposits, unlike Cu, Pb-Zn and Mo skarns, may form at depths to 11 km and that relatively deep environments favor the formation of scheelite ($CaWO_4$) skarn deposits. Newberry (1979) proposed that tungsten skarns be divided into two groups: reduced types formed in carbonaceous host rocks or at depth, and oxidized types formed in noncarbonaceous or hematitic host rocks or at lesser depths. The source of tungsten in most scheelite deposits is believed to be a felsic intrusion due to the higher concentrations of tungsten found in them and not in the intruded host rocks.

Table II. General characteristics of tungsten skarn (from Deboer, 1991, after Einaudi et al., 1981). Abbrs: bt-biotite, ep-epidote, cal-calcite, plag-plagioclase, act-actinolite, qtz-quartz, chl-chlorite, hnbl-hornblende.

Size and Grade	Typical: 0.1 to 2 m.t. 0.7% WO3	
Associated Metals	W, Mo, Cu, (Zn, Bi)	
Tectonic Setting	Continental margin, syn- to late orogenic	
Associated Igneous Rocks	qtz diorite to qtz monz.	
Mineralogy	Reduced skarn	Oxidized skarn
Prograde stage		
Pyroxene:garnet ratio	10:1 to 2:1	1:1 to 1:10
Pyroxene composition		
mole % hedenbergite	60 - 90	20 - 70
mole % johannsenite	5 - 20	0 - 5
Garnet composition		
mole % andradite	10 - 50	50 - 80
Late garnet composition		
mole % andradite	0 - 50	80 - 100
mole % spessartine	5 - 35	0 - 5
mole % almandine	5 - 40	0
Retrograde stage		
Typical assemblages	bt+plag+opaques±calcite; hnbl+opaques+qtz+cal	ep+chl+qtz+cal; act+qtz+cal+opaques
Amphibole composition		
mole % ferrotremolite	5 - 80	30 - 60
mole % tremolite	0 - 30	30 - 70
mole % ferropargasite	70 - 100	5 - 20
Diagnostic opaques	pyrrhotite, magnetite (pyrite, native bismuth)	pyrite (bismuthinite, magnetite, pyrrhotite)

1.5. Purpose of Study

This study represents a combined field and laboratory investigation of the small, but high-grade tungsten deposit at Calvert mine. This investigation will incorporate methods not used in previous studies at Calvert, including detailed geologic mapping, detailed mineral paragenesis, and fluid inclusion and stable isotope analyses. The purpose of this study is to determine the physical and geochemical conditions of ore deposition in order to aid in future tungsten skarn exploration. No previous investigations of this type have been conducted at the Calvert mine; therefore, no comparisons of ore depositional mechanisms have been made between the Calvert tungsten skarn deposit and other tungsten skarn deposits in Montana or elsewhere.

2. Regional Geology

The study area is located in the Pioneer Mountains in southwestern Montana. The geology of the region is dominated by Precambrian (Proterozoic Belt Supergroup) through early Tertiary sedimentary rocks, with Late Cretaceous to Eocene extrusive and intrusive igneous rocks scattered throughout. Figure 3 shows the location of the Pioneer Batholith (PB) amongst the many major igneous rocks in the region. These include the Boulder Batholith (BB) to the east and the Idaho Batholith (IB) to the west, as well as the Mount Powell Batholith (MPB), Philipsburg Batholith (P), Tobacco Root Batholith (TB), and the Anaconda Range plutons (ARP) just to the north.

This region is located within the eastern extent of the Sevier fold and thrust belt which is a region structurally dominated by overlapping thrust faults in Proterozoic to Cretaceous sedimentary rocks. South of Dillon is the northern extension of the Idaho-Wyoming thrust belt which includes the Medicine Lodge-Tendoy (MLT), Cabin (CT), and Fritz Creek (FCT) thrust faults that have displaced Paleozoic and Mesozoic sedimentary rocks eastward (Snee, 1978).

The Pioneer Batholith is situated within the Great Falls Tectonic Zone (GFTZ), a northeast-trending, 1.85 Ga suture zone between the Archean Medicine Hat Terrain to the north and the Archean Wyoming Terrain to the southeast. Sims et al. (2004) interpreted the GFTZ to contain accreted crust of the Wallace Terrain, as well as the Trans-Montana fold and thrust belt of Paleoproterozoic age. The Lewis and Clark Line extends at least 200 miles in an east-southeast direction from the Coeur d'Alene mining district and crosses the region just north of the Idaho and Boulder Batholiths through the cities of Missoula and Helena (Figure 3). This lineament is known to separate the batholithic terrain that hosts the Basin and Range Structural

Province to the south from an area essentially barren in plutons to the north that is characterized by faults and folds with north-northwest trends (Berger et al., 2011).

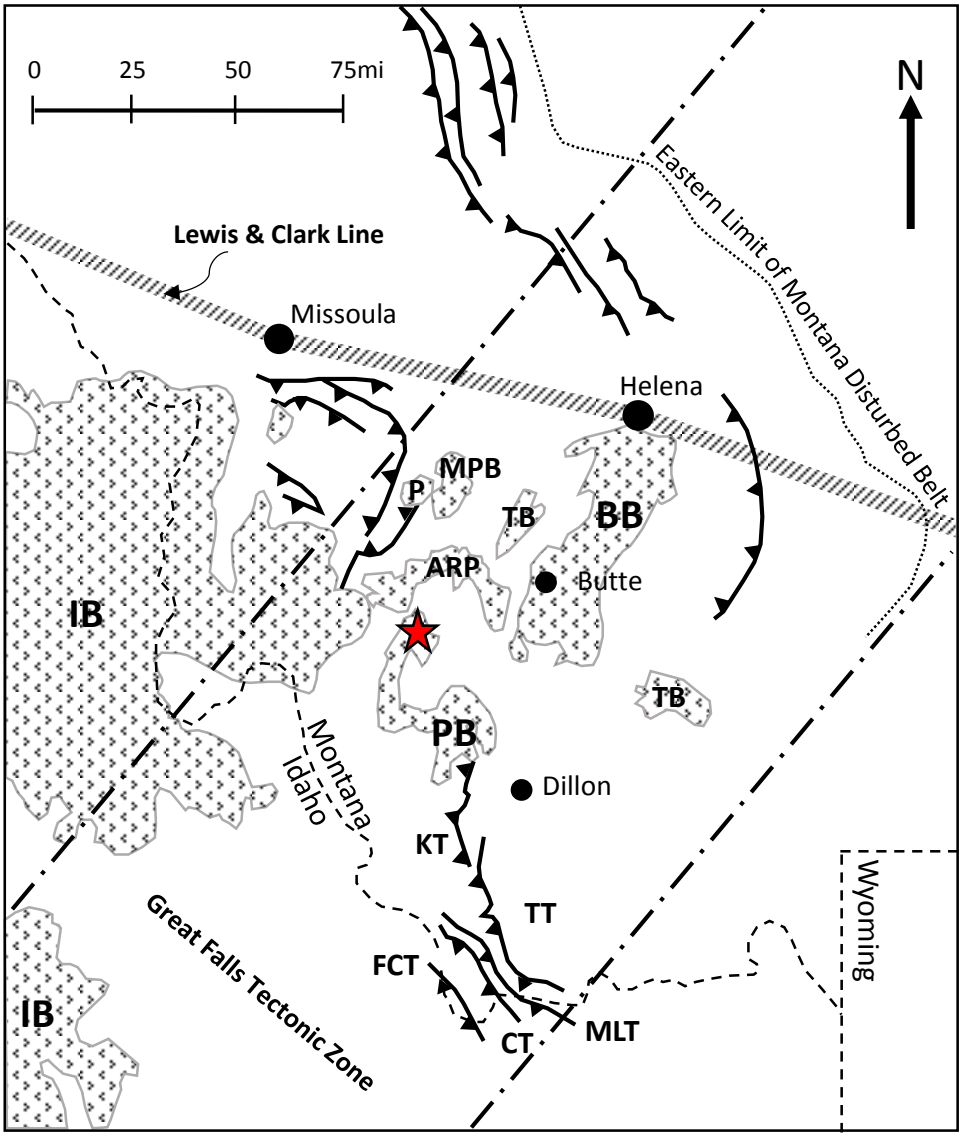

Figure 3. Regional geologic setting of the Pioneer Batholith (PB). Star identifies the location of the Calvert mine. Image modified from Snee, 1978. Abbreviations given in text.

Snee (1982) described the Pioneer Batholith as a composite body made up of plutons ranging in composition from granite to tonalite with minor pyroxenite and gabbro that was emplaced in the epizone during the time span of 83-65 Ma. Throughout the Pioneer Mountains, the batholith crosscuts the local structures and consistently intrudes to the stratigraphic level of

Paleozoic carbonate formations (e.g., Jefferson, Madison, Amsden). Proterozoic Belt sedimentary rocks are thrust over autochthonous Precambrian and Phanerozoic strata. Deboer (1991) suggested that the preservation of allochthonous Belt rocks in the west and scarcity in the east is due to west-side-down movement along the high-angle Fourth of July-Comet fault, which is a north-trending fault system situated along the Wise River and Grasshopper Creek valleys. Zen (1988) suggests that this fault is related to Tertiary Basin and Range faulting.

The geology of the Calvert Hill area has been described by Truckle (1988) as being dominated by Late Cretaceous Laramide compressional forces and plutonic intrusions and Tertiary extensions. In his M.S. thesis, Truckle inferred at least two periods of folding and thrusting in the area; the first of which he attributed to the folding and thrusting of Precambrian paragneiss over Phanerozoic metasediments. This event produced the high-angle northwest striking and southwest dipping Foolhen thrust fault (Figure 4). Truckle postulated that the Foolhen thrust fault was later folded until rupture during the second compressional event that created the Calvert thrust fault. The structure of the Calvert mine, as discussed by Truckle, is the result of three faults, from oldest to youngest: the Calvert thrust; a tensional fault following a reactivated surface; the Bryant Creek tear-fault system. The tensional stress was interpreted to have resulted from left-lateral movement along the Bryant Creek tear fault.

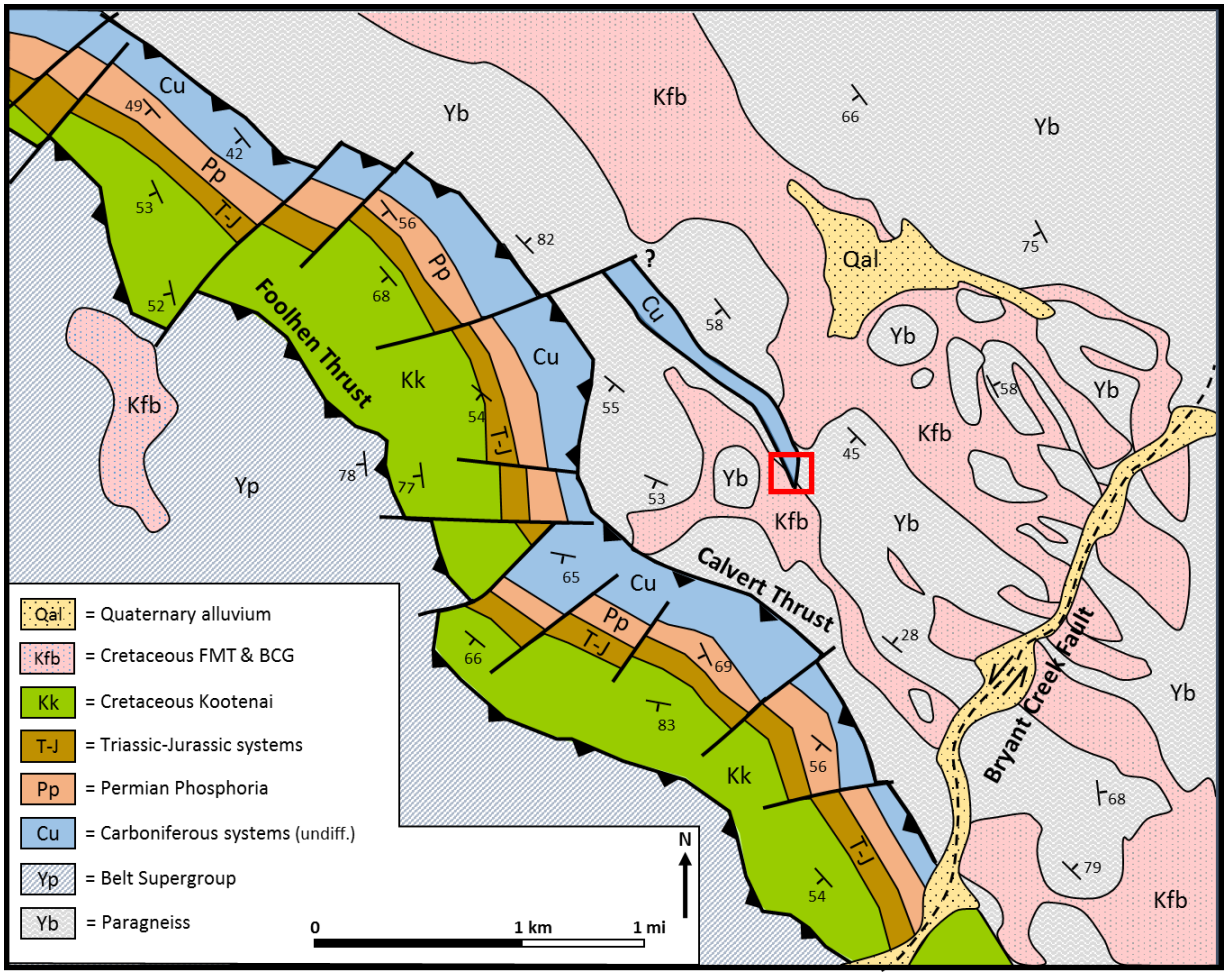

Figure 4. Geologic map of the Calvert Hill area with the location of the Calvert mine outlined in red. Image modified from Truckle (1988).

3. Methods

3.1. Geologic Mapping

Detailed outcrop and float mapping was conducted at a scale of 1:600 (1 inch = 50 feet) for an area of approximately 60,000 square meters with an aerial photograph taken from Google Earth as a base. Black-lighting was done at night with a RAYTECTORS UV Lamp. Throughout the mapping process, the rocks at Calvert were identified and structural features were measured. Hand samples were collected throughout the mine for later petrographic, geochemical, stable isotopic and fluid inclusion analyses.

The field map was converted to a raster image with the Colortrac SmartLF Gx+ T56 large format scanner by Christopher Smith at the Montana Bureau of Mines and Geology (MBMG) on the Montana Tech campus. The raster image was digitized in ArcGIS 10.3 and georeferenced with a NAIP image courtesy of the MBMG GIS Department.

3.2. Petrology/Petrography

A total of 55 hand samples were collected throughout the mapping process for petrographic, geochemical, stable isotopic and fluid inclusion analyses. These samples were taken from various locations as intact rock, loose float and dump material, and represent exoskarn with minor and significant scheelite mineralization; endoskarn; fresh, bleached and altered marble; and all igneous rocks and their various compositions and textures, including pegmatite and aplite. An additional 10 samples from the study area were taken by a Field Methods class of Montana Tech and given to the author, as well as three archived samples from the Anaconda Minerals Company Collection, located at Montana Tech.

3.2.1. Transmitted/Reflected Microscopy

Hand samples were cut into rock slabs using Highland Park models M-2 and J-3 rock saws in the rock laboratory located in the basement of the Mining and Geology building at Montana Tech. Selected slabs were trimmed to approximately 1.5 x 3 inches with a water-based trim saw and individually packaged. Samples from skarn, marble, and igneous rocks were sent to Quality Thin Sections located in Tucson, Arizona, for thin sections. Standard polished thin sections (without coverslips) were made from 18 skarn samples and two marble samples. Standard thin sections (with coverslips) were made from four igneous samples and one aplite, marble, and endoskarn sample. The marble sections were stained to identify any dolomite and the igneous sections were K-feldspar stained using sodium cobaltinitrite. Polished thin sections were examined under an Aus Jena optical microscope using transmitted and reflected light. Color microphotographs were taken using an Olympus Tough TG-810 14 megapixel camera.

Petrography samples were trimmed to useable size with a water-based trim saw to fit into a 1 inch diameter epoxy mold, along with labels identifying the sample name, author's name and the date created. An epoxy mixture of 1:4 was prepared using transparent 2lb EPO-TEK manufactured by Epoxy Technology. Epoxy mounts were polished using a Buehler AutoMet 250 to 0.05 microns. Polished mounts were examined under an Aus Jena optical microscope using reflected light. Color microphotographs were taken using an Olympus Tough TG-810 14 megapixel camera.

3.2.2. Portable X-Ray Fluorescence (XRF)

A Niton portable XRF was used to scan selected hand samples, rock slabs and polished plugs. The method of portable XRF is known to be less precise but still useful in providing active, real-time geological data which can be effective at guiding exploration. XRF results are

particularly suspect at concentrations close to detection limits (~100 ppm). The portable XRF is not meant to be an assaying tool; nonetheless, the data are useful to confirm mineralogy and to look at relative metal ratios.

Each sample was scanned with an 80 second measurement time to ensure a maximum suite of elements and to increase the accuracy of each scan. It should be pointed out that the actual area of the specimen that was scanned is approximately 16 square millimeters, whereas the hand samples and polished plugs are much larger than this, and show considerable mineralogical variation at the centimeter scale.

3.2.3. SEM

The scanning electron microscope (SEM) located in the basement laboratory of the Center for Advanced Mineral and Metallurgical Processing (CAMP) building at Montana Tech was used to determine mineralogy by means of energy dispersive X-ray analysis (EDX). Samples were prepared as described above, and carbon coated. The polished plugs were manually scanned and images were created using the backscatter electron (BSE) detector. The LEO 1430VP (Figure 5) was operated by Gary Wyss, and operating conditions were: 25 kV acceleration voltage, 17-19 mm working distance, 550 square nanometer spot size, and 100 μA beam current.

EDX spectra were collected between two EDAX Apollo 40 detectors equipped with a 3.3 window type and a collection rate of 35,000-55,000 counts per second. A collection time of 10-30 seconds, with a dead time of 25-30% provided elemental data on each phase being identified. EDX analyses are based on a standardless calibration using a ZAF correction factor which accounts for the atomic number effect, fluorescence effect, and absorption effect.

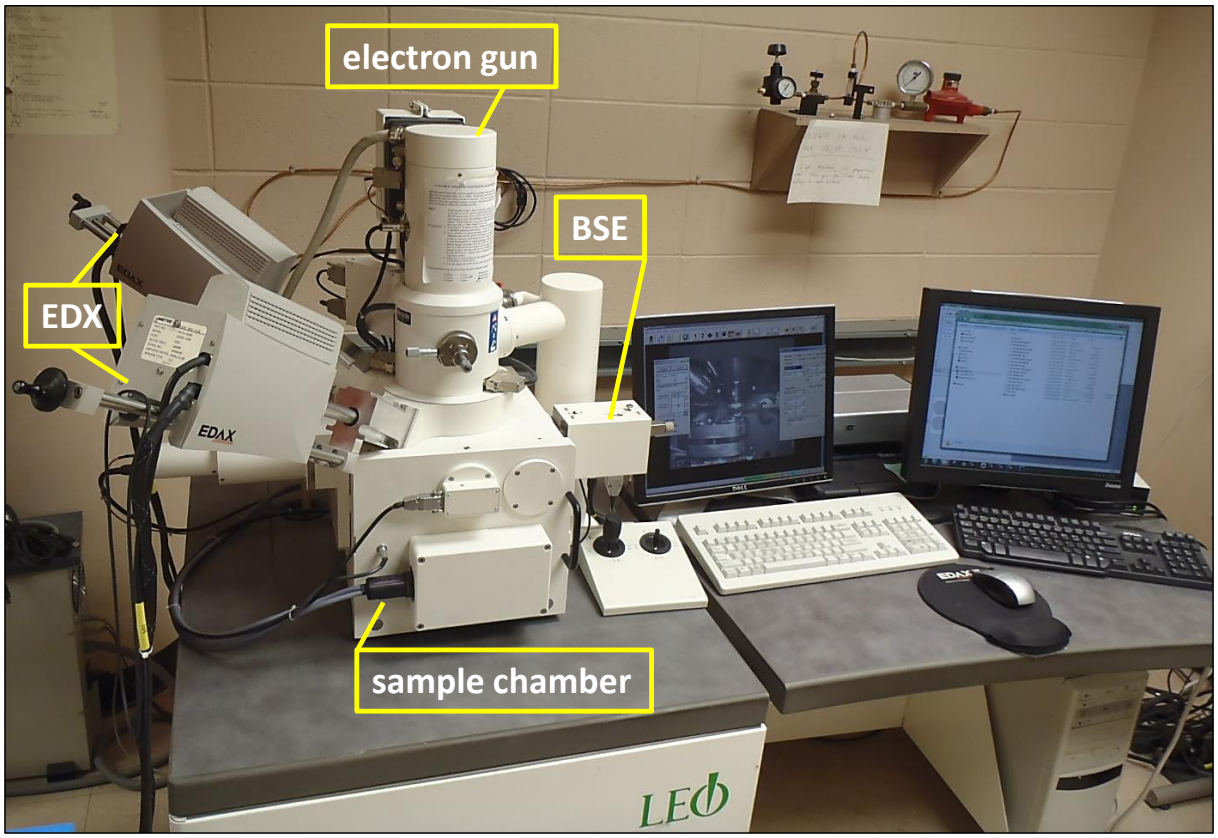

Figure 5. Scanning electron microscope (SEM) setup in the CAMP building at Montana Tech.

3.2.4. Micro Raman

Raman spectroscopy was conducted for mineral identification of select polished thin sections (with and without coverslips) using the Renishaw inVia Raman microscope located in the basement laboratory of the CAMP building at Montana Tech. Exposure time for each scan was 3-5 seconds, with 10 accumulations each scan using 514 nm, 633 nm, and 720 nm (NIR) lasers. Single scan measurements identified peak positions using the program WiRE 4.1. Raman spectra were re-analyzed with the program CrystalSleuth which is part of the RRUFF Project created by Bob Downs and Tom Laestch of the Department of Geosciences at the University of Arizona. Raman images were captured with a Renishaw CCD Camera.

3.3. Fluid Inclusions

Samples of scheelite, quartz and garnet were chosen for fluid inclusion analysis. Polished plugs were made according to the method described above, and then super-glued to a petrographic slide and cut to ~2 mm thick using an Isomet saw. The cut surfaces were polished on the Buehler AutoMet 250 polisher to 8 microns, each approximately 100 μm thick. Thick sections were submerged in acetone for 24 hours to remove the glue and epoxy from the samples.

Each sample was studied petrographically with an Aus Jena microscope to find suitable inclusions and establish mineralogic and paragenetic relationships. Inclusions of interest were sketched and the size, shape, ratio of liquid/vapor and sphericity of each vapor bubble were noted before cutting the samples into chips small enough to fit into the heating/freezing stage. Microphotographs were taken using an Olympus Tough TG-810 14 megapixel camera.

Fluid inclusions were analyzed on a Fluid Inc. adapted USGS-type gas-flow heating/freezing stage mounted on a Olympus BH-2 microscope located at Montana Tech under 320x magnification (Figure 6). The petrographic microscope, set up with the heating/freezing stage and heating element, was connected to a variac and trendicator to control the temperature, air and N_2 pressure. The inclusions were frozen with liquid nitrogen which was pushed onto the stage by a stream of N_2 gas. Heating was accomplished by passing dry nitrogen through a coiled electrical heating element. Temperatures were measured with a wire thermocouple resting on top of the rock chip. The thermocouple was calibrated using synthetic fluid inclusion standards designed to homogenize at a temperature of 375 degrees Celsius and melt at a temperature of 0.0 degrees Celsius. The calibration yielded a homogenization temperature (T_h) of 374.1 degrees Celsius (Δ 0.9°C) and a melting temperature (T_m) of 0.1 degrees Celsius (Δ0.1°C).

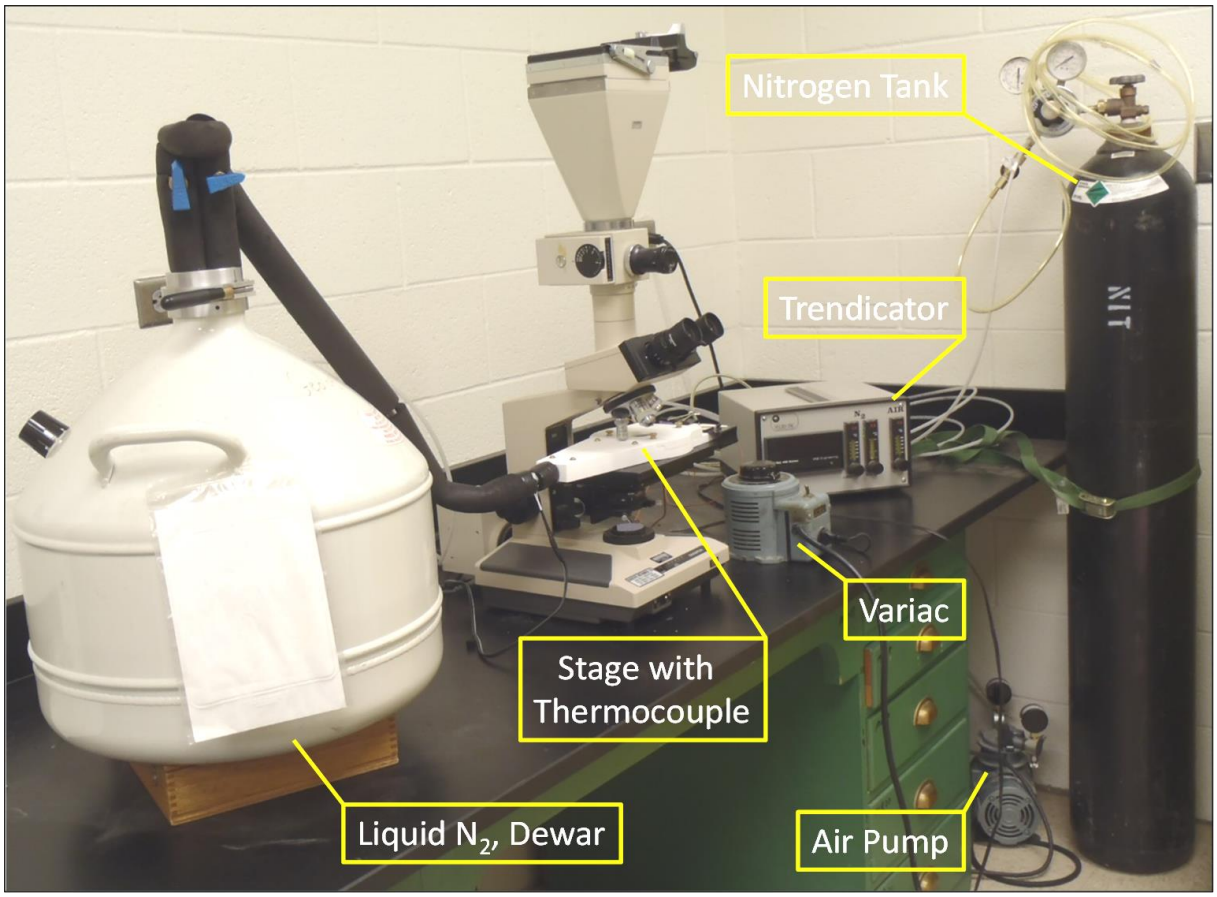

Figure 6. Modified U.S.G.S. gas-flow fluid inclusion station at Montana Tech.

Ideally, freezing experiments are completed first and then heating runs. This was done for most of the experiments when able, but a few of the experiments were conducted in reverse order due to a lack of liquid nitrogen. Low temperature data were obtained by freezing the inclusions to -50°C and observing the phase changes upon reheating. A few representative inclusions were cooled to -100°C to check for the presence of liquid CO_2. Heating rates were slowed to ~ 1°C/minute when the ice melting temperature was approached. High temperature data were taken while raising the temperature, and the heating rates were slowed to ~ 5°C/minute near the homogenization temperature. Each phase change was observed twice with excellent reproducibility, and any data for inclusions suspect of rupture or leakage were discarded.

3.3.1. Fluid Inclusion Leachate

Five scheelite samples were selected for leaching of cations from opened fluid inclusions. The samples were ground to a fine powder with an agate mortar and pestle and placed into individually labeled high-density polyethylene (HDPE) bottles. The amount of scheelite used for the procedure varied between 1-3 grams, and 10 grams of de-ionized water was added to each bottle and allowed to stand for 48 hours. Each leachate solution was filtered (0.2μm PES syringe filter) into a second set of HDPE bottles and brought to a total volume of 20 mL with de-ionized water. The solutions were preserved with 0.2g of trace metal grade HNO_3 acid. All samples were analyzed for major cations (e.g., K, Mg, Na, Ca) with the inductively coupled plasma-atomic emission spectrometer (ICP-AES) located at the Montana Bureau of Mines and Geology (MBMG) on the Montana Tech campus by Ashley Huft. It should be noted that this method determines cation ratios and cannot determine absolute metal concentrations.

3.4. Stable Isotopes

Thirty samples were collected from skarn, unaltered and altered marble for stable isotope analysis of C and O in carbonate minerals. Each sample was ground to a fine powder using a mortar and pestle, and weighted samples of 1 gram were transferred to small glass bottles. To confirm the mineralogy and to quantify the existence of impurities (e.g., Si, Al, Mg, Fe), all of the samples were scanned with a Niton portable XRF.

All samples were analyzed for $\delta^{13}C$ and $\delta^{18}O$ by Dr. Simon Poulson of the Department of Geological Sciences & Engineering at the University of Nevada-Reno. Stable isotope analyses were performed using a dual inlet Micromass IsoPrime stable isotope ratio mass spectrometer. Sample analyses were performed using the phosphoric acid reaction method of McCrea (1950), except that the reaction was performed at 90°C. Estimated analytical uncertainties are ±0.2‰ for

$\delta^{13}C$ and ±0.2‰ for $\delta^{18}O$. All stable C-isotope analyses in this study are reported in the same units as those reported by the lab, i.e., in ‰ relative to the Vienna Pee Dee Belemnite (VPDB) standard. All stable O-isotope data are reported in ‰ relative to VPDB as well as the Vienna Standard Mean Ocean Water (VSMOW) standard.

4. Results

4.1. Geology of the Study Area

Precambrian and Phanerozoic rocks crop out in the study area and are interpreted as Proterozoic paragneiss, Pennsylvanian Amsden Formation, Cretaceous igneous intrusions (tonalite, granite, aplite and pegmatite), as well as mineralized and barren skarn. Figure 7 shows the locations where the igneous intrusives are in contact with paragneiss and the marble, and depicts the spatial relationship of skarn emplacement. The dominant strike orientation of the metasedimentary rock units is to the WNW and parallels unit contacts, with southwest dips averaging 58 degrees. Within the study area, the orebody has a similar orientation, and plunges roughly south at approximately 50 degrees. The map shows the likely location of a fault which separates the Carboniferous carbonate and skarn to the west from Precambrian gneiss to the east.

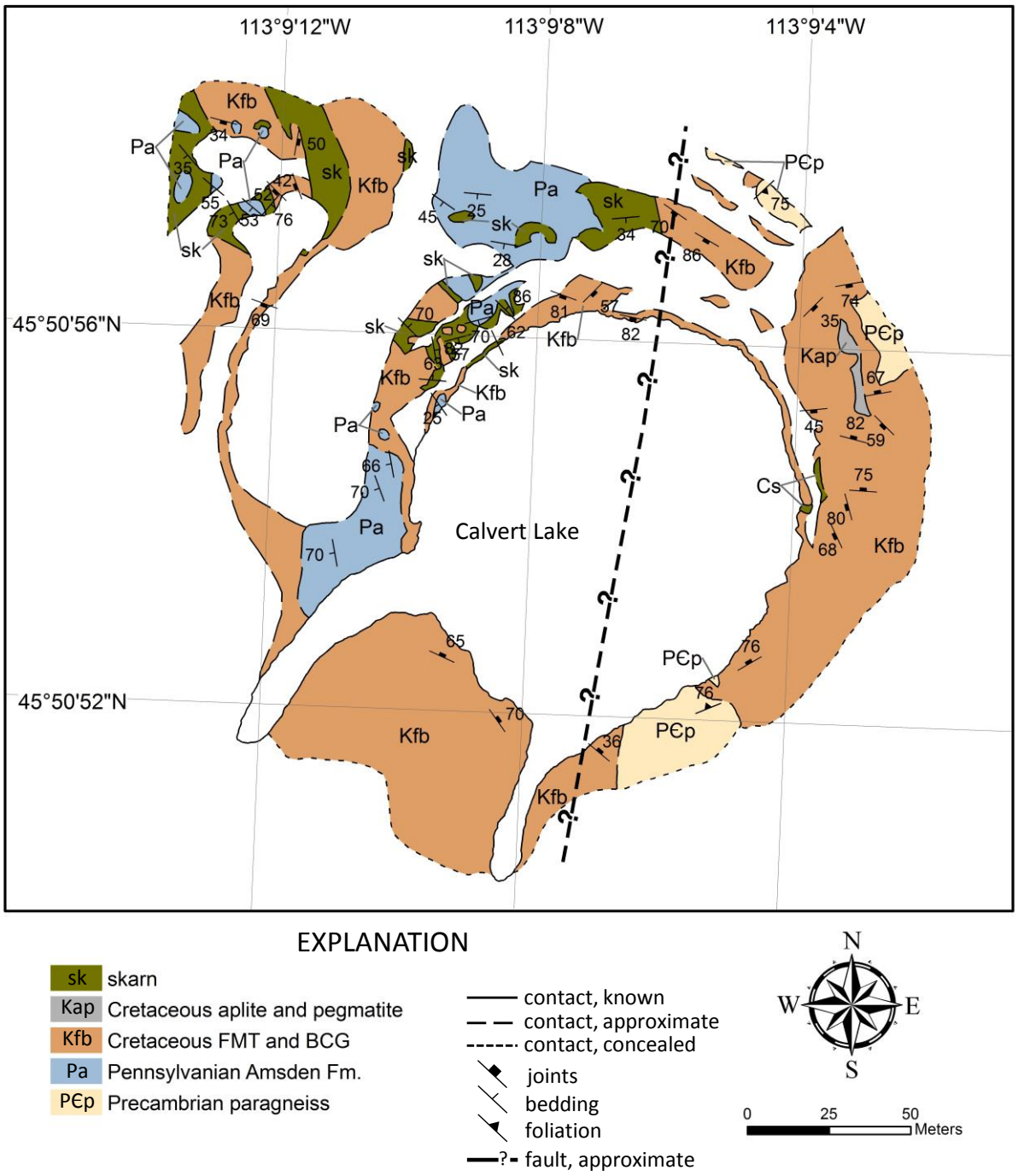

Figure 7. Simplified geologic map of the Calvert mine.

4.1.1. Paragneiss

The paragneiss outcrops as northwest-trending blocks located in the eastern portion of the study area and is bordered by coarse-grained tonalite. The paragneiss in the Calvert Hill area has been presumed to be of Precambrian age by Berger et al. (1983) because of its amphibolite grade of metamorphism and polydeformed character. Truckle (1988) described the paragneiss as being a fine-medium-grained, foliated and compositionally layered quartzo-feldspathic gneiss. Further investigation of the paragneiss was not conducted for this report but the reader is directed to the detailed description given by Truckle (1988).

4.1.2. Igneous Rocks

Two phases of the Pioneer Batholith are found within the study area, and so two periods of intrusion were delineated and their compositions are: tonalite and granite (Figure 8, data in Appendix A). Snee (1982) refers to the granodiorite-tonalite at the Calvert mine as the Foolhen Mountain Tonalite (FMT). The FMT is the dominant intrusive at the Calvert mine and is found throughout the study area. Snee and Sutter (1982) used Ar/Ar age-spectrum and conventional K/Ar dating methods on hornblende present in the FMT from the Calvert mine region, yielding an emplacement date of 72.06 ± 1.07 m.y. before present.

The FMT at Calvert exists as 1) a light-medium colored, medium-coarse grained, heavily weathered and iron-stained tonalite, and 2) a light colored, fine-medium grained, lightly weathered and iron-stained tonalite. The coarse-grained tonalite (KTD1 and KTD2) exists furthest from the skarn contact and contains coarse-grained subhedral to anhedral, poikilitic plagioclase exhibiting Carlsbad and albite twinning (Figure 9, A-B). Myrmekite is common at grain boundaries. The plagioclase is low-moderately fractured and locally altered to sericite. Quartz is fine-coarse-grained, low-moderately fractured with anhedral quartz commonly

intergrown with plagioclase. Potassium feldspar is nearly non-existent. Fine-very coarse-grained biotite exists throughout. The biotite is lightly altered to chlorite along cleavage planes that intersect fractures close to grain boundaries. Fine-medium anhedral magnetite exists throughout and is the dominant accessory mineral.

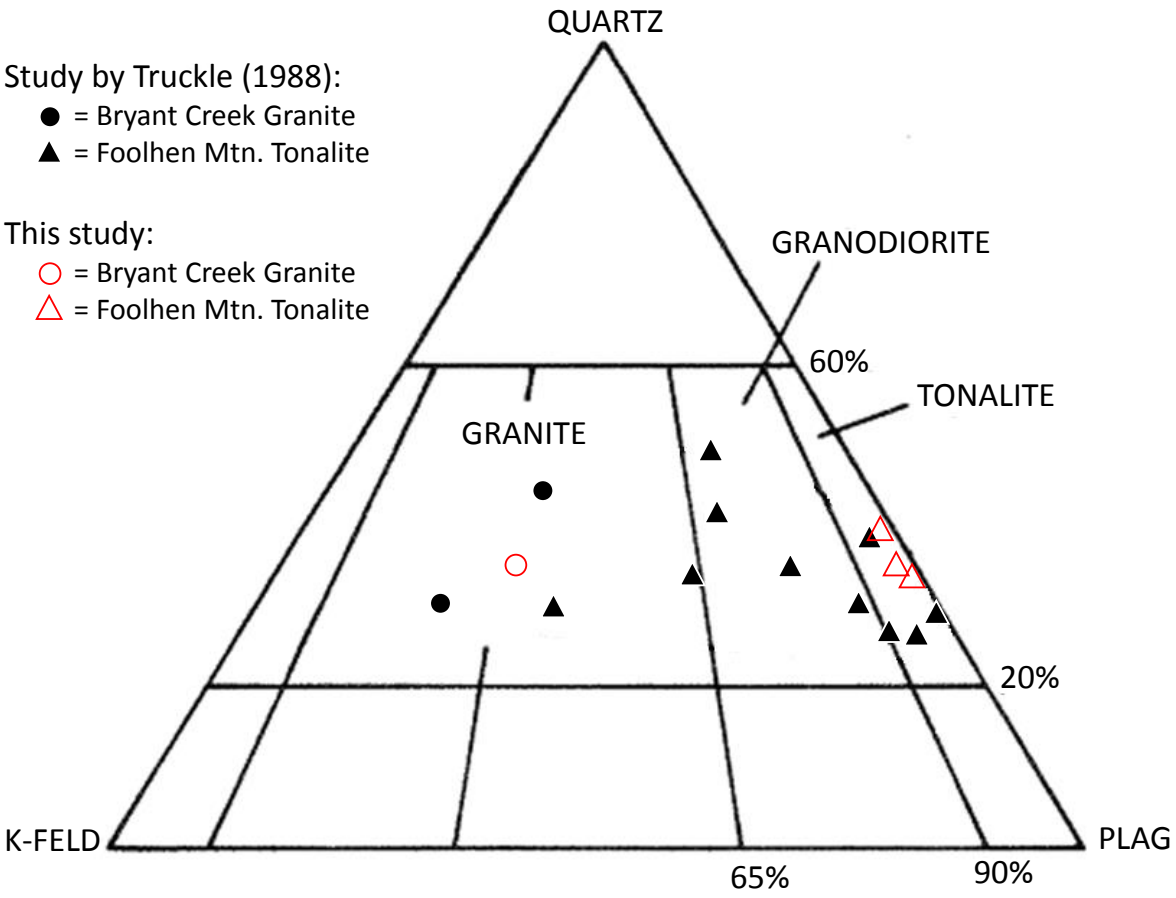

Figure 8. Modal compositions of the igneous rocks observed at Calvert mine from this study and by Truckle (1988). Minerals and percentages are summarized in Appendix A.

The fine-medium grained tonalite (KTL1) exists closest to the skarn and contains fine-medium grained, anhedral-subhedral, poikilitic plagioclase that exhibits albite twinning (Figure 9, C-D). Myrmekite is common throughout. The plagioclase is moderately-highly fractured and filled with sericite and Fe-oxides. Quartz exists as fine-coarse anhedral grains that are lightly fractured. Minimal quartz grains exhibit undulose extinction. Biotite exits as fine-medium,

anhedral-subhedral grains that are slightly altered to chlorite and Fe-oxides. An epidote-quartz endoskarn exists in the FMT at Calvert, with exposure limited to the east side of the pit. This observation is in agreement with findings from previous studies (Kemp, 2013).

The granite has been referred to as the Bryant Creek Granite (BCG) by Snee (1982), and was only observed in the western portion of the study area where it is exposed on both slopes of a trench. The BCG intrudes the FMT and is therefore younger than the tonalite, which is in agreement with the findings of Truckle (1988). The BCG (KTL2; Figure 9, E-F) contains fine-coarse-grained, anhedral-subhedral, poikilitic plagioclase exhibiting albite twinning. Myrmekite is common throughout. The plagioclase is highly fractured and altered to sericite. Highly fractured fine-coarse-grained K-feldspar exists as anhedral-subhedral and poikilitic forms exhibiting polysynthetic twinning. Quartz is fine-coarse, anhedral-subhedral, low-moderately fractured and locally cut by secondary hydrothermal quartz. Fine-grained quartz is commonly found at grain boundaries between K-feldspar and plagioclase. Biotite is highly altered to hematite, and in some places it is nearly completely altered to subhedral-euhedral hematite crystals.

Two varieties of dikes are distinguished in the study area: aplite and pegmatite. These two northwest-trending dikes intrude the tonalite in the eastern portion of the study area and have been mapped as a single unit (Kap). The dikes have not been metamorphosed suggesting that emplacement followed regional metamorphism.

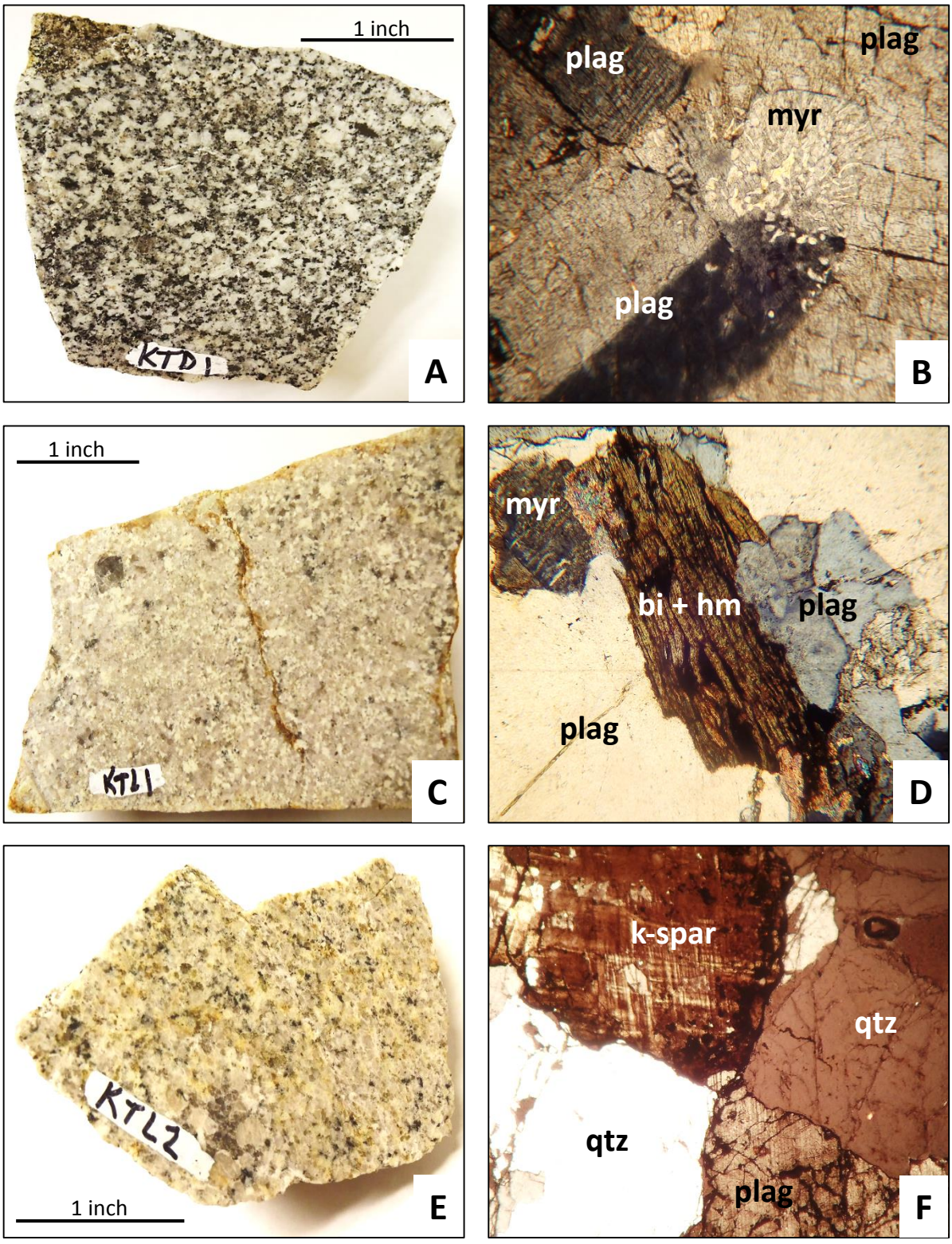

Figure 9. Igneous rock hand samples and thin section microphotographs of FMT (A-D) and BCG (E-F). All microphotographs are at 40x and all thin sections are K-feldspar stained.

4.1.3. Marble

The marble at Calvert is the host of the skarn and ore mineralization, and has been identified differently by previous researchers due to the complex nature of the stratigraphy in southwest Montana. Walker (1963) and Geach (1972) suggested that the Calvert skarn is hosted in the lower section of the Cambrian Hasmark Formation. Truckle (1988) interpreted the host rock at Calvert as Late Mississippian (Amsden Formation or Madison Group) strata. Ruppel et al. (1993) mapped Permian (Phosphoria Formation) to Pennsylvanian and Upper Mississippian (Quadrant Formation) sedimentary rocks in the Calvert mine area; units which are still mapped in the current (2007) Montana state geologic map found on the MBMG website. Kemp (2013) suggested that the mineralization at Calvert is hosted in the Amsden Formation and described it as consisting primarily of limestone, as well as mudstone, siltstone and fine-grained sandstone-rich horizons.

The Amsden Formation has also been identified as the host of skarn mineralization at other deposits in the Pioneer Mountains (Lentung, Brownes Lake, Lost Creek, and prospects in the Utopia district, see Table I). In his M.S. thesis on the skarn mineralization at Lentung (East Pioneer Mountains), Deboer (1991) identified the host rock to be the Amsden Formation and described it as a relatively clean carbonate intermediate between limestone and dolomite, with MgO contents from 5 to 11 wt.%.

No stratigraphic work was conducted for this report, but it is assumed that the host of the Calvert mineralization is the Amsden Formation based on these previous works. The Late Paleozoic strata in southwest Montana are interrupted by faulting, metamorphism, and intrusions of granitoids. According to the stratigraphic research conducted by Maughan and Roberts (1967), the Amsden Formation in southwestern Montana is Pennsylvanian age. Therefore, the

host of the skarn and ore mineralization at Calvert is interpreted to be part of the Pennsylvanian Amsden Formation which represents a shallow marine to coastal facies.

The Amsden Formation in the study area is exposed as outcrops and in trenches in the western half of the mine where it exists in sharp contact with igneous rock and skarn. The rock is a dark-blue marble consisting of granoblastic calcite, and no dolomite was observed. The emplacement of the intrusive rock(s) caused contact metamorphism which recrystallized the Paleozoic limestone to marble. The contact between the marble and limestone was not observed at the Calvert mine; therefore, the extent of the metamorphic aureole is not known.

Close to the marble/skarn contact there are zones of barren, iron-poor, calc-silicates beyond the scheelite-bearing skarn which is typical in tungsten skarn deposits (Einaudi et al. 1981). Bateman (1965) referred to these zones at the Bishop Tungsten District in California as "bleached and silicate marbles" which he suggested originated from metamorphic recrystallization accompanying destruction of carbonaceous matter. Nokleberg (1981) suggested that the barren wollastonite-grossularite-idocrase rocks surrounding the garnet-pyroxene skarns at Strawberry, California are of a metasomatic origin. The bleached marble zones at Calvert are interpreted to be of metasomatic origin due to the spatial relationship between the unaltered marble, bleached marble and the skarn (Figure 10).

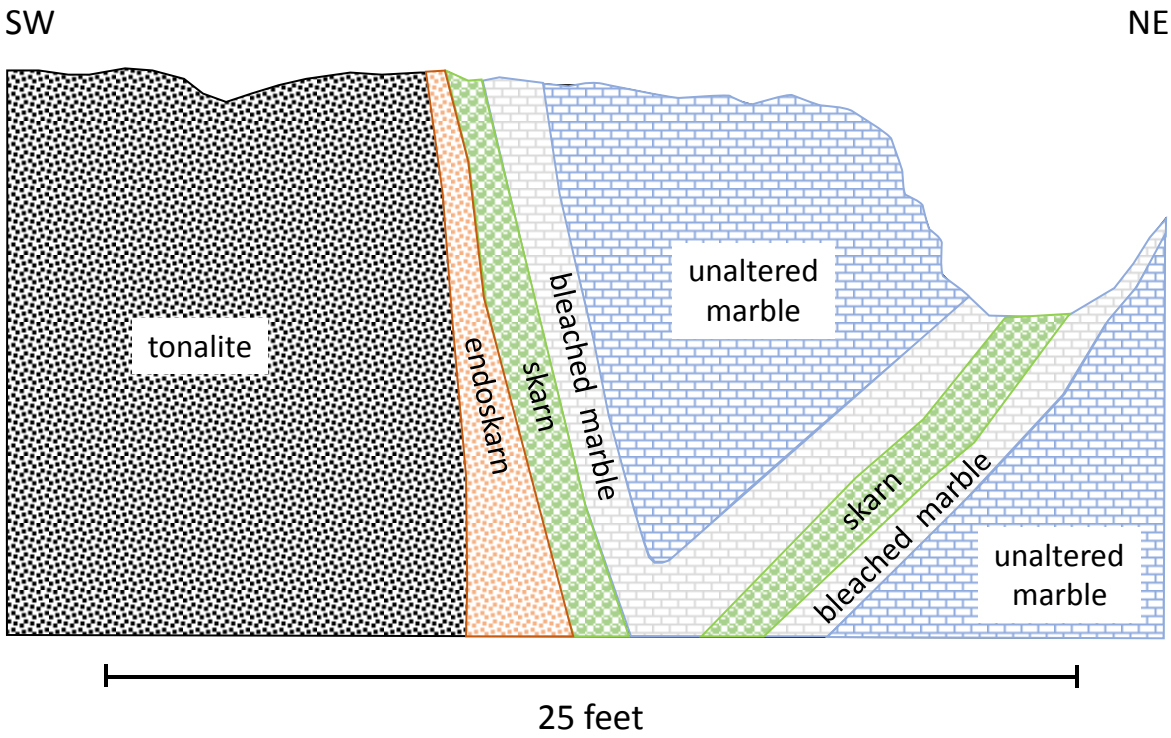

Figure 10. Spatial relationship between the FMT and marble at the Calvert mine. The bleached marble represents the extent of the metasomatic fluid propagation through the host carbonate rock.

4.2. Skarn Petrology

At the Calvert mine, skarns developed in the FMT (endoskarn) and in the marble (exoskarn). The principal skarn minerals at Calvert are garnet, epidote, amphibole, calcite and quartz together with forsterite, diopside, scheelite, magnetite, zircon, sphene, apatite, phlogopite, muscovite, hematite and chlorite as accessory minerals. Scheelite is visible when the sample is under UV light (Figure 11). There are early skarn minerals entirely or partially replaced by later predominantly hydrous minerals. Four rock types have been distinguished within the Amsden Formation at Calvert: 1) a forsterite, diopside, garnet(?) and phlogopite marble, 2) a garnet, epidote, calcite and quartz skarn containing coarse-grained scheelite (up to 2 cm in diameter), 3) an actinolite, calcite and quartz assemblage with fine-medium-grained scheelite, and 4) late chlorite and muscovite with no scheelite. Many of the garnets contain scheelite as inclusions,

along with quartz, calcite and epidote. The Calvert skarn is notable for being nearly completely absent of sulfide minerals or base metal mineralization, and is an example of a very "clean" tungsten skarn.

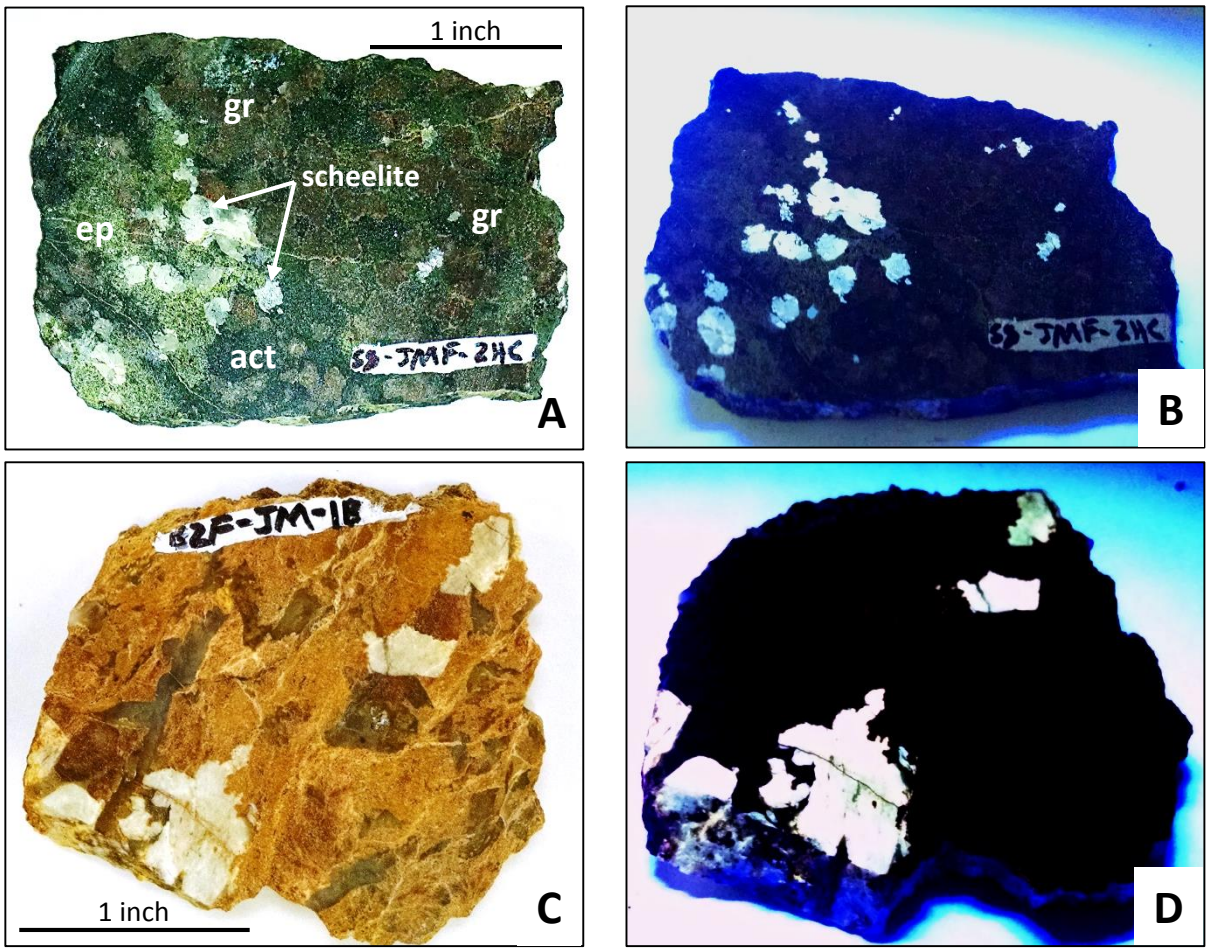

Figure 11. Calvert rock slabs under UV light. Samples represent prograde assemblages consisting of garnet-epidote-calcite with coarse-grained scheelite (A-B) and garnet-quartz-scheelite (C-D).

Although not observed in this study, there have been additional minerals reported at Calvert which include beryl, chalcopyrite, pyrite, andradite, pyrrhotite, rutile, molybdenite and cuprotungstite (Gobla, 2012). The occurrence of rare crystals of aquamarine beryl, highly sought by local mineral collectors, was first described by King (1966).

4.2.1. Skarn Paragenesis

The sequence of skarn mineralization of the Calvert deposit is shown in Figure 12. The minerals are distinguished as being formed during three stages: 1) early prograde metasomatism, 2) main-stage prograde metasomatism, and 3) retrograde alteration. A description of each stage is given below.

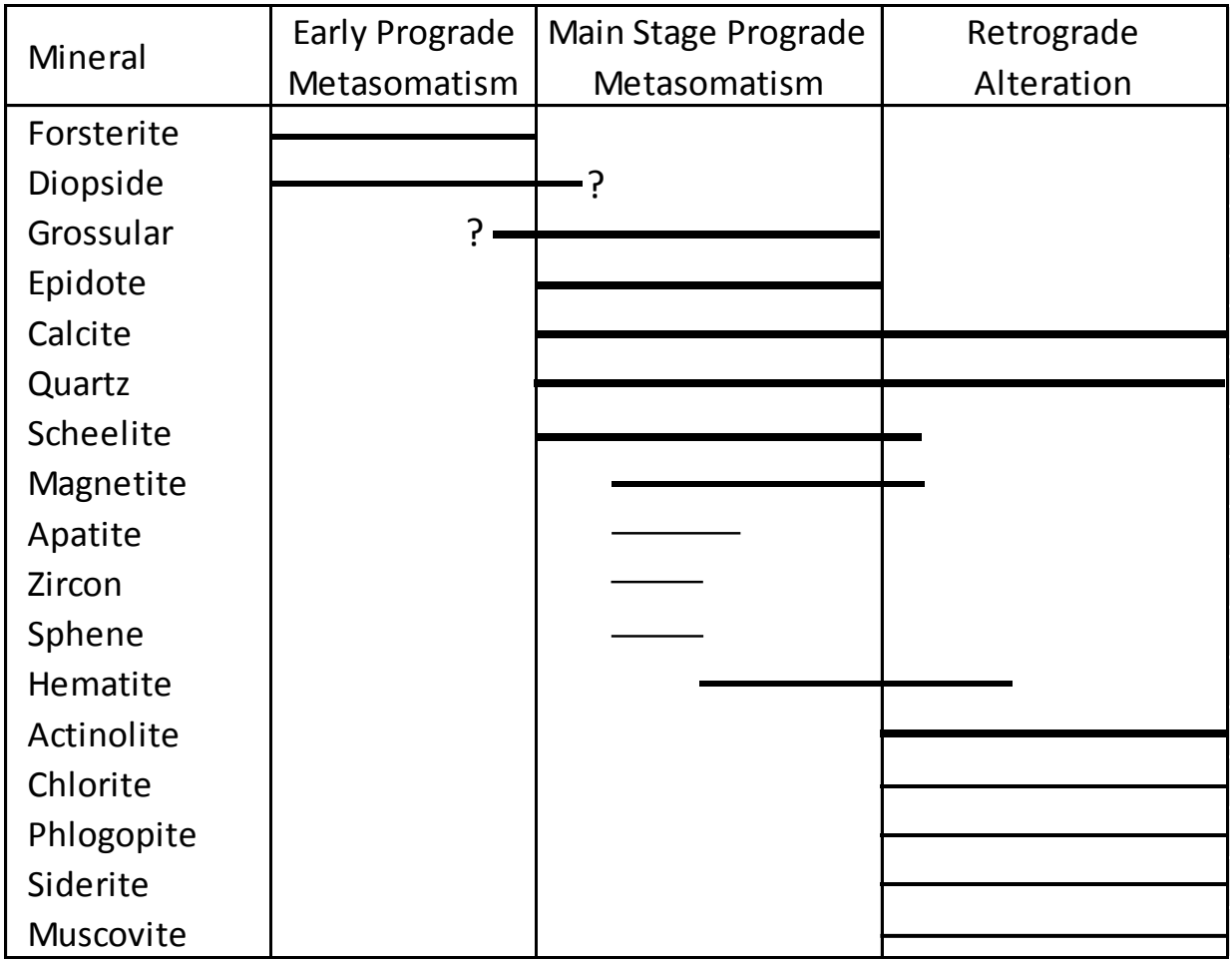

Figure 12. Paragenetic sequence of mineralization at the Calvert mine.

Early Prograde Metasomatism: An early period of prograde metasomatism is indicated by the formation of the bleached marble near the skarn contact (Figure 10; Figure 13). This zone consists of mainly calcite with minor forsterite, diopside, trace garnet(?) and secondary

phlogopite. This bleached zone suggests an early magnesium-aluminum-rich, tungsten-poor metasomatic stage, and represents the maximum extent of the metasomatic fluids.

The bleached zone varies in thickness from 2 inches to about 3 feet in the mine (Figure 13, A). Textural and mineralogical variations exist within this marble as it approaches the skarn contact. The bleached marble furthest from the skarn contact is nearly completely white and consists of granoblastic calcite with fine-medium-grained diopside and fine-coarse-grained phlogopite. The diopside exists as inclusions in calcite and along calcite grain boundaries (Figure 13, B-C). Closer to the skarn contact the bleached marble is darker and consists of fine-medium-grained anhedral calcite, forsterite, diopside, garnet(?), phlogopite, fine-medium-grained subhedral chlorite, and chalcedony filling vugs and veins (Figure 13, D-E).

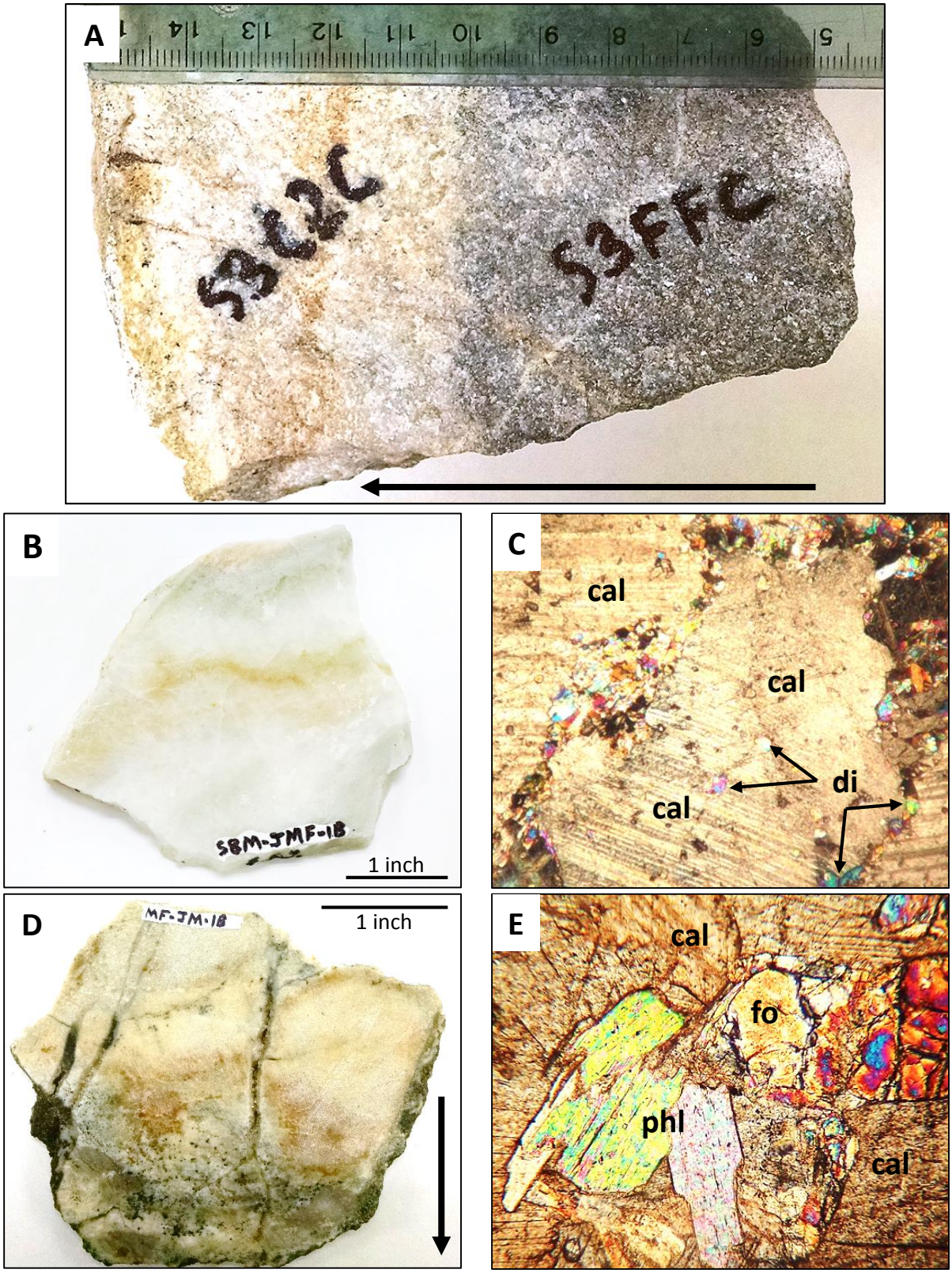

Figure 13. Bleached marble samples from Calvert. Diopside inclusions in coarse-grained marble (B-C) found far from skarn contact. At the skarn contact a forsterite-diopside-garnet(?)-phlogopite marble exists (D-E). Microphotographs are 40x magnification in PPL. Arrows show the direction to the skarn.

Main-Stage Prograde Metasomatism: The main-stage prograde skarn mineral assemblage is dominated by garnet, diopside(?), epidote, calcite and quartz together with scheelite, zircon, magnetite, apatite, hematite and sphene as accessory minerals (Figure 11). Coarse garnet (up to 8 cm) and epidote are typically found fractured and intergrown (Figure 14, A; Figure 15, A-D and F). Coarse-grained scheelite is also commonly intergrown with garnet and epidote, and occurs as fine-grained inclusions in garnet (Figure 14, B; Figure 15, A-B, Figure 16).

The garnet is light red-brown, and in thin section is commonly anisotropic with multiple growth zones, sector zoning and local oscillatory zoning. Besides scheelite, garnet hosts inclusions of calcite, quartz, epidote and accessory minerals such as zircon and sphene (Figure 14, B; Figure 16).

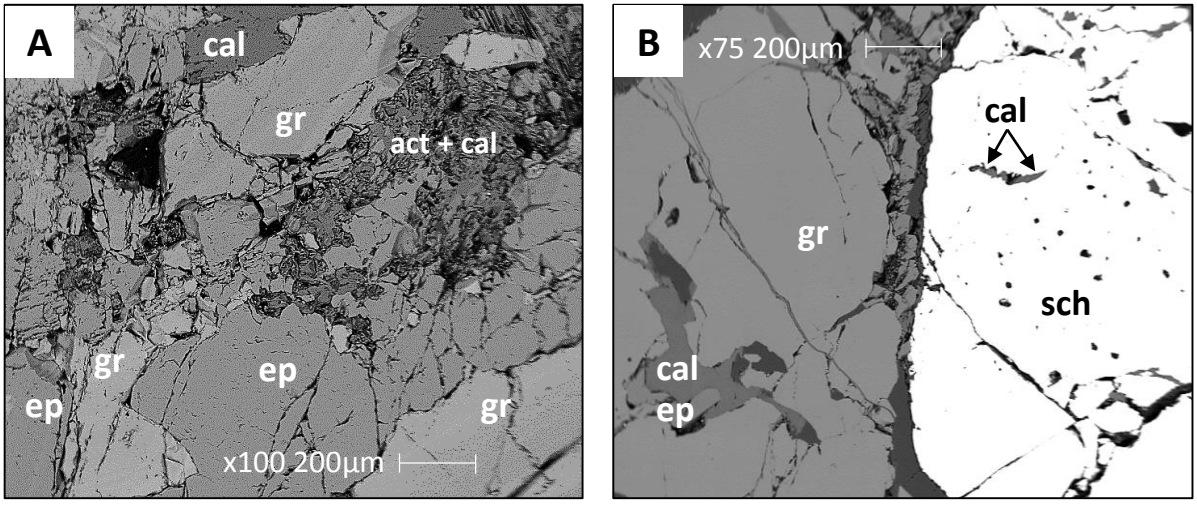

Figure 14. SEM-BSE images that show the relationship between prograde minerals garnet, epidote, and scheelite. Garnet is commonly intergrown with epidote (A). Scheelite is found intergrown with, and as inclusions in, garnet (B).

Thin section microscopy revealed what appears to be relic pyroxene associated with prograde minerals (Figure 15, E). Due to the highly altered nature of these remnant pyroxenes, optical properties were unidentifiable and compositional information was also unobtainable using SEM-EDX and Raman spectroscopy.

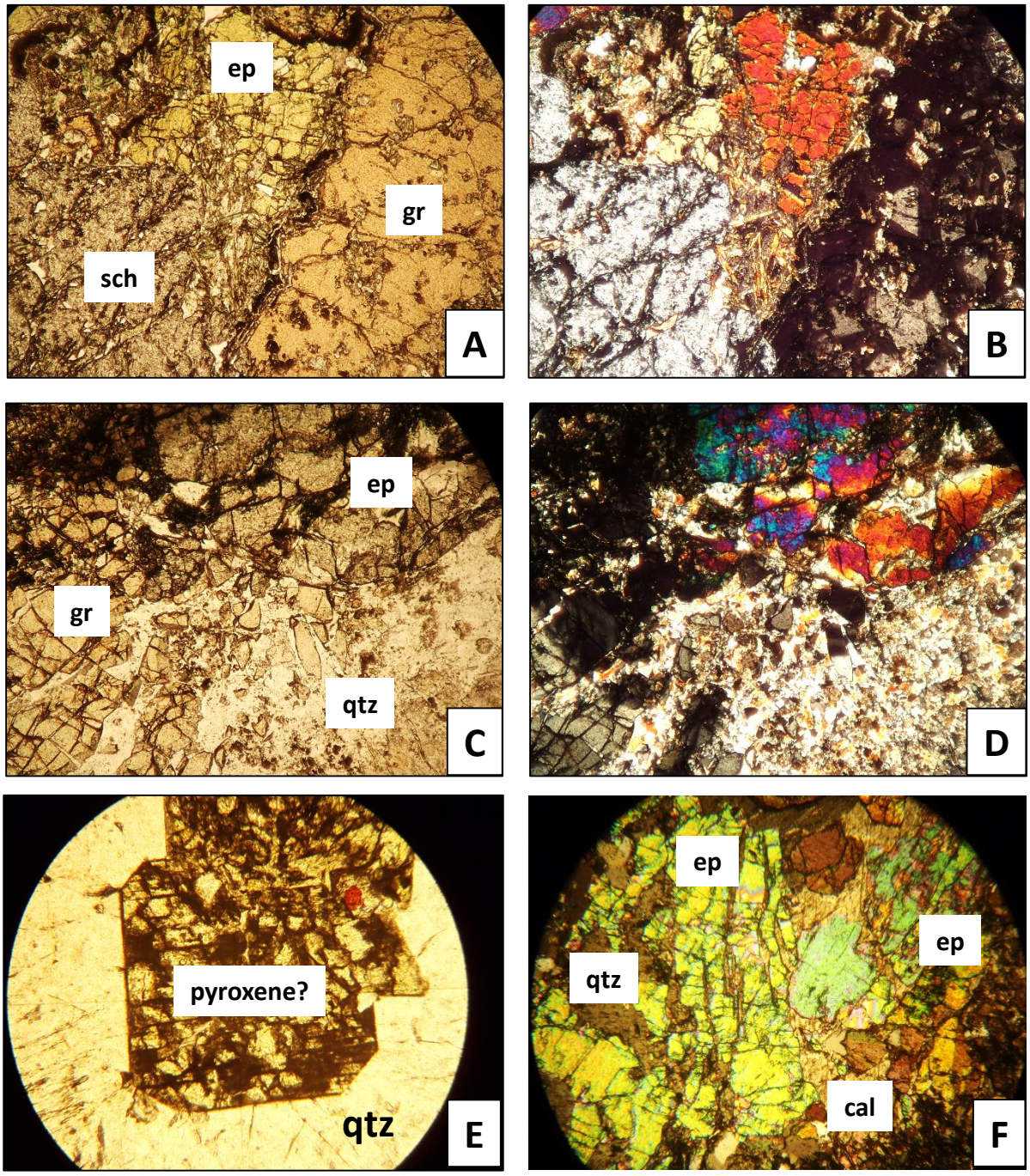

Figure 15. Microphotographs of skarn thin sections showing prograde mineral relations and textures. Scheelite intergrown with epidote and garnet in PPL (A) and XPL (B) at 40x magnification. Highly fractured and intergrown garnet and epidote containing secondary quartz as vein material (C in PPL and D in XPL; both at 40x magnification). Remnant pyroxene in prograde assemblage in PPL (E) at 100x magnification. Prograde minerals are highly fractured and filled with calcite and quartz (F in XPL at 40x magnification).

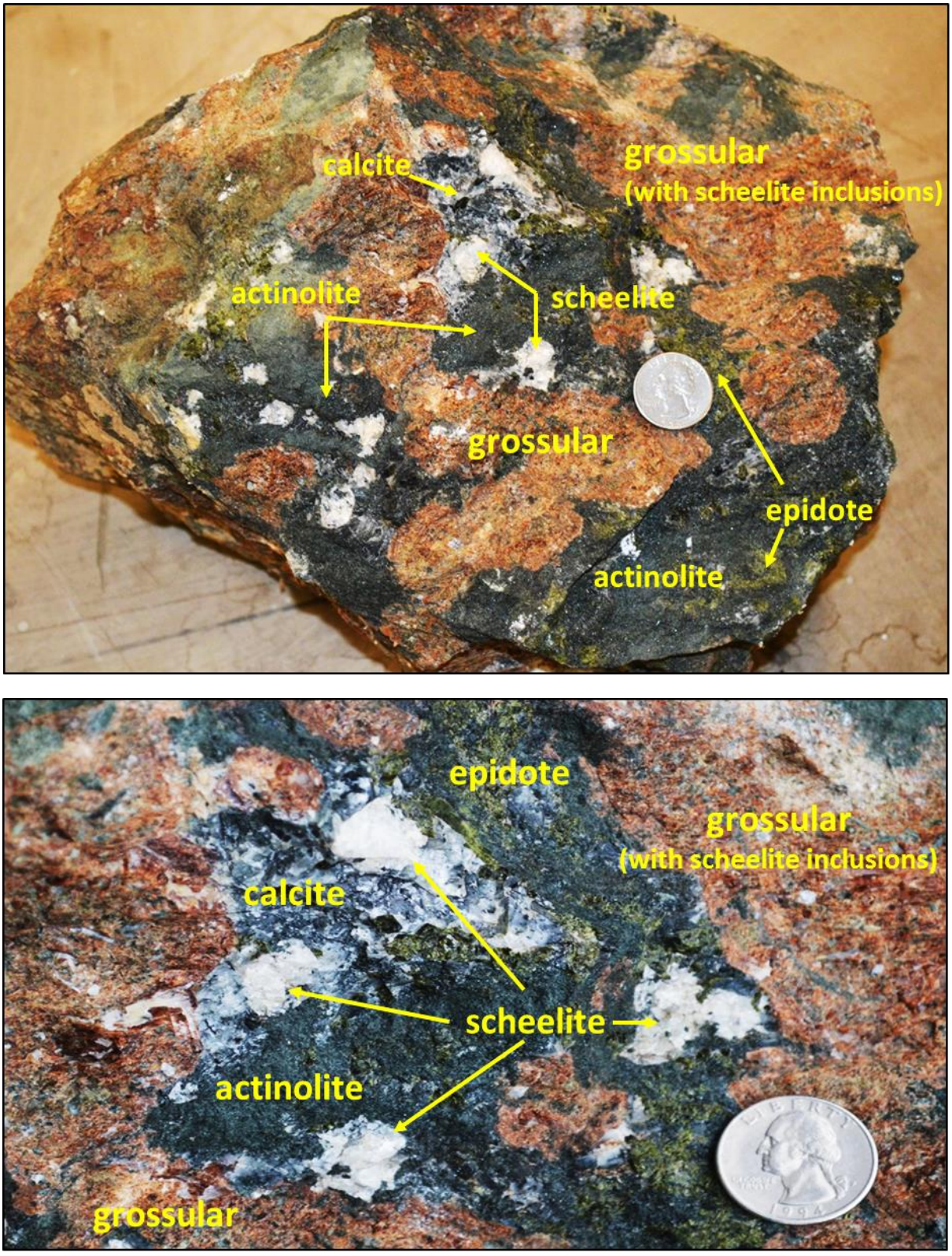

Figure 16. Calvert skarn sample showing prograde mineral assemblage of garnet+epidote+scheelite and retrograde alteration to actinolite and calcite. Small scheelite inclusions exist in grossular, and coarse scheelite exits intergrown with garnet, epidote, and calcite. Lower picture is a close-up of the top photo.

Retrograde Alteration: This stage is evident by the alteration of early higher temperature minerals and the crystallization of texturally later minerals. Retrograde alteration at the Calvert mine is extensive, with a mineral assemblage dominated by actinolite, calcite and quartz together with scheelite, hematite, muscovite, phlogopite, chlorite, magnetite and siderite as accessory minerals. Retrogression of the skarn is significant with pyroxene(?) inclusions in early scheelite altering to calcite and actinolite (Figure 17, A-B), garnet altering to calcite, quartz and hematite, and epidote altering to muscovite and hematite. Hematite occurs as subhedral-euhedral crystals in garnet and epidote, as well as an alteration product at grain boundaries and intergrown with muscovite (Figure 17, C-D). The occurrence of slightly altered prograde scheelite and fine-grained scheelite of nearly pure composition within the retrograde assemblage is evidence of scheelite remobilization, possibly during the early periods of retrograde alteration.

Large euhedral calcite crystals exist throughout the skarn at Calvert, and are generally found intergrown with epidote and actinolite (Figure 18). Vugs and fractures are commonly filled with calcite and chalcedony, and disseminated scheelite locally occurs within these late open space fillings (Figure 19).

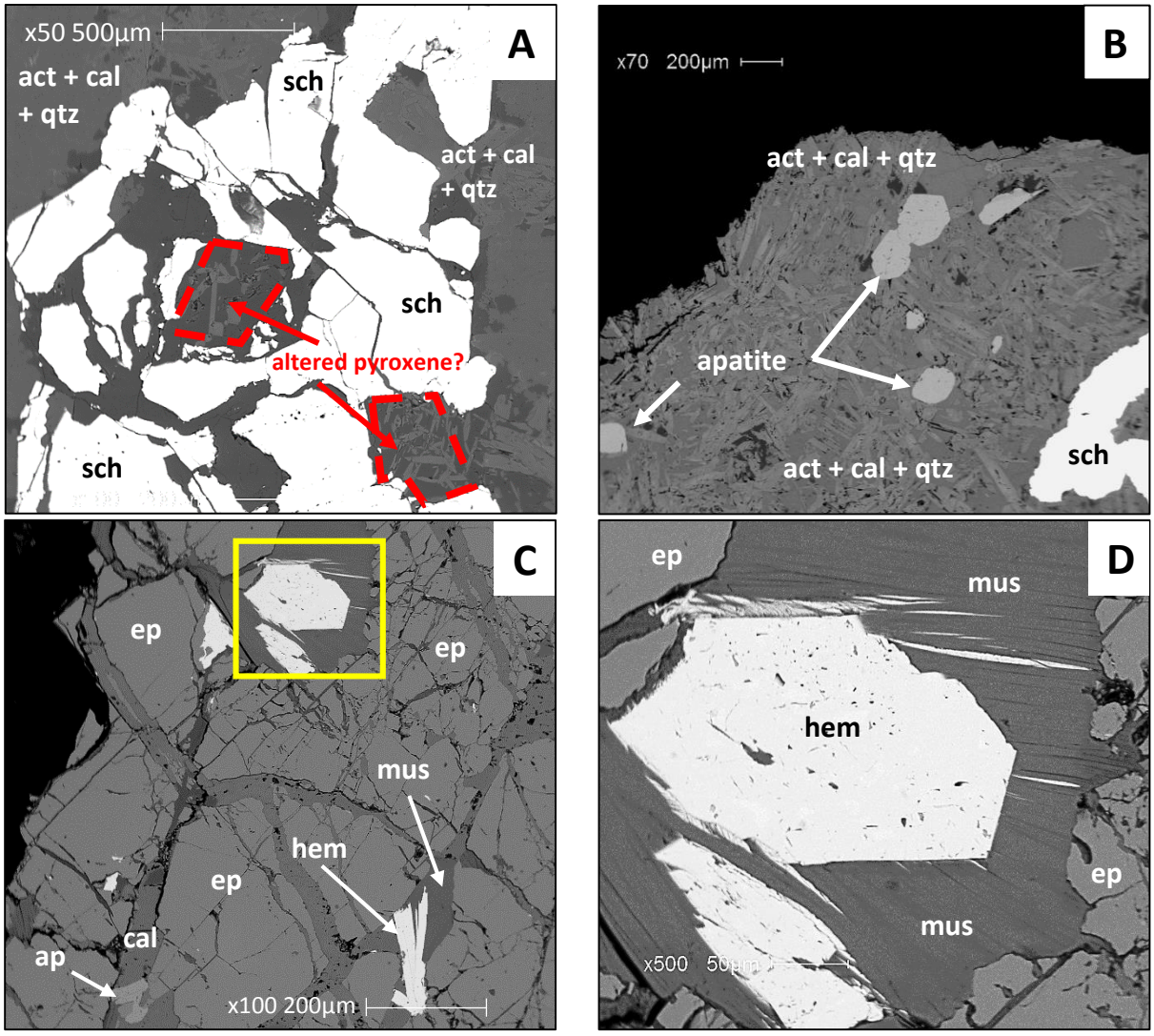

Figure 17. SEM-BSE images showing retrograde alteration of prograde skarn minerals. Pyroxene(?) inclusions in scheelite altered to actinolite and calcite (A, red outlines). Slightly altered scheelite in a retrograde matrix of actinolite, calcite and quartz (B). Fractured epidote altered to muscovite and hematite (C-D). Figure D is a close-up of bordered area in figure C.

Figure 18. Large calcite crystal in an epidote-calcite skarn hand sample.

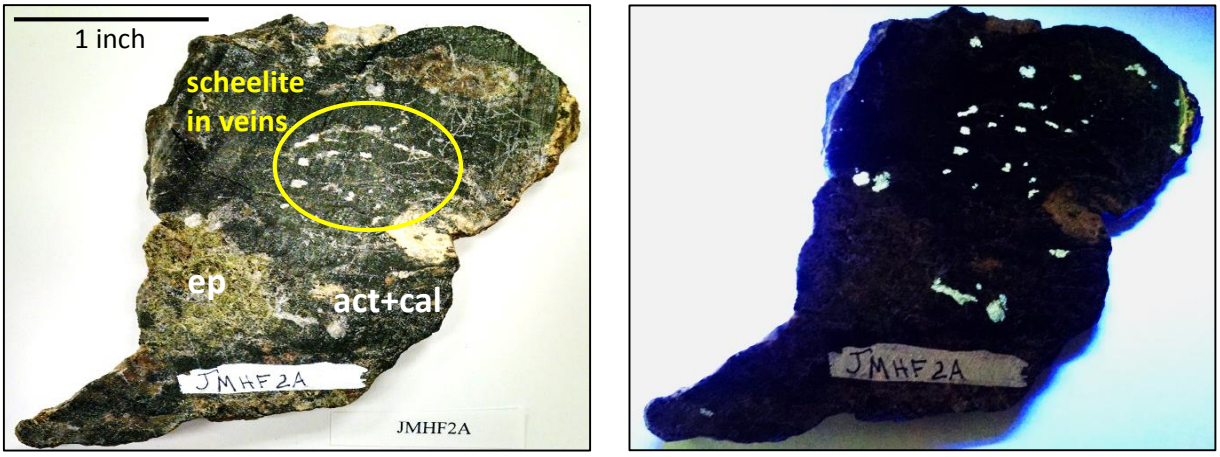

Figure 19. Retrograde actinolite-calcite hand sample under UV light. Fine-grained scheelite occurs as vein material with quartz.

4.2.2. Mineral Chemistry

In this section, mineral compositions from SEM-EDX analyses of the skarn minerals garnet, epidote, actinolite, scheelite, calcite and apatite are presented and discussed. Mineral chemistries aid in constraining the physical and chemical conditions during skarn evolution. Chemical analyses of skarn minerals can also be used to classify the skarn types (Einaudi et al., 1981; Meinert, 1992).

Garnet

A common feature of the garnet at Calvert is an epidote+quartz+calcite reaction rim separating early core growth from later rim growth (Figure 20). SEM-EDX analysis was used to determine if any compositional change exists between the garnet core and rim for the samples. The compositional variations of the Calvert garnets are shown in Table III and graphically presented in Figure 21. Mole fraction calculations show that the garnets are predominantly grossular, indicating a metasomatic addition of aluminum and ferric iron.

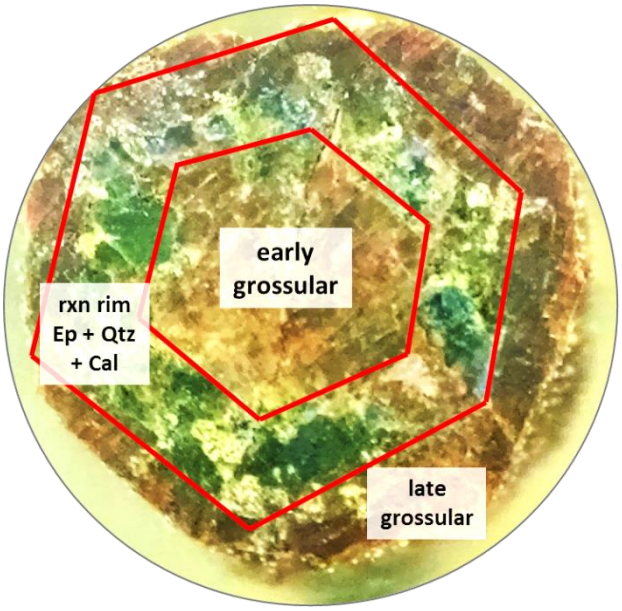

Figure 20. Polished plug of garnet sample GF-2A exhibiting an epidote+calcite+quartz reaction rim separating an early garnet core from a late garnet rim. Plug is 1 inch across.

Table III. SEM-EDX results for selected garnet samples analyzed. Based on the formula: $Ca_3(Al,Fe)_2Si_3O_{12}$

		Atomic %						
Sample	Type	Ca	Al	Fe	Mg	Mn	Si	Formula
JMHF7A-1	grossular	18.8	10.4	4.4	0.0	2.0	22.5	$(Ca_{2.7}Mn_{0.3})(Al_{1.4}Fe_{0.6})(SiO_4)_3$
JMHF7A-5	grossular	18.3	10.0	4.9	0.0	2.4	22.7	$(Ca_{2.6}Mn_{0.4})(Al_{1.3}Fe_{0.7})(SiO_4)_3$
GF-1A2	grossular	18.8	9.9	4.6	0.0	1.8	22.7	$(Ca_{2.7}Mn_{0.3})(Al_{1.4}Fe_{0.6})(SiO_4)_3$
GF-2A2	grossular	20.3	9.9	4.8	0.0	1.3	22.6	$(Ca_{2.8}Mn_{0.2})(Al_{1.3}Fe_{0.7})(SiO_4)_3$
GF-2A3	grossular	19.6	10.1	7.0	0.0	2.5	25.8	$(Ca_{2.7}Mn_{0.3})(Al_{1.2}Fe_{0.8})(SiO_4)_3$
GF-2A4	grossular	20.8	11.3	5.8	0.0	2.0	26.8	$(Ca_{2.7}Mn_{0.3})(Al_{1.3}Fe_{0.7})(SiO_4)_3$
GF-2A5	grossular	20.2	10.2	6.8	0.0	2.1	26.7	$(Ca_{2.7}Mn_{0.3})(Al_{1.2}Fe_{0.8})(SiO_4)_3$
GF-2A6	grossular	20.8	10.8	6.0	0.0	1.6	26.5	$(Ca_{2.8}Mn_{0.2})(Al_{1.3}Fe_{0.7})(SiO_4)_3$
GF-2A7	grossular	22.0	11.7	4.8	0.0	1.0	26.5	$(Ca_{2.9}Mn_{0.1})(Al_{1.4}Fe_{0.6})(SiO_4)_3$
GF-2A8	grossular	14.9	14.2	7.3	0.0	0.4	21.9	$(Ca_{2.9}Mn_{0.1})(Al_{1.3}Fe_{0.7})(SiO_4)_3$
GF-2A9	grossular	22.0	11.4	4.9	0.0	0.7	26.2	$(Ca_{2.9}Mn_{0.1})(Al_{1.4}Fe_{0.6})(SiO_4)_3$
GF-2A10	grossular	20.5	10.5	5.9	0.0	1.7	26.1	$(Ca_{2.8}Mn_{0.2})(Al_{1.3}Fe_{0.7})(SiO_4)_3$
GF-2A11	grossular	21.3	10.6	4.0	0.0	0.7	22.7	$(Ca_{2.9}Mn_{0.1})(Al_{1.5}Fe_{0.5})(SiO_4)_3$
GF-2A12	grossular	21.1	11.1	5.1	0.0	1.0	26.0	$(Ca_{2.9}Mn_{0.1})(Al_{1.4}Fe_{0.6})(SiO_4)_3$
GF-2A13	grossular	20.3	8.8	5.0	0.0	1.2	20.3	$(Ca_{2.8}Mn_{0.2})(Al_{1.3}Fe_{0.7})(SiO_4)_3$
GF-2A14	grossular	21.8	10.9	5.4	0.0	1.1	26.1	$(Ca_{2.9}Mn_{0.1})(Al_{1.3}Fe_{0.7})(SiO_4)_3$
GF-2A15	grossular	21.4	10.8	5.2	0.0	1.2	26.0	$(Ca_{2.8}Mn_{0.2})(Al_{1.3}Fe_{0.7})(SiO_4)_3$
GF-2A16	grossular	20.6	10.7	4.0	0.0	1.0	22.8	$(Ca_{2.9}Mn_{0.1})(Al_{1.5}Fe_{0.5})(SiO_4)_3$
GF-2A17	grossular	21.8	11.0	5.1	0.0	0.6	25.9	$(Ca_{2.9}Mn_{0.1})(Al_{1.4}Fe_{0.6})(SiO_4)_3$
GF-2A18	grossular	21.2	11.6	4.3	0.0	0.8	25.9	$(Ca_{2.9}Mn_{0.1})(Al_{1.5}Fe_{0.5})(SiO_4)_3$
GF-2A19	grossular	19.5	9.2	5.7	0.0	1.8	22.8	$(Ca_{2.7}Mn_{0.3})(Al_{1.2}Fe_{0.8})(SiO_4)_3$
GF-2A20	grossular	20.4	9.6	5.2	0.0	1.3	22.8	$(Ca_{2.8}Mn_{0.2})(Al_{1.3}Fe_{0.7})(SiO_4)_3$
GF-2A21	grossular	19.1	8.5	6.6	0.0	1.9	22.8	$(Ca_{2.7}Mn_{0.3})(Al_{1.1}Fe_{0.9})(SiO_4)_3$
GF-2A22	grossular	20.7	11.0	4.9	0.0	1.2	25.5	$(Ca_{2.8}Mn_{0.2})(Al_{1.4}Fe_{0.6})(SiO_4)_3$
GF-2A23	grossular	19.1	10.3	6.0	0.0	2.0	25.5	$(Ca_{2.7}Mn_{0.3})(Al_{1.3}Fe_{0.7})(SiO_4)_3$
GF-2A29	grossular	20.2	8.9	5.8	0.2	1.1	22.5	$(Ca_{2.8}Mn_{0.2})(Al_{1.2}Fe_{0.8})(SiO_4)_3$
GF-2A30	andradite	18.6	4.3	11.5	0.2	3.2	22.8	$(Ca_{2.6}Mn_{0.4})(Fe_{1.5}Al_{0.5})(SiO_4)_3$
GF-2A31	andradite	19.0	4.8	10.5	0.2	2.3	22.8	$(Ca_{2.7}Mn_{0.3})(Fe_{1.4}Al_{0.6})(SiO_4)_3$

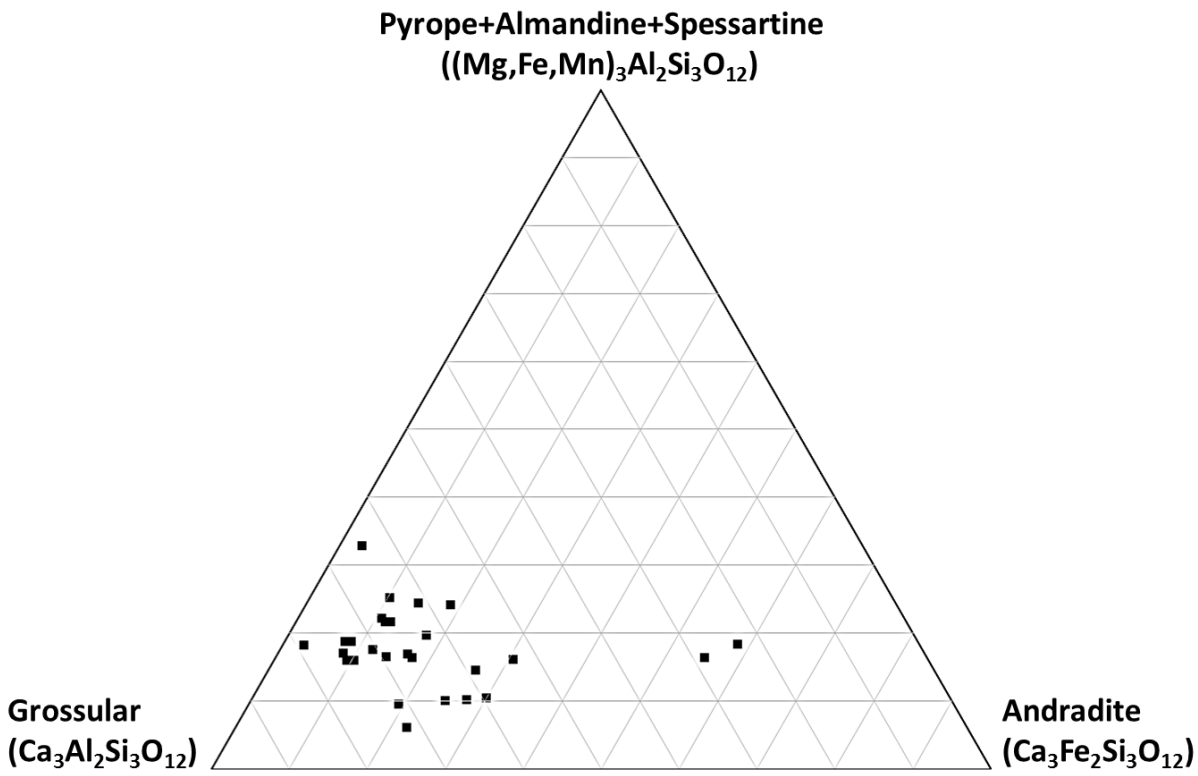

Figure 21. Modal compositions of the Calvert garnets analyzed by SEM-EDX. The Calvert garnet is predominantly grossular.

According to the data, a minor andradite phase has been identified (Figure 21). These data were taken very close to the reaction rim minerals, and may represent an artifact of sampling (3 garnets analyzed). Further analyses of the Calvert garnets is required to determine if this composition is primary or secondary.

Epidote

The SEM-EDX results of the Calvert epidotes are given in Table IV. These data show a narrow compositional range for the Calvert epidote, with minimal substitution of manganese for calcium and a 2:1 ratio of aluminum to iron. Optical properties (birefringence, pleochroism, etc.) and chemical analyses (Al/Fe^{3+} ratio) have identified these as epidote and not clinozoisite.

Table IV. SEM-EDX results for epidote samples analyzed. Based on the formula: $Ca_2(Al,Fe)_3Si_3O_{12}(OH)$

		Atomic %					
Sample	Type	Ca	Al	Fe	Mn	Si	Formula
JMHF7A-13	epidote	13.6	14.9	6.1	0.2	22.7	$(Ca_{1.97}Mn_{0.03})Al_{2.1}Fe_{0.9}Si_3O_{12}(OH)$
SST-JM-1A3	epidote	13.2	15.3	5.4	0.0	22.8	$Ca_2Al_{2.2}Fe_{0.8}Si_3O_{12}(OH)$
GF-1A5	epidote	10.2	11.7	5.0	7.6	22.3	$(Ca_{1.2}Mn_{0.8})Al_{2.1}Fe_{0.9}Si_3O_{12}(OH)$
GS-2A1	epidote	13.1	14.0	6.9	0.0	22.5	$Ca_2Al_2Fe_1Si_3O_{12}(OH)$
GS-2A12	epidote	13.5	14.2	6.6	0.3	21.9	$(Ca_{1.96}Mn_{0.04})Al_{2.1}Fe_{0.9}Si_3O_{12}(OH)$
GS-2A17	epidote	13.3	14.1	6.6	0.3	22.0	$(Ca_{1.96}Mn_{0.04})Al_{2.1}Fe_{0.9}Si_3O_{12}(OH)$
GS-2A18	epidote	13.7	14.4	6.4	0.2	22.1	$(Ca_{1.97}Mn_{0.03})Al_{2.1}Fe_{0.9}Si_3O_{12}(OH)$

Amphibole

The compositional variations in the Calvert amphiboles are shown in Table V. These data show that the amphiboles are calcic, falling completely within the tremolite-ferroactinolite series. According to Nesse (2012), compositions with more than 90% magnesium are tremolite, between 90% and 50% magnesium are actinolite, and less than 50% magnesium are ferro-actinolite. These results show that the Calvert amphiboles are actinolite in composition.

Table V. SEM-EDX results for amphibole samples analyzed. Based on the formula: $Ca_2(Mg,Fe)_5Si_8O_{22}(OH)_2$

		Atomic %						
Sample	Type	Ca	Al	Fe	Mg	Mn	Si	Formula
JMHF7A-16	actinolite	7.3	1.2	6.2	10.8	0.8	30.9	$Ca_2(Mg_{2.9}Fe_{1.6}Al_{0.3}Mn_{0.2})Si_{8.1}O_{22}(OH)_2$
JMHF7A-17	actinolite	7.4	2.7	7.7	9.3	1.1	30.3	$Ca_2(Mg_{2.3}Fe_{1.8}Al_{0.6}Mn_{0.3})Si_{7.3}O_{22}(OH)_2$
JMHF7A-18	actinolite	7.3	1.6	6.9	10.4	0.8	30.4	$Ca_2(Mg_{2.6}Fe_{1.8}Al_{0.4}Mn_{0.2})Si_{7.7}O_{22}(OH)_2$
JMHF8C-3	actinolite	5.8	2.0	5.2	8.2	0.7	23.5	$Ca_2(Mg_{2.6}Fe_{1.6}Al_{0.6}Mn_{0.2})Si_{7.3}O_{22}(OH)_2$
JMHF8C-14	actinolite	7.2	2.2	6.1	10.6	0.9	30.1	$Ca_2(Mg_{2.7}Fe_{1.5}Al_{0.6}Mn_{0.2})Si_8O_{22}(OH)_2$
JMHF8C-15	actinolite	7.2	2.0	6.7	10.3	1.2	30.1	$Ca_2(Mg_{2.5}Fe_{1.7}Al_{0.5}Mn_{0.3})Si_{7.5}O_{22}(OH)_2$
JMHF8C-19	actinolite	6.7	1.5	6.0	10.3	1.1	29.2	$Ca_2(Mg_{2.7}Fe_{1.6}Al_{0.4}Mn_{0.3})Si_{7.7}O_{22}(OH)_2$
JMHF8C-21	actinolite	6.7	1.4	5.8	10.3	0.9	29.4	$Ca_2(Mg_{2.8}Fe_{1.6}Al_{0.4}Mn_{0.2})Si_8O_{22}(OH)_2$
JMHF8C-22	actinolite	5.6	2.2	6.0	7.0	1.5	31.3	$Ca_2(Mg_{2.1}Fe_{1.8}Al_{0.7}Mn_{0.4})Si_{9.4}O_{22}(OH)_2$
JMHF8C-31	actinolite	6.8	3.2	7.1	8.9	0.9	27.6	$Ca_2(Mg_{2.2}Fe_{1.8}Al_{0.8}Mn_{0.2})Si_{6.9}O_{22}(OH)_2$
JMHF8C-40	actinolite	7.0	2.8	6.5	9.5	0.8	28.4	$Ca_2(Mg_{2.4}Fe_{1.7}Al_{0.7}Mn_{0.2})Si_{7.3}O_{22}(OH)_2$
GF-1A6	actinolite	6.7	1.0	6.3	10.3	0.9	29.8	$Ca_2(Mg_{2.7}Fe_{1.7}Al_{0.3}Mn_{0.3})Si_8O_{22}(OH)_2$
GS-2A4	actinolite	7.4	1.6	6.9	10.0	0.9	29.5	$Ca_2(Mg_{2.6}Fe_{1.8}Al_{0.4}Mn_{0.2})Si_{7.6}O_{22}(OH)_2$
GS-2A6	actinolite	7.3	2.4	7.8	8.8	1.0	29.0	$Ca_2(Mg_{2.2}Fe_{1.9}Al_{0.6}Mn_{0.3})Si_{7.2}O_{22}(OH)_2$
GS-2A10	actinolite	7.3	0.0	6.6	10.3	1.0	30.2	$Ca_2(Mg_{2.9}Fe_{1.8}Mn_{0.3})Si_{8.4}O_{22}(OH)_2$
GS-2A27	actinolite	7.4	1.5	6.1	10.3	1.0	30.4	$Ca_2(Mg_{2.7}Fe_{1.6}Al_{0.4}Mn_{0.3})Si_8O_{22}(OH)_2$
GS-2A32	actinolite	5.1	1.1	4.3	6.8	0.7	20.4	$Ca_2(Mg_{2.6}Fe_{1.7}Al_{0.4}Mn_{0.3})Si_{7.9}O_{22}(OH)_2$
S1-JMF-1C4	actinolite	6.9	1.6	6.5	9.9	1.0	29.8	$Ca_2(Mg_{2.6}Fe_{1.7}Al_{0.4}Mn_{0.3})Si_{7.9}O_{22}(OH)_2$
S1-JMF-1C5	actinolite	6.8	2.0	6.0	10.4	0.9	29.1	$Ca_2(Mg_{2.7}Fe_{1.6}Al_{0.5}Mn_{0.2})Si_{7.6}O_{22}(OH)_2$

Scheelite

Most of the scheelite at Calvert fluoresces typical bluish-white, but locally fluoresces yellow under longwave UV light (Figure 22). This yellowish fluorescence is typical for higher molybdenum concentrations, and represents a possible powellite presence. However, SEM-EDX analyses of this sample showed no variation in molybdenum content (Figure 23, right); therefore, the cause of the different color of fluorescence is not known.

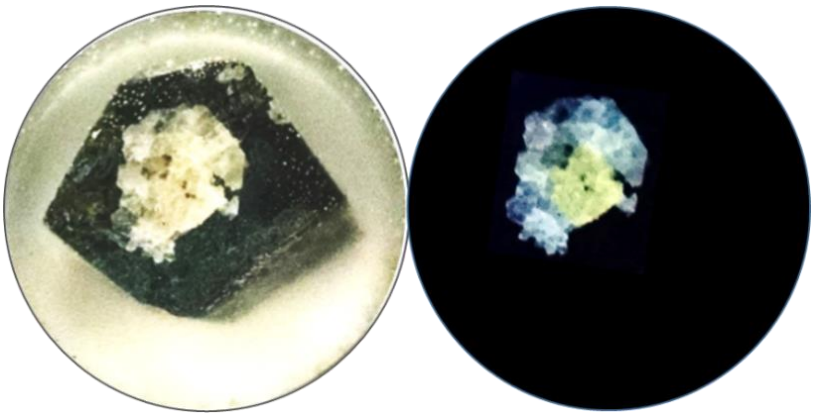

Figure 22. Zoned scheelite in an actinolite-calcite matrix under UV light. Sample CAL-IS. Each border is approximately the plug border and the field of view of each plug is 1 inch.

Portable XRF data show a strong correlation between W and Mo (Figure 23, left; data in Appendix A), with a correlation coefficient of 0.83. No deviations from this correlation are predicted since molybdenite or other molybdenum-bearing minerals were not observed. This positive correlation of molybdenum and tungsten suggests that molybdenum accompanied tungsten in scheelite, and that scheelite is the source of molybdenum at Calvert.

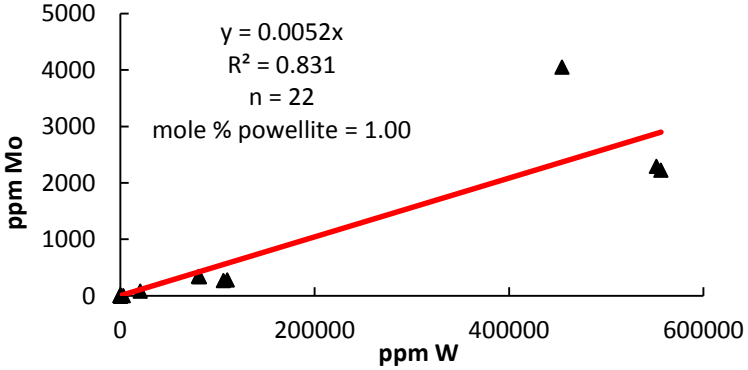

SEM-EDX		
Sample	Powellite mole %	Scheelite mole %
JMHF8C-12	1.77	98.23
JMHF8C-17	2.05	97.95
S1-JMF-1C3	1.67	98.33
CAL-IS	0.00	100.00
CAL-IS	0.00	100.00
CAL-IS	0.00	100.00
Avg.	**0.92**	**99.09**

Figure 23. The relationship between W and Mo from the Calvert skarn deposit. XRF data (Appendix A) suggest a mole % powellite of 1.00 (left). SEM-EDX measured a mole % powellite of 0.92 (right).

The portable XRF data suggests a mole % powellite of 1.00, whereas the SEM-EDX measured an average mole % powellite of 0.92 (Figure 23). These results show very good agreement between the two methods.

Calcite and Apatite

SEM-EDX analyses of calcites show narrow compositional variations and minimal impurities. Early skarn calcite is typically pure, with no magnesium or manganese content. Late skarn calcite contains iron and manganese impurities averaging 1.5 wt.% Fe and 2.4 wt.% Mn. Analyses of several apatite grains show that the skarn apatite composition averages 1.9 wt.% fluorine and 22.6 wt.% phosphorous. Magnesium and manganese are absent in the apatite.

4.3. Fluid Inclusions

Fluid inclusions were analyzed from garnet, scheelite and quartz. The inclusions chosen for study were larger and generally isolated or occurred as part of random, three dimensional distributions not associated with obvious fractures and are taken as primary based on the criteria of Roedder (Table 2-1, 1984). Primary inclusions ranged from 6.5 to 50 μm in diameter and at 25°C consisted of two phase liquid + vapor (L+V) with the vapor phase occupying 7 to 12% volume (Figure 24). In all cases, no solid phases or other fluid phases (e.g., CO_2 or CH_4) were observed. In addition, no evidence of boiling was noted.

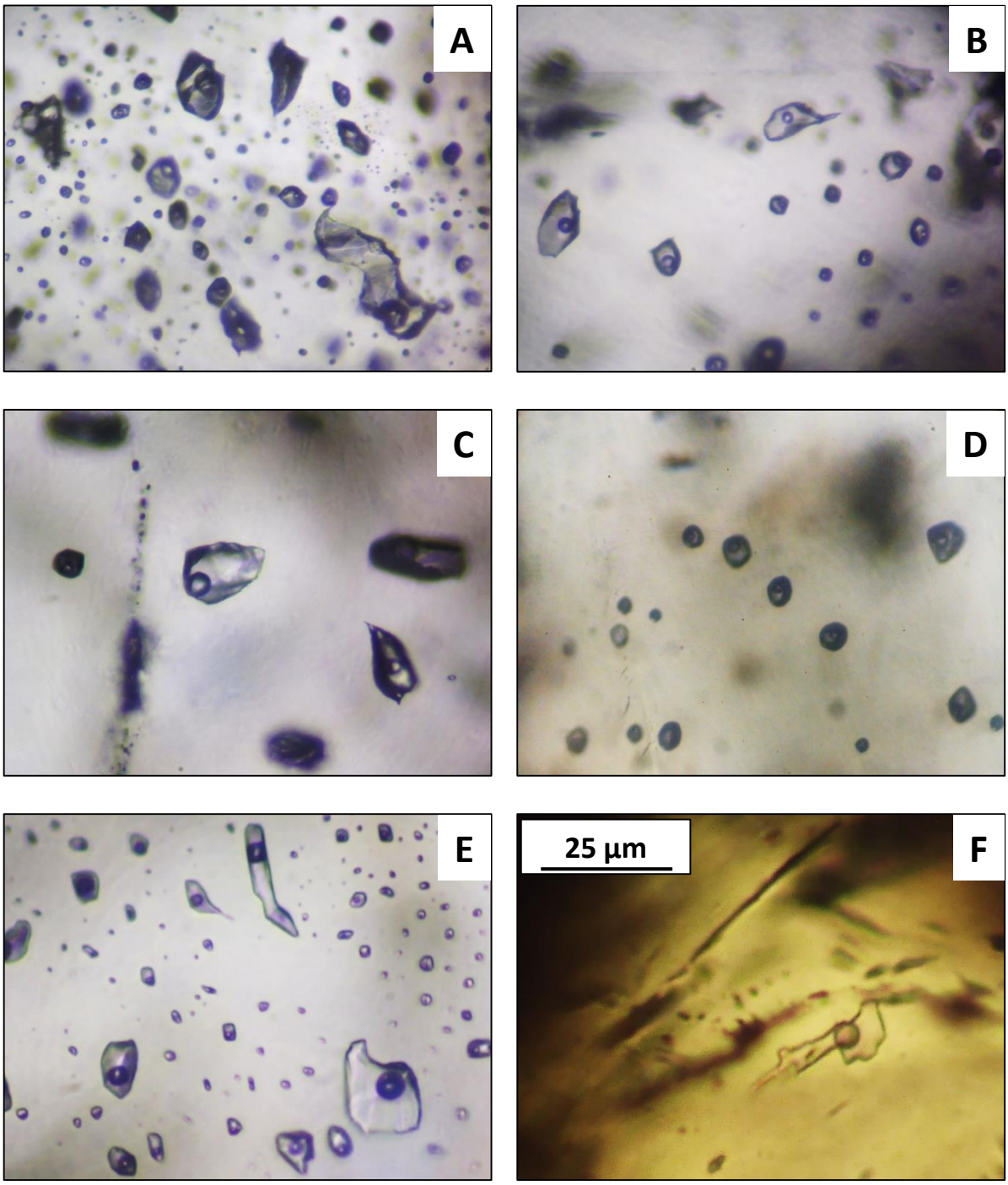

Figure 24. Two phase fluid inclusions in scheelite (A-C), quartz (D-E), and garnet (F). Microphotographs are taken in PPL at 320x magnification. Scale is the same for all photographs.

Minor cooling was required to freeze the fluids despite the relatively small size of most of the inclusions. All fluids froze within the range of -48° to -23°C with an average of -39.5°C. This range in temperature for which the fluids froze implies an absence of $CO_{2(l)}$ content, and no three-phase fluid inclusions or CO_2-clathrates were observed. Eutectic melting temperatures upon reheating were generally not observed, with noticeable melting not occurring below -10°C. Final ice melting temperatures (T_m) ranged from -3.0° to -1.4°C for garnet, -4.9° to -4.2°C for quartz, and -8.1° to -1.2°C for scheelite (Figure 25). All the inclusions exhibited noncritical homogenization to the liquid phase upon heating. Homogenization temperatures (T_h) ranged from 248.8° to 267.8°C for garnet, 209.0° to 264.0°C for quartz, and 200.5° to 288.6°C for scheelite (Figure 25).

These data show a dominant population of fluid inclusions with a homogenization temperature range of 250°-260°C and evidence for a period of cooling-off (Figure 26). All fluid inclusions encountered in this study appear to represent simple H_2O-salt mixtures because no CO_2 clathrates were observed during freezing runs. In order to nucleate a CO_2 clathrate on warming from below zero, an inclusion needs to have > 1.5 mole % of CO_2 (Diamond, 1992).

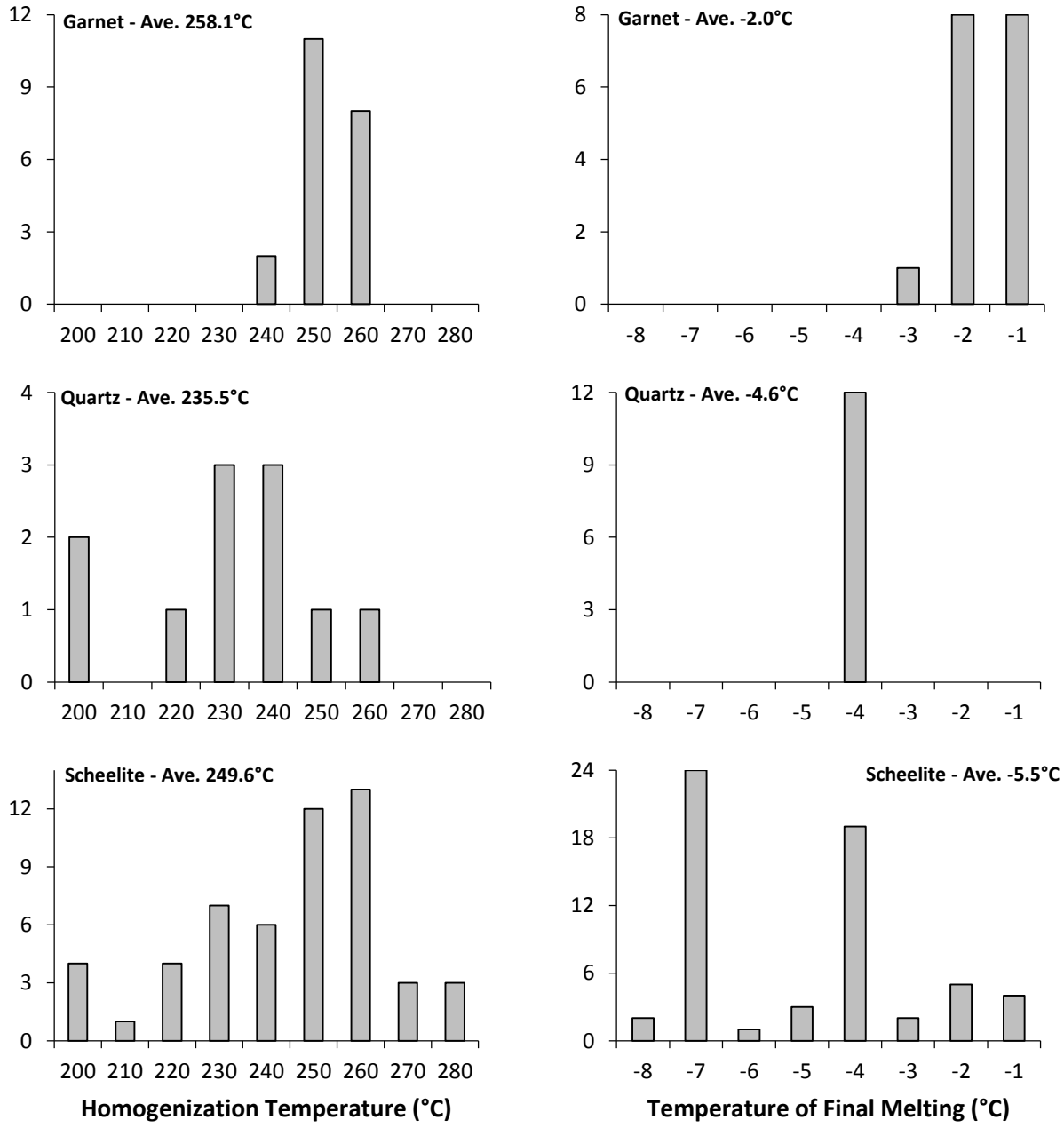

Figure 25. Homogenization temperatures and temperatures of final melting for fluid inclusions in this study.

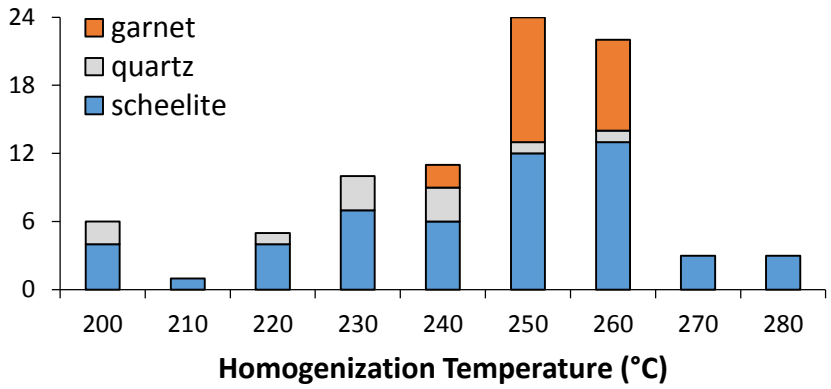

Figure 26. Histogram of homogenization temperatures for all fluid inclusions in this report.

4.3.1. Salinities

Salinities were determined using the freezing point depression after Potter et al. (1978),

$$w_s = 0 + 1.76958\theta - 4.2384 \times 10^{-2}\theta^2 + 5.2778 \times 10^{-4}\theta^3 \pm 0.028 \quad (1)$$

in which w_s is the wt.% NaCl equivalent (eq.) in the solution and θ is the freezing point depression, or 0 minus the T_m. Figure 27 is a plot of salinity vs. homogenization temperatures for all data where both measurements were obtained. These data show clusters, possibly an artifact of sampling bias, centered at salinities of 3.2 wt.%, 7.3 wt.%, and 11.2 wt.% NaCl eq. Scheelite is associated with all three salinities and is the only mineral with inclusions >10 wt.% NaCl eq. (from a ~2 cm prograde scheelite crystal). Salinities in quartz and garnet inclusions average 7.2 wt.% and 3.4 wt.% NaCl eq., respectfully. It is assumed that salinity increased throughout skarn formation because garnet is the dominant prograde mineral, having mineralized very early with inclusions of scheelite, and the scheelite data with salinity >10 wt.% comes from a large (~2 cm) prograde scheelite crystal (JMSFB, data in Appendix A). The clusters in salinities may represent different degrees of mixing between a saline magmatic fluid and less

saline groundwater, and the increase in salinity could have occurred as a result of the formation of abundant epidote in the prograde assemblage.

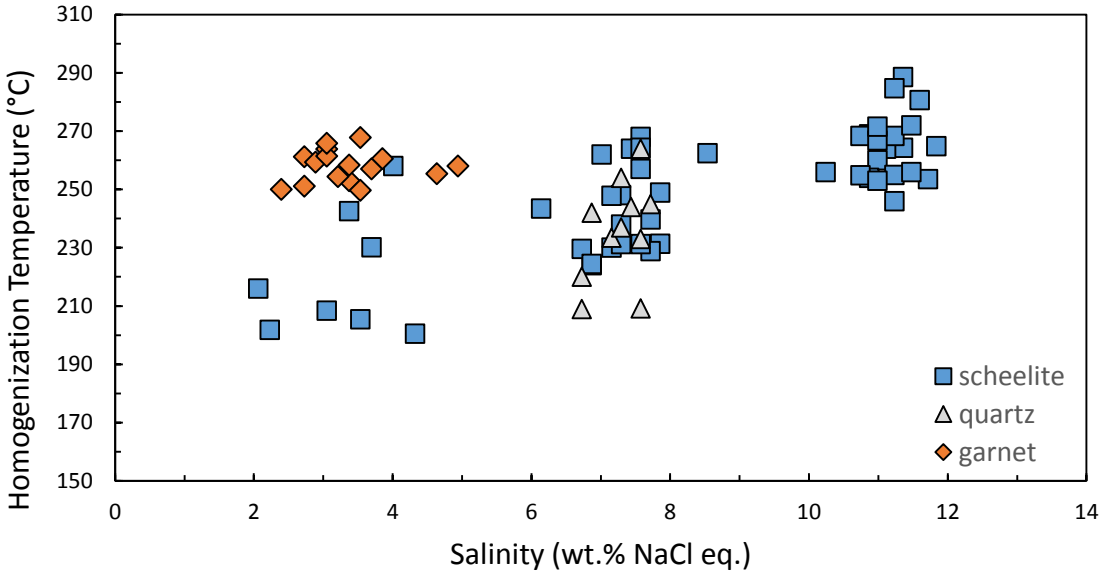

Figure 27. Plot of salinity versus homogenization temperatures.

4.3.2. Temperature and Pressure

Table VI shows the results of the salt leachates from inclusions in selected scheelite samples. The dominant cation in the scheelite fluid inclusions is calcium, although some calcium could have come from the host scheelite. Detection limits are: 0.21 mg/L for Na; 0.06 mg/L for K; 0.01 mg/L for Ca; 0.01 mg/L for Mg.

Table VI. Leachate results from fluid inclusions in scheelite samples. All concentrations reported in mg/L.

Field ID	Al	B	Ca	K	Li	Mg	Mn	Mo	Na	Se	Sr
7304-1	0.08	--	7.51	0.41	--	0.14	--	0.15	0.90	0.05	--
JH-FM	--	--	4.99	0.50	--	0.27	--	0.11	0.52	--	0.01
B2F-JM	--	--	7.18	0.23	--	0.13	--	0.39	0.45	0.06	--
CAL-IS	1.18	--	9.00	0.25	--	0.09	--	0.10	0.56	--	0.01
JMSF	--	0.05	6.61	0.94	0.01	0.13	--	0.16	1.91	--	0.01

Previous work by Truesdell (1976) and Fournier (1981) have shown that, above about 180°C, sodium and potassium mass ratios (Na/K) of geothermal waters can be used as a geothermometer. Temperatures of entrapment were estimated using Na/K geothermometry after Fournier (Equation 2) and Truesdell (Equation 3),

$$T = 1217 / (\log (Na/K) + 1.483) - 273.15 \quad (2)$$

$$T = 855.6 / (\log (Na/K) + 0.8573) - 273.15 \quad (3)$$

in which *T* is the temperature of entrapment in degrees Celsius and *Na/K* is the cation mass ratio reported from analysis of the inclusion leachates. Table VII shows the results of the calculated ratio (Na/K) and temperatures of entrapment for the five selected scheelite leachate samples. As seen in Table VII, the estimated temperatures of entrapment for sample JH-FM are anomalously high (538° and 704°C). This scheelite sample comes from a highly altered epidote-actinolite skarn, and the fluid inclusion leachate could represent a mixture of multiple generations of fluids. Therefore, data from the JH-FM sample was not used in the calculation of the average entrapment temperatures.

Table VII. Measured Na/K ratios and calculated entrapment temperatures for selected scheelite leachate samples.

Field ID	Na/K	Fournier T (ºC)	Truesdell T (ºC)
7304-1	2.23	392	437
JH-FM	1.04	538	704
B2F-JM	1.97	411	469
CAL-IS	2.24	390	435
JMSF	2.03	407	462

These calculations estimate entrapment temperatures between 400°C (Fournier) and 450°C (Truesdell). It should be noted that this geothermometer assumes equilibrium between the fluid and two feldspars (plagioclase and alkali-feldspar). This assumption would be valid for high temperature fluid equilibrated with granite, but not necessarily with a tonalite.

Since it has been demonstrated that the fluids were not boiling at the time of entrapment, a pressure correction must be added to the homogenization temperature to obtain the true entrapment temperature of the inclusions. Using data from Potter (1977), a pressure correction was determined using a homogenization temperature of 250°C and an estimated temperature of entrapment range of 400°-450°C from the leachate analyses (Figure 28). Roedder (1984) demonstrated that solutions in the system Na-K-Ca-Mg-Cl-Br-SO_4-H_2O are predicted accurately (± 1.0% error) by the NaCl-H_2O pressure correction curves.

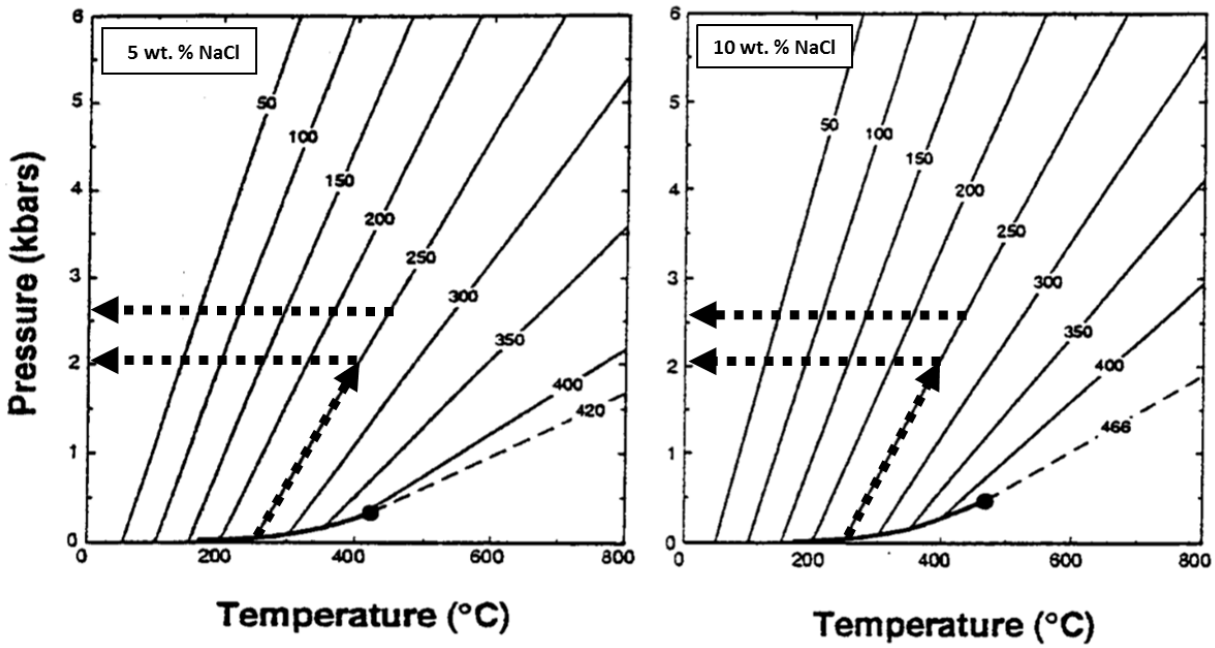

Figure 28. Pressure correction diagrams for the H_2O-NaCl system at 5 wt.% (left) and 10 wt.% NaCl (right). Both diagrams use homogenization temperatures from fluid inclusion analyses (average of 250°C) and geothermometry from inclusion leachates (400°-450°C) to predict a pressure of 2-2.5 kbar.

Since salinities ranged from 3.2 wt.% to 11.2 wt.% NaCl eq., pressure determinations were made using T-P diagrams of the H_2O-NaCl system at 5 wt.% and 10 wt.% NaCl equivalent. Both diagrams predict a corresponding pressure of formation between 2 and 2.5 kbars. If it is assumed that fluid pressures were lithostatic, then this corresponds to a depth of 7 to 8.75 km, assuming a geobaric gradient of 3.5 km/kbar. According to Roedder (1984), these data also correspond to a fluid density of 0.8 g/cm^3. If hydrostatic pressure is assumed, the estimated

depth of skarn formation would be > 25 km. This value is not realistic; therefore, lithostatic pressure is assumed.

4.4. Stable Isotopes of Calcite

The results of the stable isotope analyses of calcites, along with a brief description of where the calcite samples came from, are shown in Table VIII. Average $\delta^{18}O$ (VSMOW) and $\delta^{13}C$ (VPDB) values of the unaltered marble are 25.2‰ and 0.6‰, respectfully. Average $\delta^{18}O$ and $\delta^{13}C$ values of the bleached marble are 18.0‰ and -0.6‰, respectfully. Average $\delta^{18}O$ and $\delta^{13}C$ values of the skarn calcite are 11.2‰ and -7.0‰, respectfully.

Table VIII. Stable isotope results of selected calcite samples.

Sample	$\delta^{13}C$ VPDB, ‰	$\delta^{18}O$ VPDB, ‰	$\delta^{18}O$ VSMOW, ‰	Comments
DMIP	0.2	-6.0	24.7	unaltered marble
S3FFC	0.9	-5.0	25.8	unaltered marble
Average	**0.6**	**-5.5**	**25.2**	
JMFH6A	0.6	-11.5	19.0	bleached marble
SSA-JMF4-1	-1.9	-10.9	19.6	bleached marble
S8M-JMF-1A	-1.1	-13.9	16.6	bleached marble
S3MOS	-0.4	-13.4	17.1	bleached marble
MIPIS	-0.5	-15.1	15.3	bleached marble
S3C2C	-0.4	-11.9	18.6	bleached marble
MIPISC	-0.4	-10.9	19.7	bleached marble
Average	**-0.6**	**-12.5**	**18.0**	
JMSF	-6.0	-19.9	10.4	skarn
JMFIS	-7.7	-17.2	13.2	skarn
B2F-JM-1D	-7.4	-18.4	11.9	skarn
SS-JM-3F	-5.3	-17.0	13.4	skarn
S2-JMA3-1	-6.8	-22.4	7.8	skarn
MF-JM-1A	-6.3	-16.8	13.6	skarn
JMHF2D	-9.0	-17.9	12.5	skarn
JMISS	-7.9	-16.4	14.0	skarn
GSF-1S	-7.4	-17.8	12.6	skarn
JH-FM-1C	-9.4	-19.4	10.9	skarn
S12-JMF-1E	-5.9	-22.5	7.7	skarn
JMHF6A-vein	-5.0	-18.5	11.9	fracture filling
CAL-IS	-7.7	-20.3	10.0	skarn
JMIC	-7.5	-20.2	10.0	skarn
4XIS	-6.6	-20.2	10.1	skarn
IJMI	-6.8	-18.4	11.9	skarn
CISJM	-7.3	-19.6	10.7	skarn
4JMI	-5.5	-20.9	9.3	skarn
ICJMIS	-7.5	-20.0	10.3	skarn
Average	**-7.0**	**-19.1**	**11.2**	

Figure 29 shows the results of the stable isotope analysis. The top image is a $\delta^{13}C$-$\delta^{18}O$ diagram in which both skarn and marble carbonate samples are plotted. This plot shows a large depletion of both ^{18}O and ^{13}C in the skarn calcite relative to the calcite in the marble protolith which had average $\delta^{18}O$ and $\delta^{13}C$ values of 25.2‰ (VSMOW) and 0.6‰ (VPDB), respectfully. These data also show that the marble underwent minimal ^{18}O or ^{13}C depletion except within close proximity to the skarn (largest zone of bleached marble observed at Calvert was ~ 3ft). The histograms in Figure 29 show that these bleached zones are slightly depleted in $\delta^{18}O$ (7.2‰) and $\delta^{13}C$ (1.2‰) with respect to the country rock. Samples collected from completely metasomatized country rock exhibit large depletions in $\delta^{18}O$ (14.0‰) and $\delta^{13}C$ (7.6‰) with respect to the country rock, and can provide insight into the role of wall-rock interaction with magmatic fluids.

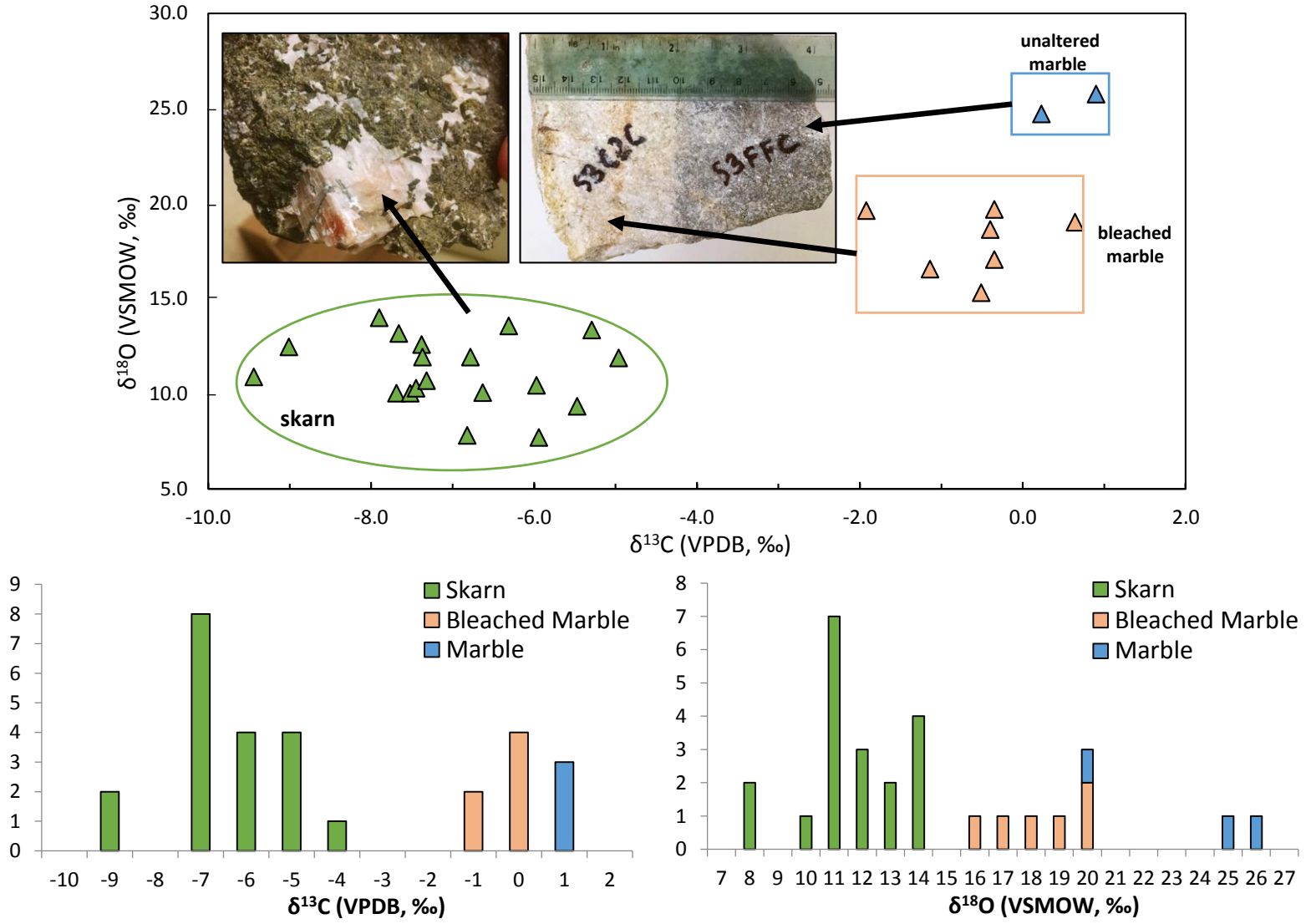

Figure 29. Results of isotopic analysis on calcite samples and representative photographs of sample locations (top). Frequency distributions of $\delta^{13}C$ (bottom left) and $\delta^{18}O$ carbonate values (bottom right).

5. Discussion

In this chapter, field relationships, petrographic observations, and stable isotope and fluid inclusion results are used to estimate the physical and chemical conditions during skarn formation. These estimates are followed by a discussion on tungsten solubility, the possible source(s) of the hydrothermal fluids, and the controlling factors of mineralization at the Calvert mine. Finally, the Calvert deposit is compared to previous studies of tungsten skarns in Montana and elsewhere.

5.1. Mineral Assemblage

The prograde mineral assemblage of the Calvert skarn consists of garnet, epidote, calcite and quartz which can be used to constrain the temperature of the prograde skarn fluids. The formation of epidote minerals can occur during early high-temperature as well as later lower-temperature stages of skarn formation (Klemd, 2004). Einaudi et al. (1981) showed that epidote minerals can form at temperatures greater than 400°C but only at low mole fraction CO_2 values ($X_{CO2} < 0.05$). Klemd discussed mixed volatile reactions involving epidote minerals and evaluated mineral stabilities with T-X_{CO2} graphs in the CASCH and CF*SCH systems. He showed that in addition to pressure and temperature, epidote mineral stability also depends on the Al/Fe^{3+} ratio. According to Klemd's diagrams, Fe-poor epidote (clinozoisite) and quartz assemblages are stable only at $X_{CO2} \leq 0.1$ and temperatures between 280°-480°C. Klemd discussed how in highly oxidizing conditions, as is the case in many skarns, epidote shows an enlarged stability range with respect to X_{CO2} due to the presence of ferric iron. The epidote at Calvert has a 2:1 ratio of Al/Fe^{3+}, and while the stability field of epidote would be expanded relative to clinozoisite, the higher concentration of Al would constrain X_{CO2} to lower values.

Similar results were obtained by Will et al. (1990), who evaluated mineral stabilities with T-X_{CO2} graphs in the CFMASCH system with quartz and fluid in excess at 2 kbar and temperatures between 380° and 510°C. In this diagram the stability field of Fe-poor clinozoisite-bearing assemblages are restricted to $X_{CO2} < 0.15$.

5.2. Fluid Chemistry

Mole Fraction CO_2: No CO_2 vapor, liquid or clathrate crystals (upon cooling) were observed in any of the fluid inclusions, which suggests a mole fraction $CO_2 < 1.5\%$ (Diamond, 1992). This information, along with the prograde mineral assemblage, can be used to further constrain the physical and chemical conditions prevalent during prograde skarn formation. Figure 30 is a T-X_{CO2} diagram from Klemd (2004) showing the stability of epidote as a function of temperature and X_{CO2} in the vapor phase. According to this phase diagram, the prograde skarn mineral assemblage consisting of garnet, epidote, quartz and calcite is stable at low X_{CO2} (< 1.5%) and within the estimated entrapment temperatures from leachate experiments (400° to 450°C), and is therefore consistent with the observations made in this study.

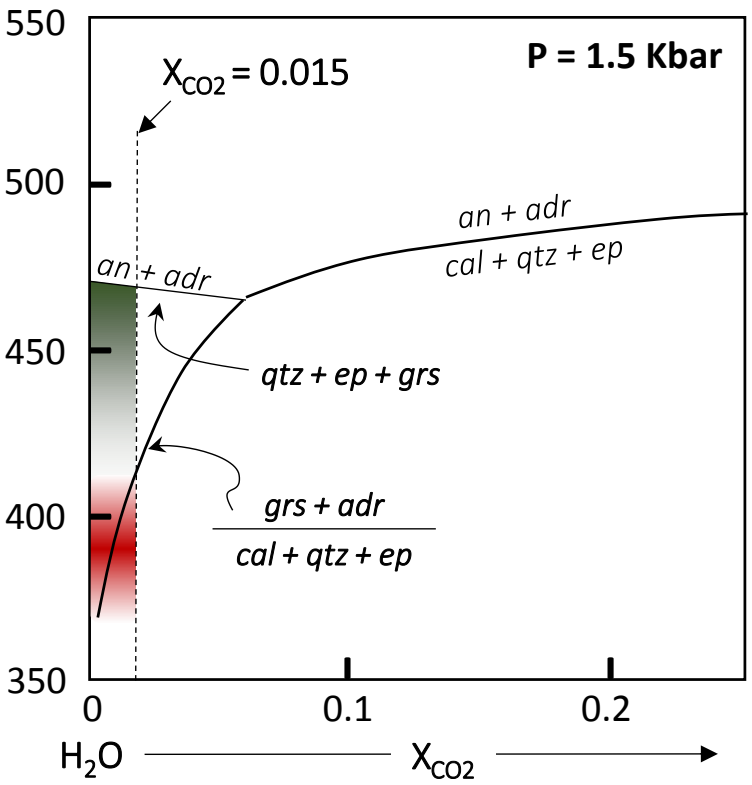

Figure 30. T-X_{CO2} projection calculated at 1500 bars in the CF*SCH system for 0 < X_{CO2} < 0.45. Red shaded region shows equilibrium for garnet, quartz and epidote in the presence of calcite at X_{CO2} < 1.5%. Green shaded region shows the upper stability of epidote in the presence of garnet and quartz (no calcite). Abbreviations are grossular (grs), andradite (adr), epidote (ep), anorthite (an), quartz (qtz), and calcite (cal). Modified from Klemd, 2004.

Figure 30 also shows that the observed reaction rim of epidote, quartz and calcite that separates early garnet core growth from later garnet rim growth (Figure 20) can result from small fluctuations in mole fraction CO_2, possibly due to irregular degrees of fluid mixing, as controlled by the following reaction:

$$\underset{\text{(epidote)}}{2Ca_2(Al,Fe)_3Si_3O_{12}(OH)} + \underset{\text{(calcite)}}{5CaCO_3} + \underset{\text{(quartz)}}{3SiO_2} = \underset{\text{(grossular)}}{2Ca_3Al_2Si_3O_{12}} + \underset{\text{(andradite)}}{Ca_3Fe_2Si_3O_{12}} + 5CO_2 + H_2O \qquad \text{5-1}$$

Fugacity of Oxygen: The stability of certain skarn minerals can help to constrain conditions of skarn formation as a function of temperature and oxygen fugacity. The fugacity of oxygen during skarn formation is the result of the oxidation conditions imposed on the hydrothermal fluid by the intrusion and the chemical effects of the host rock. Newberry and Swanson (1986) have shown that tungsten skarn-associated intrusions typically have a high oxygen fugacity, but interaction of magmatic fluids with reduced wallrock may nonetheless produce a reduced skarn.

Figure 31 shows that, at the temperatures determined by leachate experiments and based on the presence of hematite and magnetite in the skarn, the oxygen fugacity for the prograde and retrograde skarn was about 10^{-21} and 10^{-23} bars, respectfully. The occurrence of magnetite and hematite, with little to no sulfides, tends to support the conclusion of oxidizing conditions during skarn formation. Moreover, the widespread occurrence of Fe(III)-bearing epidote in the prograde mineral assemblage further confirms the oxidizing conditions of the Calvert skarn. The occurrence of molybdenum within scheelite rather than molybdenite is further evidence of an oxidized environment (Newberry, 1998). In some locations, iron and manganese were incorporated into the skarn calcite. This suggests that local reducing conditions were present in the Calvert skarn since iron in its oxidized state (Fe^{+3}) would not be available for incorporation into the calcite matrix.

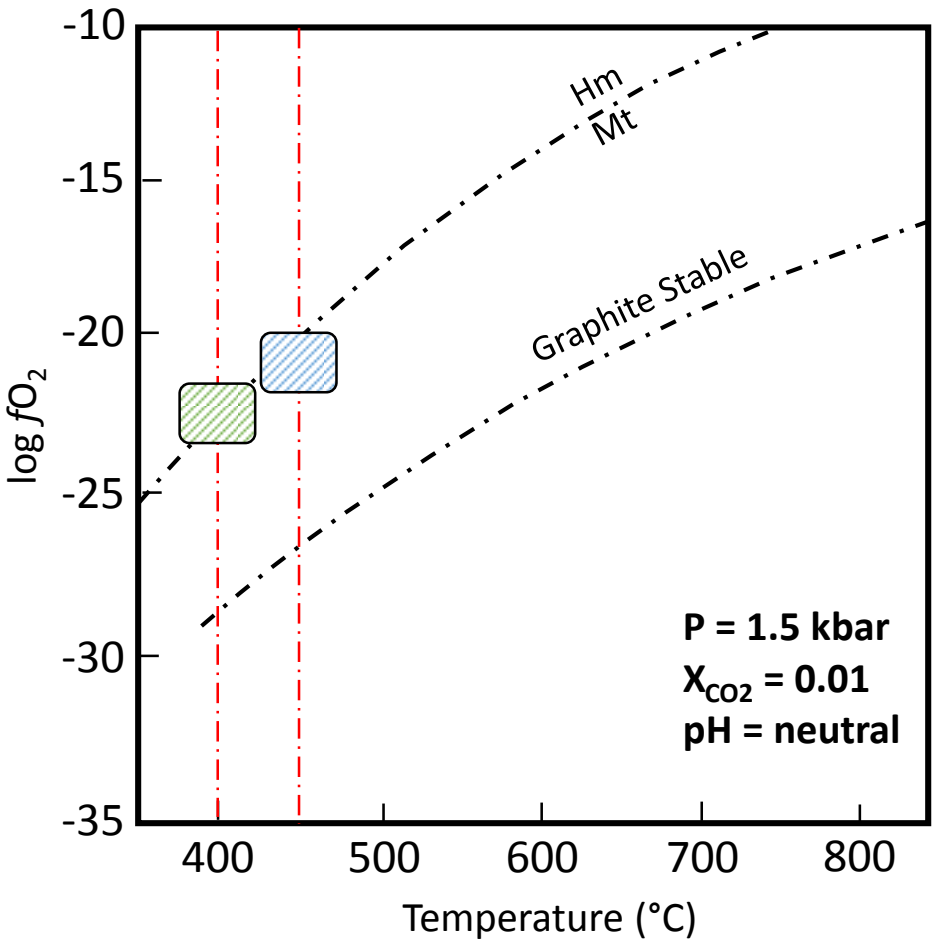

Figure 31. T-log fO_2 plot showing the conditions of prograde skarn formation (blue hachured area) and for retrograde alteration (green hachured area). Temperatures are constrained from leachate analyses (red lines). Field lines are plotted for 1.5 kbar. Modified from Deboer, 1991.

pH and Calcium Activity: Chemical determinations of minerals from the Calvert skarn deposit show that a large proportion of the skarn minerals at Calvert are calcium-rich (diopside, grossular, Ca-amphibole, epidote, calcite, apatite, scheelite). This observation suggests high calcium activity during skarn formation, most likely due to the dissolution of the calcic marble protolith. Carbonate dissolution would also neutralize acidic hydrothermal fluids, raising pH. A high concentration of calcium is also indicated by the fluid inclusion leachate results.

5.3. Stable Isotope Interpretation

Taylor and O'Neil (1977) demonstrated that the large difference in carbon and oxygen isotope compositions between igneous rocks and marble allows tracking of the progressive interaction between skarn fluid and carbonate wallrock as well as estimating mole fraction CO_2 values in oxidized skarn fluids. Mass ratios of oxygen and carbon in skarn-forming fluid (F) to that in host marble (R) resulting from the reaction of marble to skarn were computed using the equation (shown here for oxygen) after Taylor (1971 and 1974):

$$\text{F/R} = \frac{\delta^{18}O_{rock(f)} - \delta^{18}O_{rock(i)}}{\delta^{18}O_{H_2O(i)} - (\delta^{18}O_{rock(f)} - \Delta_{rock-H_2O})} \quad (4)$$

where subscript *f* and *i* represent final and initial isotopic values, respectfully. Isotopic fractionation data from Zheng (1999) and Ohmoto and Rye (1979) were used in the calculations. Values of $\delta^{18}O_{H2O\,(i)}$ and $\delta^{13}C_{CO2\,(i)}$ were taken from Bowman et al. (1985a) as 7.5‰ (VSMOW) and -5.5‰ (VPDB), and are typical values of magmatic fluids. The values of $\delta^{18}O_{rock\,(i)}$ and $\delta^{13}C_{rock\,(i)}$ were assumed to be 30.6‰ (VSMOW) and 0.0‰ (VPDB), which is typical of Paleozoic marine limestone. Since it has been shown that the mole fraction CO_2 was ≤ 1.5%, a value of $X_{CO2} = 0.01$ was used. Equilibrium exchange was assumed, and all computed F/R ratios should be regarded as minima because of the possibilities of incomplete exchange.

The same calculations can be used for oxygen as well as carbon. The only difference comes with regard to the amount of oxygen versus carbon in the fluid and in the wallrock. At $X_{(CO2)} = 0.01$ the fluid contains 101 times more oxygen than carbon on an atomic basis, and the limestone wallrock contains 3 times more oxygen than carbon. Therefore, for each mole of carbon that is exchanged between the fluid and rock, there are 101/3 moles of oxygen exchanged for the equivalent amount of fluid.

The solid curve in Figure 32 represents the $\delta^{13}C$-$\delta^{18}O$ trend computed from equation (4) that would result from progressive interaction between igneous fluids ($\delta^{13}C_i$ = -5.5‰, $\delta^{18}O_i$ = 7.5‰, $X_{(CO2)}$ = 0.01) and the wallrock carbonate ($\delta^{13}C_i$ = 0.0‰, $\delta^{18}O_i$ = 30.6‰). The square (□) represents the $\delta^{13}C$ and $\delta^{18}O$ values of the igneous fluid endmember at 400°C and the diamond (◊) represents the initial $\delta^{13}C$ and $\delta^{18}O$ values of marine limestone. The curve is marked with atomic oxygen ratios of magmatic fluid (F) to marble rock (R). The interaction between the magmatic fluid and carbonate rock causes the $\delta^{18}O$ isotopic composition of the carbonate rock to change first, with $\delta^{13}C$ changing only after F/R ratio > 4. Eventually the system will reach equilibrium between the carbonate rock and the magmatic fluid with a value that is offset by an isotopic fractionation that is temperature dependent.

The lowest $\delta^{18}O$ values of the skarn calcites can only be explained by very high F/R ratios (> 40). The higher $\delta^{18}O$ values of the bleached marble can be explained by much lower F/R ratios, between 1 and 4. Based on this evidence it appears the system was H_2O-dominated throughout all stages of development and a single fluid with a mole fraction CO_2 of about 0.01 was responsible for the resulting isotopic depletions of the skarn calcite from that of the protolith marble.

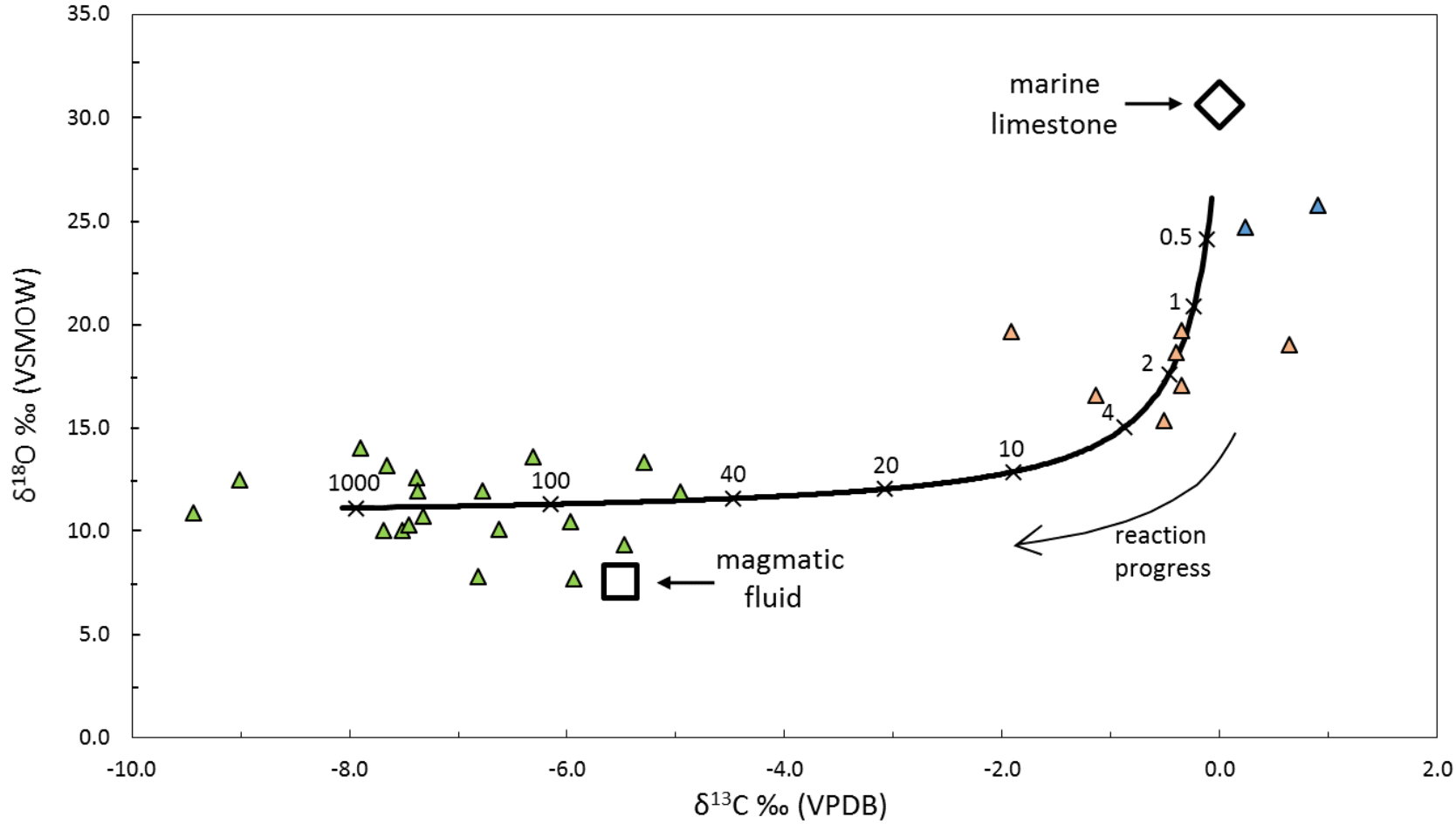

Figure 32. Plot of $\delta^{13}C$ vs. $\delta^{18}O$ values for carbonates at the Calvert mine. Symbols are: data points (Δ); marine limestone (◊); magmatic fluid (□). Solid line represents the ^{13}C and ^{18}O depletions in calcite resulting from the interaction (at 400°C) of average marble and magmatic fluid ($\delta^{13}C$ = -5.5‰, $\delta^{18}O$ = 7.5‰, X_{CO2} = 0.01). Solid line is marked off in atomic ratios of magmatic fluid (F) to marble rock (R). Equilibrium carbon and oxygen isotope fractionations of Zheng (1999) and Ohmoto & Rye (1979) were assumed in these calculations

5.4. Tungsten Solubility, Fluid Source and Ore Deposition

Research on the hydrothermal solubility and speciation of tungsten has been discussed in many literary works. Experiments conducted by Foster (1977) on scheelite solubility in KCl solutions (1.0 and 0.5 m) at 1 kbar from 250° to 550°C showed that scheelite solubility increased with both temperature and salinity, and concluded that tungstic acid was the dominant species in solution. Wesolowski (1984) determined that in near neutral pH, mildly to strongly saline conditions, at temperatures between 150°-300°C and a total W concentration of 10^{-4} to 10^{-5} m, the most important species are WO_4^{2-} and HWO_4^-, with H_2WO_4 only important at low pH.

Wood and Vlassopoulos (1989) conducted experiments on the solubility of WO_4^{2-} at 500°C and 1 kbar in various solutions of HCl, NaOH, NaCl and KCl, and found no dependence of W solubility on HCl concentration (up to 5.0 molal HCl). They instead found an increase in W solubility in NaOH (0.01-1.0 m), NaCl (1.0-6.0 m) and KCl (1.0 m) solutions, leading them to suggest that W-Cl complexes are not important in W transport, but W-Na ion pairs (e.g., $NaHWO_4$) may be. Wood and Samson (2000) calculated the solubilities of scheelite and ferberite in NaCl-HCl-H_2O solutions at temperatures from 200° to 600°C, pressures from 500 to 1000 bars, pH from 3 to 6, and m_{NaCl} from 0.1 to 5.0 moles/kg H_2O. They concluded that chloride, fluoride and carbonate complexing of tungsten are not important in natural hydrothermal solutions, and showed instead the importance of cation-tungstate oxyacids in W solubility (e.g., $NaWO_4^-$, H_2WO_4, HWO_4^-, $NaHWO_4$). These results show that the moderate Cl^- concentrations of the Calvert ore fluids estimated from fluid inclusion work are not needed for W transport. However, high Na^+ activities could have enhanced W solubility as $NaWO_4^-$ or $NaHWO_4$.

The source of the hydrothermal fluids is not definitely known, and no geochemical analyses of the igneous and marble rocks at Calvert were conducted for this report. Isotopic data from this study indicates that the source of the fluids is magmatic. Research done by Deboer (1991) shows that unaltered Amsden Formation in the Pioneer Mountains contains low concentrations of W and Mo. He coupled his results with the fact that W-Mo mineralization is found in a variety of carbonate units within the Paleozoic section where in contact with the Pioneer Batholith to suggest that the source of the W and Mo was the magma itself.

At Calvert, a possible source is the tonalite intrusion that is in contact with the skarn and contains an epidote-quartz endoskarn (Figure 33, A). If so, this would result in the formation of a proximal skarn mineral assemblage indicative of temperatures approaching that of a tonalite solidus (~ 650°C; Schmidt, 1993). Alternatively, the skarn-forming fluids may have come from the granite (Figure 33, B), which has a slightly lower solidus temperature (~ 620°C; Blatt et al., 2006). A third possible source that is presented here is a deep-seated porphyry-style deposit (Calvert is situated within the Great Falls Tectonic Zone). This would result in the formation of distal skarn mineralogy of lower temperatures and more oxidized conditions (Figure 33, C).

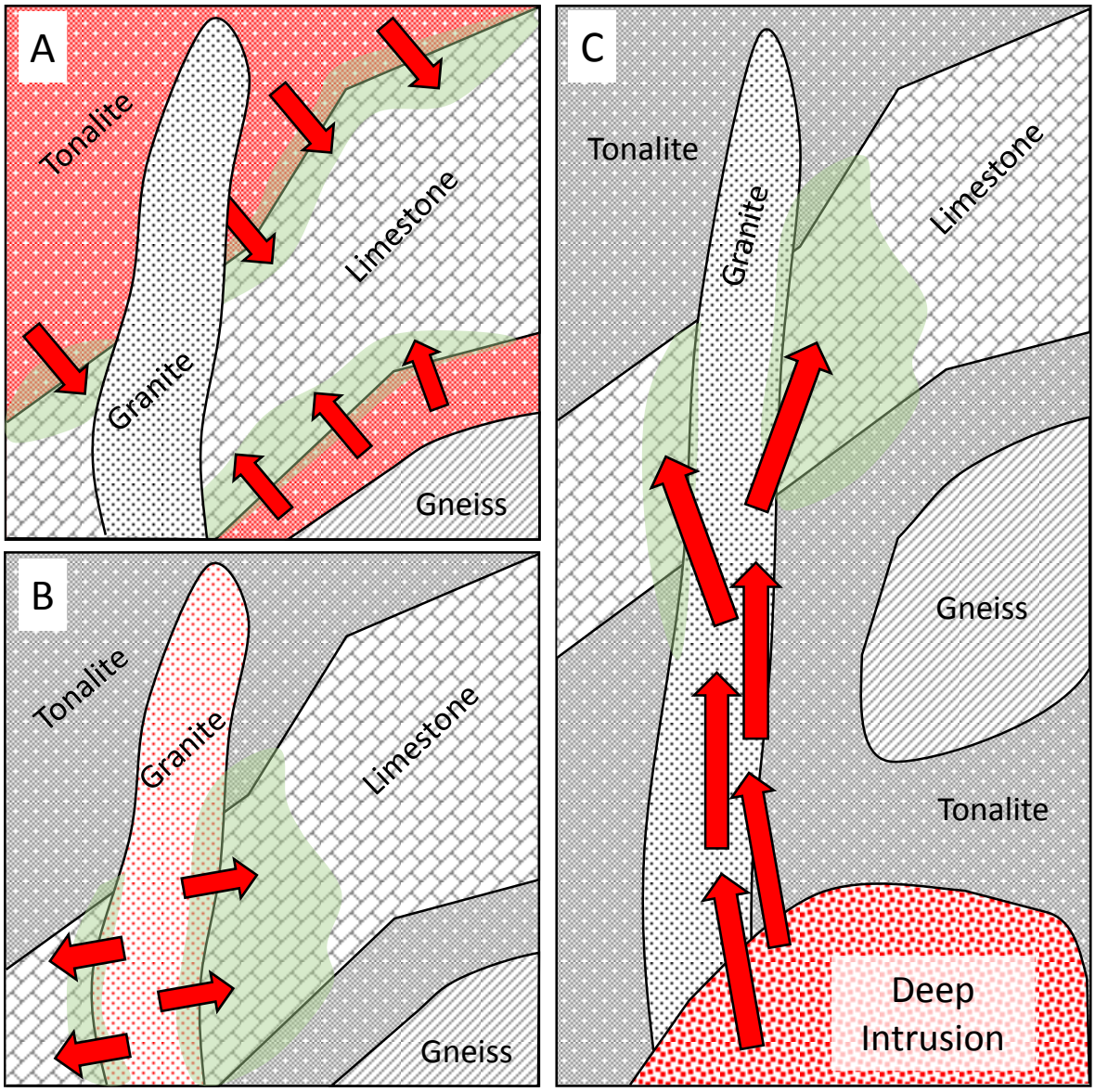

Figure 33. Diagrams showing possible sources of W-bearing fluid. These include the FMT (A), the BCG (B), and a deep-seated deposit (C).

Possible mechanisms of tungsten precipitation at Calvert are changes in temperature, pH, and the activity of calcium, along with dilution from fluid mixing. The results of the fluid inclusion leachate suggest an entrapment temperature of 400°-450°C which is most likely lower than the temperature of a magmatic fluid as it exsolved from the parent melt. This decrease in temperature can cause a decrease in the solubility of tungsten complexes in solution as discussed by Wood and Samson (2000).

Assuming the magmatic fluids were acidic, this acidity would cause the dissolution of the carbonate wallrock according to reaction 5-2:

$$CaCO_{3\,(wallrock)} + H^{+}_{\,(magmatic\ fluid)} \leftrightarrow Ca^{2+} + HCO_3^{-} \qquad 5\text{-}2$$

where the dissolution of the carbonate wallrock increases the activity of calcium in the system. If the tungsten was transported in solution as a tungstate, tungstic acid, or in cation-tungstate oxyacid, then high Ca^{2+} activity is a critical requirement for scheelite deposition, possibly according to the reactions:

$$NaWO_4^{-} + Ca^{2+} \leftrightarrow CaWO_{4\,(scheelite)} + Na^{+} \qquad 5\text{-}3$$

$$HWO_4^{-} + Ca^{2+} \leftrightarrow CaWO_{4\,(scheelite)} + H^{+} \qquad 5\text{-}4$$

Scheelite becomes increasingly insoluble as the acidic fluid is neutralized upon reaction with the carbonate wallrock and will precipitate in the presence of Ca^{2+} as proposed by Wesolowski (1984).

5.5. Comparison to Other Tungsten Skarns

The Calvert deposit shares many similarities and a few differences with other scheelite skarn deposits (e.g., LenTung in Montana, Kara in Tasmania, CanTung in Canada). Of the well-studied skarns, Calvert is most similar to the LenTung deposit in the East Pioneer Mountains of Montana. This deposit developed where the Amsden Formation was contacted by a granodiorite satellite pluton of the Pioneer Batholith. Both deposits contain very few sulfides. No sulfides were observed in the Calvert samples for this report, but minor pyrite, chalcopyrite, pyrrhotite, molybdenite and cuprotungstite have been reported elsewhere (Golba, 2012). Sulfides at LenTung occur locally throughout the skarn, but make up less than 1% of the rock (Deboer, 1991).

The LenTung deposit shows an increase in salinity from early stages of skarn formation (5.8 wt.%) to late stages of skarn formation (8.5 wt.% NaCl eq.). Deboer attributed this to simple cooling of the hydrothermal fluids and suggested that dilution with meteoric water was not an important process in scheelite precipitation. At Calvert, the increase in salinity from early skarn formation (3.2 wt.%) to late skarn formation (11.2 wt.%) is interpreted as being either the result of mixing between magmatic fluid and meteoric fluid, or the loss of water to hydrous skarn mineral formation (e.g., epidote, actinolite, micas).

Mineral assemblages and stable isotopic compositions of carbonates at Calvert closely resemble those of the Elkhorn skarn in Montana (Bowman et al., 1985a). At Elkhorn, zoned contact skarns have replaced late Precambrian to Paleozoic dolomitic marbles where it is contacted by the Black Butte quartz diorite. Both deposits contain prograde mineral assemblages including garnet, epidote, quartz and calcite together with sphene, apatite and magnetite as accessory minerals. Both deposits also show very similar depletions in ^{13}C and ^{18}O values in

skarn calcite relative to the host rocks. Moreover, isotopic depletions due to fluid/rock interaction suggest very similar mole fraction CO_2 values for Elkhorn ($X_{CO2} = 0.02$) and Calvert ($X_{CO2} = 0.01$).

The Kara deposit in Tasmania is extremely rich in magnetite, very poor in sulfides, lacks pyrrhotite and appears to be highly oxidized (Singoyi, 1995). This skarn deposit developed from a Devonian granitoid intrusion into Cambrian and Ordovician calcic marble. Other important similarities include prograde temperatures (450°-600°C), retrograde temperatures (< 400°C), confining pressures (1 kbar), low powellite content (≤ 6%), and oxidizing conditions. The garnet composition at Kara is andradite-rich, whereas the garnet at Calvert is grossular-rich, but the dominant pyroxene component at both deposits is diopside. Unlike at Calvert, where the major scheelite and magnetite mineralization occurred during the main prograde stage, major scheelite and magnetite mineralization at Kara accompanied hydrous minerals in the late stages of skarn formation (Singoyi, 1995).

The CanTung deposit is hosted in Cambrian calcitic marble, contains abundant sulfides, and is an example of a reduced skarn (Mathieson and Clark, 1984; Bowman et al., 1985b). Fluid inclusion studies by Mathieson and Clark interpreted a low-salinity aqueous brine fluid (< 10 wt.% NaCl) as the ore fluid, which is similar to the Calvert skarn ore fluid (3.2-11.2 wt.% NaCl eq.). The Calvert and CanTung deposits share similar temperature and pressure ranges of skarn formation, with Calvert ranging 400°-450°C and pressures of 2-2.5 kbar, the CanTung E-Zone skarn ranging 400°-520°C and pressures of 2-3 kbar (Marshal et al., 2003), and the CanTung Open Pit orebody ranging 400°-595°C and pressures of 2-4 kbar (Yuvan, 2006).

6. Conclusions and Recommendations

6.1. Conclusions

The Calvert scheelite-bearing skarn developed in the Pennsylvanian Amsden Formation during the emplacement and cooling of satellite plutons of the Pioneer Batholith. Thermal effects accompanying the intrusion of the Foolhen Mountain Tonalite produced contact metamorphism which recrystallized the limestone to marble. The Bryant Creek Granite intruded the tonalite either during or after it completely cooled.

A dilute, oxidizing and W-bearing fluid phase could have originated from the initial emplacement of the Foolhen Mountain Tonalite, as a result of the later intrusion of the Bryant Creek Granite, or possibly from a deep-seated porphyry-style deposit. Evidence in this study (e.g., temperature, amount of hydrous minerals, etc.) suggests that the Calvert skarn is a distal skarn and that additional fluids might have come from a secondary deep-seated magma. Whatever the source, these fluids migrated out along permeable stratigraphic horizons depositing the prograde assemblage dominated by garnet, diopside(?), epidote, calcite and quartz together with scheelite, zircon, magnetite, apatite, hematite and sphene as accessory minerals. The favorable stratigraphic horizon to host the W-bearing skarn appears to be clean carbonates within the Amsden Formation with enhanced permeability possibly due to fracturing accompanying batholith emplacement, and possibly intensified by hydro-fracturing (increase in pore-fluid pressure) as magmatic fluids (and/or volatilized CO_2) were exsolved.

The estimated conditions of the main-stage prograde metasomatic skarn formation at Calvert are as follows:

Pressure: 2 to 2.5 kbar (7 to 8.75 km depth)

Temperature: 400° to 450°C

Mole fraction CO_2: 0.01

log fO_2: 10^{-21} to 10^{-23} bars

Salinity: 3.2 to 11.2 wt.% NaCl eq.

Continued cooling of the pluton(s) generated hydrothermal fluids which caused retrograde alteration of prograde minerals to lower temperature minerals including actinolite, calcite and quartz together with scheelite, hematite, muscovite, phlogopite, chlorite, magnetite and siderite as accessory minerals. The major amounts of retrograde alteration at Calvert suggests an influx of meteoric water was responsible for the retrograde alteration.

The Calvert deposit is a calcic-type skarn and is characterized by calcium-rich skarn minerals having chemistries that are indicative of an oxidizing environment. It contains iron, evident by the occurrence of magnetite, hematite and siderite, but not in abundance, evident by the iron-poor calc-silicate minerals (e.g., grossular, actinolite, and epidote). The occurrence of iron-oxides with no pyrite also supports the conclusion of an oxidizing environment. The widespread occurrence of calcium-rich minerals suggests a high calcium activity, which is important in scheelite mineralization.

The precipitation of scheelite most likely resulted from cooling coupled with an increase in the activity of calcium due to fluid/rock interaction with the calcite-marble host rock. The presence of scheelite in both prograde and retrograde mineral assemblages indicates multiple periods of scheelite solubility and mineralization (e.g., remobilization). This remobilization

could possibly be due to local decreases in calcium activity from continued introduction of magmatic fluid, which would decrease pH and increase salinity.

Fluid inclusion microthermometry of the Calvert skarn minerals show that the early mineral assemblage was formed at higher temperatures (up to 450°C) and as temperatures declined the mineral assemblage was dominated by hydrous minerals. Major scheelite mineralization occurred during the hotter period of skarn development, although a subordinate proportion also formed at lower temperatures during retrograde alteration.

Salinity values for the skarn minerals (garnet, quartz, scheelite) cluster at 3.2 wt.%, 7.4 wt.%, and 11.2 wt.% NaCl eq. Since the homogenization temperatures average between 250°-260°C, these data form a horizontal trend parallel to the salinity axis on the temperature-salinity plot. This suggests a mixing between a high salinity magmatic fluid and low salinity fluids of a meteoric origin, or possibly a loss of water to the formation of hydrous skarn minerals.

The protolith marble at Calvert shows a narrow variation in $\delta^{13}C$ and $\delta^{18}O$ values that average 0.6‰ (VPDB) and 25.2‰ (VSMOW), respectfully. Both the carbon and oxygen values are depleted relative to marine limestone values of 0.0‰ and 30.6‰, respectfully. The skarn calcite generally has isotopically lighter carbon and oxygen than the protolith marble, with values ranging from -5.0‰ to -9.4‰ for carbon and 7.7‰ to 14.0‰ for oxygen. The observed depletion towards isotopic magmatic values indicates an interaction between the marble and metasomatic fluids derived from the source igneous body.

6.2. Recommendations

An electron microprobe analysis could more accurately obtain quantitative compositions of the Calvert skarn minerals, which can be used to classify the skarn type. Redox conditions prevailing during skarn evolution influence the skarn type formed and can be inferred from the

determination of relative ratios of Fe^{+2}/Fe^{+3} in skarn minerals. Variations in MgO and/or Al_2O_3 activities would require changes in pyroxene and garnet compositions that yield changes in f_{O2}, aCaO, $a$$Al_2O_3$, aMgO, and $a$$Fe_2O_3$ as well (Brown and Essene, 1985).

Whole rock and trace element analysis of each of the intrusive rocks could help determine the identity of the source of tungsten at Calvert. Samples should be taken from proximal (altered) and distal (unaltered) tonalite, as well as from the granite that cross-cuts the tonalite. Additional samples should be obtained from outside of the area to use as baselines for sample comparison. A deep exploration hole can be drilled to test the idea of a buried pluton. Further examination would be needed to determine the location and depth of a borehole if additional work is required to locate the W source.

More fluid inclusion analyses are recommended from the prograde epidote, calcite, scheelite inclusions in garnet and retrograde actinolite and calcite. This could further constrain the T-P regime of the skarn and mitigate effects of sampling bias.

Oxygen isotope zonation ($\delta^{18}O$) in skarn garnet can be used to constrain the extent of the infiltration of meteoric fluids during hydrothermal mineralization (D'Errico et al., 2012). Garnet growth can record the infiltration of external fluids in metamorphic or hydrothermal systems, for example, in its major element zoning or in its oxygen isotope composition, which can now be measured at high spatial resolution using a secondary ion microprobe (SIMS).

Leachate samples were above the detection limits, but not by much. When performing the leachate experiment, it is recommended that more mass of the solid phase be used (e.g., 3x or 5x more solid than used in this study) in the same mass of water.

Since magmatic fluid interaction with host rock results in a general depletion of heavy isotopic compositions in carbonate protoliths, determination of carbon and oxygen isotopic

compositions of carbonates can be an important method in distinguishing barren marbles from marbles that have been metasomatically altered. This method is relatively inexpensive, and can be used as an effective exploration tool in skarn exploration.

References

Arth, J.G., Zen, E-an, Sellers, G., and Hammarstrom, J., 1986, High Initial Sr Isotopic Ratios and Evidence for Magma Mixing in the Pioneer Batholith of Southwest Montana: Journal of Geology, v. 94, p. 419-430.

Bateman, P.C., 1965, Geology and Tungsten Mineralization of the Bishop District, California: U.S. Geological Survey Professional Paper 470, p. 208.

Berger, B.R., Snee, L.W., Hanna, W., and Benham, J.R., 1983, Mineral Resource Potential of the West Pioneer Wilderness Study Area, Beaverhead County, Montana: U.S. Geological Survey Miscellaneous Field Studies Map MF-1585A, 21 p.

Berger, B.R., and Benham, J.R., 1984, West Pioneer Wilderness Study Area, Montana, Wilderness Mineral Potential-Assessment of Mineral-Resource Potential in U.S. Forest Service Lands Studied 1964-1984: U.S. Geological Survey Professional Paper 1300, p. 757-760.

Berger, B.R., Hildenbrand, T.G., O'Neill, J.M., 2011, Control of Precambrian Basement Deformation Zones on Emplacement of the Laramide Boulder Batholith and Butte Mining District, Montana, United States: U.S. Geological Survey Scientific Investigations Report 5016.

Blatt, H., Tracy, R.J., Owens, B.E., 2006, Petrology: Igneous, Sedimentary, and Metamorphic, 3rd Edition: New York, W.H. Freeman, 529 p.

Bowman, J.R., O'Neil, J.R., and Essene, E.J., 1985a, Contact Skarn Formation at Elkhorn, Montana II: Origin and Evolution of C-O-H Skarn Fluids: American Journal of Science, v. 285, p. 621-660.

Bowman, J.R., Covert, J.J., Clark, A.H., and Mathieson, G.A., 1985b, The CanTung E-Zone Scheelite Skarn Orebody, Tungsten, Northwest Territories: Oxygen, Hydrogen, and Carbon Isotope Studies: Economic Geology, v. 80, p. 1872-1895.

Brown, P.E., and Essene, E.J., 1985, Activity Variations Attending Tungsten Skarn Formation, Pine Creek, California: Contributions to Mineralogy and Petrology, v. 89, p. 358-369.

Collins, B.I., 1975, Petrogenesis of the Lost Creek Scheelite-Bearing Skarns, Pioneer Mountains, Montana: Northwest Geology, p. 46-52.

Collins, B.I., 1977, Formation of Scheelite-bearing and Scheelite-barren Skarns at Lost Creek, Pioneer Mountains, Montana: Economic Geology, v. 72, p. 1505-1523.

Crump, T.R., 1976, The Relationship of Scheelite Mineralization to Late-stage Changes in Selected Tactites in Southwestern Montana [M.S. thesis]: Tuscon, Arizona, University of Arizona, 108 p.

Deboer, 1991, Geology and Mineralization of the Lentung Tungsten Skarn Deposit Near Brownes Lake Pioneer Mountains, Montana [M.S. thesis]: Bellingham, Washington, Western Washington University, 200 p.

D'Errico, M.E., Lackey, J.S., Surpless, B.E., Loewy, S.L., Wooden, J.L., Barnes, J.D., Strickland, A., and Valley, J.W., 2012, A Detailed Record of Shallow Hydrothermal Fluid Flow in the Sierra Nevada Magmatic Arc from low-$\delta^{18}O$ Skarn Garnets: Geology, v. 40, p. 763-766.

Diamond, L.W., 1992, Stability of CO_2 Clathrate Hydrate + CO_2 Liquid + CO_2 Vapour + Aqueous KCl-NaCl Solutions: Experimental Determination and Application to Salinity Estimates of Fluid Inclusions: Geochemica et Cosmochimica Acta, v. 56, p. 273-280.

Einaudi, M.T., Meinert, L.D., and Newberry, R.J., 1981, Skarn Deposits: Economic Geology 75th Anniversary Volume, p. 317-391.

Einaudi, M.T., and Burt, D.M., 1982, Introduction - Terminology, Classification, and Composition of Skarn Deposits: Economic Geology, v. 77, p. 745-754.

Foster, R.P., 1977, Solubility of Scheelite in Hydrothermal Chloride Solutions: Chemical Geology, v. 20, p. 27-43.

Foster, D.A., Mueller, P.A., Heatherington, A., Gifford, J.N., and Kalakay, T.J., 2012, Lu-Hf Systematics of Magmatic Zircons Reveal a Proterozoic Crustal Boundary Under the Cretaceous Pioneer Batholith, Montana: Lithos 142-143, p. 216-225.

Fournier, R.O., 1981, Application of Water Geochemistry to Geothermal Exploration and Reservoir Engineering; Chapter 4 in Geothermal Systems: Principles and Case Histories, L. Ryback and L.J. P. Muffler eds., Wiley New York, p. 109-143.

Franklin, R.J., 1989, Lentung Project Summary, unpublished U.S. Borax and Chemical Corporation report, 9 p.

Gammons, C.H., Pape, B.L., Parker, S.R., Poulson, S.R., and Blank, C.E., 2013, Geochemistry, Water Balance, and Stable Isotopes of a “clean” Pit Lake at an Abandoned Tungsten Mine, Montana, USA: Applied Geochemistry 36, p. 57-69.

Geach, R.D., 1972, Mines and Mineral Deposits (Except Fuels) Beaverhead County, Montana: U.S. Bureau of Mines Bulletin 85, 194 p.

Gobla, M.J., 2012, Montana Mineral Locality Index: Rocks and Minerals, v. 87, p. 208-240.

Hammarstrom, J.M., 1982, Chemical and Mineralogical Variation in the Pioneer Batholith, Southwest Montana: U.S. Geological Survey Open-File Report 82-148, 178 p.

Kalakay, T.J., John, B.E., and Lageson, D.R., 2001, Fault-Controlled Pluton Emplacement in the Sevier Fold-and-Thrust Belt of Southwest Montana, USA: Journal of Structural Geology, vol. 23, p. 1151-1165.

Kemp, R.T., 2013, Geological Report on the Calvert Tungsten Property, Beaverhead County, Montana, unpublished report for U.S. Tungsten Co., 84 p.

King, R.H., 1966, Beryl in a Montana Tactite Body: The American Mineralogist, v. 51, p. 502-503.

Klemd, R., 2004, Fluid Inclusions in Epidote Minerals and Fluid Development in Epidote-Bearing Rocks: Reviews in Mineralogy, v. 56, p. 197-234.

Marshal, D., Falck, H., Mann, B., Kirkham, G., and Mortensen, J., 2003, Geothermometry and Fluid Inclusion Studies of the E-Zone Biotite Skarn, CanTung Mine, Tungsten, NWT: Abstracts of the 31st Yellowknife Geoscience Forum, p. 60.

Mathieson, G.A., and Clark, A.H., 1984, The CanTung E-Zone Scheelite Skarn Orebody, Tungsten, Northwest Territories: A Revised Genetic Model: Economic Geology, v. 79, p. 883-901.

Maughan, E.K., and Roberts, A.E., 1967, Big Snowy and Amsden Groups and the Mississippian-Pennsylvanian Boundary in Montana: U.S. Geological Survey Professional Paper 554-B, 27 p.

McCrea, J.M., 1950, On the Isotope Chemistry of Carbonates and a Paleotemperature Scale: Journal of Chemical Physics 18, p. 849-857.

McMannis, W.J., 1965, Resume of Depositional and Structural History of Western Montana: Bulletin of the American Association of Petroleum Geologists, v. 49, p. 1801-1823.

Meinert, L.D., 1983, Variability of Skarn Deposits: Guides to Exploration-Advances in the Past Half-Century: Iowa, Kendall/Hunt Publishing, p. 301-316.

Meinert, L.D., 1992, Skarns and Skarn Deposits: Geoscience Canada, v. 19, p. 145-162.

Meinert, L.D., Dipple, G.M., and Nicolescu, S., 2005, World Skarn Deposits: Economic Geology 100th Anniversary Volume, Society of Economic Geologists, Littleton, Colorado, USA, p. 299-336.

Mellon, S.A., 1978, Stratigraphic Controls on Scheelite-bearing Tactite Within the Amsden Group at the Lost Creek Mining District, Beaverhead County, Montana [M.S. thesis]: Rapid City, South Dakota, South Dakota School of Mines and Technology, 62 p.

Myers, W.B., 1952, Geology and Mineral Deposits of the Northwest Quarter Willis Quadrangle and Adjacent Brown's Lake Area, Beaverhead County, Montana: U.S. Geological Survey Open-File Report 52-105, 46 p.

Nesse, W.D., 2012, Introduction to Mineralogy (2nd ed.). New York, NY: Oxford University Press, Inc.: New York, New York, p. 326.

Newberry, R.J., 1979, Systematic Variations in W-Mo-Cu Skarn Formation in the Sierra Nevada: Geological Society of America Abstracts with Programs, v. 11, p. 486.

Newberry, R.J., and Einaudi, M.T., 1981, Tectonic and Geochemical Setting of Tungsten Skarn Mineralization in the Cordillera: Arizona Geological Digest, v. 14, p. 99-112.

Newberry, R.J., and Swanson, S.E., 1986, Scheelite Skarn Granitoids: an Evaluation of the Roles of Magmatic Source and Process: Ore Geology Reviews, v. 1, p. 57-81.

Newberry, R.J., 1998, W- and Sn-Skarn Deposits: a 1998 Status Report: In Mineralized Intrusion-Related Skarn Systems: Min. Assoc. Can. Short Course 26, p. 289-335.

Nokleberg, W.J., 1981, Geologic Setting, Petrology, and Geochemistry of Zoned Tungsten-Bearing Skarns at the Strawberry Mine, Central Sierra Nevada, California: Economic Geology, v. 26, p. 111-133.

Ohmoto, H., and Rye, R.O., 1979, Isotopes of Sulfur and Carbon, in Barnes, H.L. Ed., Geochemistry of Hydrothermal Ore Deposits, New York, John Wiley & Sons, p. 509-567.

Pattee, E.C., 1960, Tungsten Resources of Montana: Deposits of the Mount Torrey Batholith, Beaverhead County: U.S. Bureau of Mines Report of Investigations 5552, 41 p.

Pearson, R.C., and Zen, E-an, 1985, Geologic Map of the Eastern Pioneer Mountains, Beaverhead County, Montana: U.S. Geological Survey Miscellaneous Field Studies Map MF-1806-A.

Potter, R.W., 1977, Pressure Corrections for Fluid-Inclusion Homogenization Temperatures Based on the Volumetic Properties of the System NaCl-H_2O: U.S. Geological Survey Journal of Research, v. 5, p. 603-607.

Potter, R.W., Clynne, M.A., and Brown, D.L., 1978, Freezing Point Depression of Aqueous Sodium Chloride Solutions: Economic Geology, v. 73, p. 284-285.

Roedder E., 1984, Fluid Inclusions: Reviews in Mineralogy, v. 12, 646 p.

Ruppel, E.T., and Lopez, D.A., 1984, The Thrust Belt in Southwest Montana and East-Central Idaho: U.S. Geological Survey Professional Paper 1278, 41 p.

Ruppel, E.T., O'Neill, J.M., and Lopez, D.A., 1993, Geologic Map of the Dillon 1° x 2° Quadrangle, Idaho and Montana: U.S. Geological Survey Miscellaneous Investigations Series Map I-1803-H.

Sando, W.J., 1985, Mississippian and Pennsylvanian Stratigraphy in Southwest Montana and Adjacent Idaho: U.S. Geological Survey Bulletin 1656, 89 p.

Schmidt, M.W., 1993, Phase Relations and Compositions in Tonalite as a Function of Pressure: An Experimental Study at 650°C: American Journal of Science, v. 293, p. 1011-1060.

Schutz, J.L., 1986, Geology of Precious Metal Mineralization in the Baldy Mountain District, Beaverhead County, Montana [M.S. thesis]: Fort Collins, Colorado, Colorado State University, 190 p.

Sims, P.K., O'Neill, J.M., Bankey, V., Anderson, E., 2004, Precambrian Basement Geolgoic Map of Montana – An Interpretation of Aeromagnetic Anomalies: U.S. Geological Survey Scientific Investigations Map 2829.

Singoyi, B., 1995, Mineral Paragenesis, Geochemistry and Fluid Characteristics of the Kara Scheelite-Magnetite Skarn Deposit, Northwestern Tasmania [MS Thesis]: Hobart, Tasmania, University of Tasmania, 161 p.

Sloss, L.L., and Moritz, C.A., 1951, Paleozoic Stratigraphy of Southwestern Montana: Bulletin of the American Association of Petroleum Geologists, v. 35, p. 2135-2169.

Smith, D.L., and Gilmour, E.H., 1980, The Mississippian and Pennsylvanian (Carboniferous) Systems in Montana: Montana Bureau of Mines and Geology, Memoir 46, 32 p.

Snee, L.W., 1978, Petrography, K-Ar Ages, and Field Relations of the Igneous Rocks of Part of the Pioneer Batholith, Southwestern Montana [M.S. thesis]: Columbus, Ohio, Ohio State University, 110 p.

Snee, L.W., 1982, Emplacement and Cooling of the Pioneer Batholith, Southwestern Montana [Ph.D. thesis]: Columbus, Ohio, Ohio State University, 320 p.

Snee, L.W., and Sutter, J.F., 1982, Geochronological Data for the Pioneer Mountains, Southwestern Montana: Part I-$^{40}Ar/^{39}Ar$ Age Spectrum and Conventional K/Ar Dates for Unaltered Plutons: U.S. Geological Survey Open-File Report 9740-00375, 51 p.

Suttner, L.J., 1969, Stratigraphic and Petrographic Analysis of Upper Jurassic-Lower Cretaceous Morrison and Kootenai Formations, Southwest Montana: Bulletin of the American Association of Petroleum Geologists, v. 53, p. 1391-1410.

Taylor, H.P., 1971, Oxygen Isotope Evidence for Large-Scale Interaction Between Meteoric Ground Waters and Tertiary Granodiorite Intrusions, Western Cascade Range, Oregon: Journal of Geophysical Research, v. 76, p. 7855-7874.

Taylor, H.P., 1974, The Application of Oxygen and Hydrogen Isotope Studies to Problems of Hydrothermal Alteration and Ore Deposition: Economic Geology, v. 69, p. 7855-7874.

Taylor, H.P., and O'Neil, J.R., 1977, Stable Isotope Studies of Metasomatic Ca-Fe-Al-Si Skarns and Associated Metamorphic and Igneous Rocks, Osgood Mountains, Nevada: Contributions to Mineralogy and Petrology, v. 63, p. 1-50.

Truckle, 1988, Geology of the Calvert Hill Area, Beaverhead County, Montana [M.S. thesis]: Butte, Montana, Montana College of Mineral Science and Technology, 94 p.

Truesdell, A.H., 1976, Summary of Section III, Geochemical Techniques in Exploration: Proc. 2nd U.N. Symposium on the Development and Use of Geothermal Resources, San Francisco, 1975, v. 1, p. 1iii-1xxix.

Walker, D.D., 1963, Tungsten Resources of Western Montana: U.S. Bureau of Mines, Report of Investigations 6334, 60 p.

Wesolowski, D., 1984, Geochemistry of Tungsten in Scheelite Deposits: The Skarn Ores at King Island, Tasmania [Ph.D. thesis]: University Park, PA, The Pennsylvania State University, 431 p.

Will, T.M., Powell, R., Holland, T., Guiraud, M., 1990, Calculated Greenschist Facies Mineral Equilibria in the System –CaO-FeO-MgO-Al_2O_3-TiO_2-SiO_2-CO_2-H_2O: Contributions to Mineralogy and Petrology, v. 104, p. 353-368.

Wood, S.A., and Samson, I.M., 2000, The Hydrothermal Geochemistry of Tungsten in Granitoid Environments: I. Relative Solubilities of Ferberite and Scheelite as a Function of T, P, pH, and m_{NaCl}: Economic Geology, v. 95, p. 143-182.

Wood, S.A., and Vlassopoulos, D., 1989, Experimental Determination of the Hydrothermal Solubility and Speciation of Tungsten at 500°C and 1 kbar: Geochimica et Cosmochimica Acta, v. 53, p. 303-312.

Yuvan, J., 2006, Fluid Inclusion and Oxygen Isotope Studies of High-Grade Quartz-Scheelite veins, CanTung Mine, Northwest Territories, Canada: Products of a Late-Stage Magmatic-Hydrothermal Event [M.S. thesis]: Columbia, Missouri, University of Missouri-Columbia, 94 p.

Zen, E-an, Marvin, R.F., and Mehnert, H.H., 1975, Preliminary Petrographic, Chemical, and Age Data on Some Intrusive and Associated Contact Metamorphic Rocks, Pioneer Mountains, Southwestern Montana: Geological Society of America Bulletin, v. 86, p. 367-370.

Zen, E-an, 1988, Bedrock Geology of the Vipond Park 15-Minute, Stine Mountain 7.5-Minute, and Maurice Mountain 7.5-Minute Quadrangles, Pioneer Mountains, Beaverhead County, Montana: U.S. Geological Survey Bulletin 1625, 49 p.

Zheng, Y.F., 1999, Oxygen Isotope Fractionation in Carbonate and Sulfate Minerals: Geochemical Journal 33, p. 109-126.

Zimbelman, D.R., 1984, Geology of the Polaris 1SE Quadrangle, Beaverhead County, Montana [M.S. thesis]: Boulder, Colorado, University of Colorado, 154 p.

Appendix A: XRF, Fluid Inclusion and Petrographic Data

Table IX. Portable XRF data.

SAMPLE	Ca	Ca Error	W	W Error	Mo	Si	Al	Fe	Mn	Cl	Au	Au Error	Zn	Cu	P	P Error	S	S Error	Balance
1705/JMHF7A	37228	634	182	34	2	512339	9655	10199	2064	690	< LOD	5	47	28	< LOD	811	828	117	43%
1706/JMHF7A	30097	528	133	30	< LOD	512959	8004	4957	1707	210	< LOD	5	35	22	< LOD	761	571	102	44%
1707/JMHF7A	36388	627	159	34	< LOD	521414	7256	9662	1957	204	< LOD	5	52	21	< LOD	748	599	99	42%
1708/SFJM-1	21900	806	110183	3634	281	124152	1696	< LOD	< LOD	10719	< LOD	360	< LOD	< LOD	24206	689	2605	130	70%
1709/SFJM-1	20395	533	106277	872	268	109797	1631	< LOD	< LOD	12829	< LOD	83	< LOD	< LOD	21262	353	2608	108	72%
1710/S1-JMF-1C	63620	1034	81573	660	341	129017	2770	11290	2317	13715	210	48	< LOD	152	16949	423	2289	142	68%
1711/S1-JMF-1C	95418	1356	80614	661	343	136428	5162	17564	5482	12072	247	49	< LOD	207	16315	454	2059	151	62%
1712/GF-1A	189262	4957	196	26	6	69914	20394	23819	10194	16610	< LOD	6	64	66	< LOD	443	934	166	67%
1713/GF-1A	208893	1793	480	47	5	77100	22440	27221	11607	16333	< LOD	7	76	85	< LOD	464	903	172	63%
1714/GF-2A	235877	6737	60	32	6	206826	91426	71708	12676	1693	< LOD	8	177	73	< LOD	665	303	165	37%
1715/GF-2A	211826	2182	266	57	4	221584	86921	84591	14289	1711	< LOD	9	290	129	< LOD	680	< LOD	757	37%
1716/JMHF10A	229214	1907	102	41	< LOD	186577	31329	25734	19387	10816	< LOD	7	96	44	< LOD	574	1375	175	49%
1717/JMHF10A	255253	2052	65	43	< LOD	217669	36857	32385	24162	819	< LOD	7	115	45	< LOD	669	1076	182	43%
1718/JMHF10A	146997	1493	76	25	< LOD	351270	12478	25457	12318	4961	< LOD	6	276	57	< LOD	710	1267	156	43%
1719/JMHF10A	144678	1492	64	23	2	188833	11582	25998	14376	15980	< LOD	6	233	43	< LOD	528	2154	175	60%
1720/ST-JMF-T1D	64988	928	105	35	< LOD	435625	7640	18766	3601	4326	< LOD	5	105	24	< LOD	742	292	113	45%
1721/ST-JMF-T1D	63871	2030	67	22	< LOD	441795	8365	19371	3547	4956	< LOD	6	114	34	< LOD	767	380	119	44%
1722/JMHF8C	142784	1491	3109	92	7	123547	3790	27092	4622	34927	< LOD	11	179	46	< LOD	486	2673	194	65%
1723/JMHF8C	187106	1809	20483	241	81	196637	4240	37262	8305	7954	51	18	234	83	808	411	1113	162	51%
1724/GF-3A	246247	6732	< LOD	42	4	222553	42593	51681	16175	694	< LOD	8	320	37	< LOD	678	< LOD	243	40%
1725/GF-3A	305500	8135	87	30	< LOD	113542	35477	42454	16124	4604	< LOD	7	212	52	< LOD	542	769	179	48%
1726/GF-4A	288899	2263	213	47	3	95725	32845	42226	17927	8153	< LOD	7	108	65	< LOD	538	2571	220	51%
1727/GF-4A	238918	1919	89	40	< LOD	68783	22509	30609	13196	12033	< LOD	6	83	41	< LOD	491	3649	225	61%
1728/JMHF7A	6970	325	26	16	< LOD	320840	2432	994	336	29747	< LOD	4	21	22	< LOD	574	1458	152	64%
1729/JMHF7A	12531	332	53	19	< LOD	505405	2697	1095	378	10492	< LOD	5	26	26	< LOD	730	372	106	47%
1730/JMHF7A	58455	1028	96	26	< LOD	407021	8864	37760	6318	6132	< LOD	6	223	59	< LOD	714	569	127	46%
1731/JMHF7A	39460	767	40	22	< LOD	326076	5263	29252	4873	17061	< LOD	6	165	31	< LOD	615	923	139	56%
1732/JMHF7A	24148	850	< LOD	27	< LOD	535845	4989	4178	1299	999	< LOD	5	42	16	< LOD	801	400	102	43%
1733/JMHF7A	16210	374	< LOD	26	5	552525	4526	2550	1050	1050	< LOD	5	30	< LOD	< LOD	758	287	104	42%
1734/JMHF7A	206943	2000	210	49	< LOD	267064	34912	57780	23623	902	< LOD	8	291	56	< LOD	692	403	157	39%
1735/JMHF7A	37605	634	70	34	< LOD	531172	6399	10364	1818	617	< LOD	5	68	26	< LOD	802	< LOD	219	41%
1736/T1-JMF-1F	24272	511	55	31	< LOD	382391	2633	12358	1579	8543	< LOD	5	85	30	< LOD	918	1267	111	55%
1738/T1-JMF-1F	12192	325	< LOD	20	< LOD	188125	1437	3049	679	22016	< LOD	4	24	11	< LOD	358	2073	115	76%
1739/SST-JM-1A	915	82	< LOD	26	< LOD	550688	2534	153	92	2633	< LOD	5	< LOD	19	< LOD	789	< LOD	141	44%
1740/SST-JM-1A	846	83	< LOD	27	< LOD	543221	2335	112	79	1920	< LOD	5	< LOD	17	< LOD	773	< LOD	178	45%
1741/SST-JM-1A	225762	2059	138	48	< LOD	147933	101044	59091	3549	1915	< LOD	8	46	70	< LOD	532	< LOD	765	44%
1742/SST-JM-1A	150513	1702	119	43	< LOD	156219	91225	57924	2814	4907	< LOD	7	81	42	< LOD	514	709	148	44%
1743/SSA-JMFA-4	55815	1753	240	28	< LOD	478271	4949	14380	4749	1632	13	5	87	62	< LOD	759	< LOD	190	79%
1745/SSA-JMFA-4	218303	1662	221	29	3	301483	3024	11642	5147	953	10	5	94	56	< LOD	719	1151	456	45%
1746/SSA-JMFA-4	357616	2270	178	30	< LOD	135422	< LOD	4381	3278	1203	15	5	90	64	< LOD	599	< LOD	253	49%
1747/SSA-JMFA-4	325202	8611	84	26	< LOD	177515	< LOD	3297	2202	1011	11	5	65	41	< LOD	620	382	165	48%

Table X. Portable XRF data (cont'd).

Sample	Ca	Ca Error	W	WO3	W Error	Mo	Si	Al	Fe	Mn	Mg	Cl	Se	Se Error	Zn	Zn Error	Cu	Cu Error
1848/BGSJM	324597	2413	529	666	62	3	75249	14097	27544	21842	< LOD	952	< LOD	6	125	13	40	16
1850/JMHF5F	57815	1740	158	199	55	8	317852	10651	70342	12065	32882	96	< LOD	7	410	31	58	24
1851/GSF-IS	375184	2631	136	171	33	< LOD	46130	15670	25452	23750	< LOD	235	< LOD	5	108	11	27	14
1852/SSA-JMFA	132191	2038	272	343	75	< LOD	117491	35678	237859	12820	17229	< LOD	< LOD	6	311	23	< LOD	31
1853/SSA-JMFA	44249	1580	1991	2511	68	< LOD	439321	3090	13868	41473	7663	< LOD	51	6	227	17	250	19
1854/JM-5F2-C	193327	2152	346	437	42	4	194863	106609	90215	6886	< LOD	742	< LOD	5	57	11	54	16
1855/SST-JM-1B	16183	752	< LOD		36	3	276269	134288	49622	1074	16100	97	< LOD	4	89	9	30	12
1856/S2-JMA3-2	268114	2338	54	68	32	5	198627	57890	75010	4532	< LOD	215	< LOD	5	195	14	34	15
1857/TI-JMF-1B	176419	2001	81	103	53	4	202468	84375	89892	11915	14327	< LOD	7	3	273	16	34	15
1858/TI-JMF-1B	114785	3621	< LOD		42	< LOD	306994	11045	63792	11358	47978	450	4	3	548	20	34	13
1859/B2F-JM-1C	80170	5818	454309	572838	39402	4054	244379	< LOD	< LOD	< LOD	< LOD	484	781	513	< LOD	1466	< LOD	787
1860/JMSF	87755	2519	551605	695519	12922	2294	204484	< LOD	611	< LOD	< LOD	< LOD	956	140	< LOD	459	318	139
1861/JMSF	105231	2991	556175	701281	13261	2229	228124	< LOD	2401	< LOD	< LOD	1138	845	139	< LOD	465	394	141

Sample	Au	Au Error	Ag	Ag Error	Ti	Ti Error	K	P	P Error	S	S Error	Cs	Cs Error	Te	Te Error	Balance
1848/BGSJM	15	9	13	8	< LOD	282	2372	< LOD	581	932	192					53%
1850/JMHF5F	< LOD	12	< LOD	7	< LOD	88	842	< LOD	586	475	109					50%
1851/GSF-IS	< LOD	8	< LOD	17	291	84	3267	< LOD	511	< LOD	924	158	18	222	56	51%
1852/SSA-JMFA	< LOD	23	< LOD	10	10359	272	1851	< LOD	439	< LOD	169	165	20	178	59	43%
1853/SSA-JMFA	62	10	< LOD	8	< LOD	234	237	3156	539	< LOD	159					44%
1854/JM-5F2-C	< LOD	9	21	11	2420	121	929	< LOD	611	< LOD	744	153	18	181	55	40%
1855/SST-JM-1B	< LOD	6	< LOD	13	2270	113	61995	< LOD	547	< LOD	166	100	15	132	45	44%
1856/S2-JMA3-2	< LOD	8	22	12	1260	93	< LOD	< LOD	690	< LOD	750	167	19	238	58	39%
1857/TI-JMF-1B	< LOD	9	24	12	545	77	884	< LOD	605	< LOD	674	174	19	267	59	42%
1858/TI-JMF-1B	8	5	< LOD	8	< LOD	119	1141	< LOD	707	< LOD	204					44%
1859/B2F-JM-1C	< LOD	2655	53	23	< LOD	98	< LOD	54090	3134	6041	457					16%
1860/JMSF	611	325	72	25	< LOD	118	< LOD	72116	1373	5181	250	2939	501	6798	1604	7%
1861/JMSF	749	327	81	31	< LOD	139	< LOD	85663	1640	6094	306	1067	234	3234	779	< LOD

Table XI. Fluid inclusion data.

No.	Sample	Mineral	Type	Size (μm)	T(f°C)	T(m°C)	T(h°C)	Salinity wt%NaCl eq.
1	JMSFB	scheelite	L/V	22.5	-43.0	-7.6		11.2
2	JMSFB	scheelite	L/V	10.0	-46.0	-7.3		10.9
3	JMSFB	scheelite	L/V	12.0	-45.0	-7.5		11.1
4	JMSFB	scheelite	L/V	20.0	-42.0	-7.5		11.1
5	JMSFB	scheelite	L/V	12.0		-7.3	254.7	10.9
6	JMSFB	scheelite	L/V	15.0		-7.2		10.7
7	JMSFB	scheelite	L/V	17.5		-7.9	280.6	11.6
8	JMSFB	scheelite	L/V	17.5	-39.4	-7.7	288.6	11.4
9	JMSFB	scheelite	L/V	20.0	-38.5	-8.1	264.8	11.8
10	JMSFB	scheelite	L/V	16.0	-46.0	-7.7	264.3	11.4
11	JMSFB	scheelite	L/V	12.0		-7.3	268.9	10.9
12	JMSFB	scheelite	L/V	22.5	-45.0	-7.5	264.0	11.1
13	JMSFB	scheelite	L/V	12.0		-7.2	268.3	10.7
14	JMSFB	scheelite	L/V	7.0		-7.6	268.4	11.2
15	JMSFB	scheelite	L/V	9.0		-7.4	266.8	11.0
16	JMSFB	scheelite	L/V	7.5		-7.4	271.5	11.0
17	JMSFB	scheelite	L/V	22.0	-41.4	-7.6	284.7	11.2
18	JMSFB	scheelite	L/V	30.0	-48.3		277.8	
19	JMSFB	scheelite	L/V	22.5	-39.9	-7.4	260.0	11.0
20	JMSFB	scheelite	L/V	20.0	-40.5	-7.8	272.0	11.5
21	JMSFB	scheelite	L/V	12.5	-44.8	-6.8	256.0	10.2
22	JMSFB	scheelite	L/V	17.5	-44.0	-8.0	253.5	11.7
23	JMSFB	scheelite	L/V	15.0	-47.0	-7.6	255.0	11.2
24	JMSFB	scheelite	L/V	15.0	-33.9	-7.3	254.0	10.9
25	JMSFB	scheelite	L/V	15.5	-33.6	-7.8	256.0	11.5
26	JMSFB	scheelite	L/V	15.0	-33.5	-7.2	254.8	10.7
27	JMSFB	scheelite	L/V	17.5	-37.3	-7.6	246.0	11.2
28	JMSFB	scheelite	L/V	13.0	-38.3	-7.4	253.0	11.0
29	7304-1B	scheelite	L/V	6.5	-38.0	-5.5	262.4	8.5
30	7304-1B	scheelite	L/V	17.5	-45.0	-4.8	257.0	7.6
31	7304-1B	scheelite	L/V	17.5	-41.0	-4.8	268.0	7.6
32	7304-1B	scheelite	L/V	26.0	-45.0	-4.6	248.0	7.3
33	7304-1B	scheelite	L/V	26.0	-38.0	-4.7	264.0	7.4
34	7304-1B	scheelite	L/V	18.0		-4.4	262.0	7.0
35	7304-1B	scheelite	L/V	13.0			252.8	
36	7304-1B	scheelite	L/V	17.0			256.0	
37	7304-1B	scheelite	L/V	20.0		-3.8		6.1
38	7304-1B	scheelite	L/V	15.0		-4.6		7.3
39	S1-JMF-1C	scheelite	L/V	22.5	-37.6	-2.5	390.5	4.2
40	S1-JMF-1C	scheelite	L/V	37.0	-23.7	-1.2	216.0	2.1

Table XII. Fluid inclusion data (cont'd).

No.	Sample	Mineral	Type	Size (μm)	T(f°C)	T(m°C)	T(h°C)	Salinity wt%NaCl eq.
41	S1-JMF-1C	scheelite	L/V	12.0	-37.9	-1.8	208.4	3.1
42	S1-JMF-1C	scheelite	L/V	40.0	-33.0	-2.2	230.2	3.7
43	S1-JMF-1C	scheelite	L/V	15.0	-33.3	-2.4	258.0	4.0
44	CAL-IS	scheelite	L/V	22.5	-35.9	-4.5	230.0	7.2
45	CAL-IS	scheelite	L/V	13.0	-39.0	-4.6	238.0	7.3
46	CAL-IS	scheelite	L/V	23.0	-36.0	-5.0	231.4	7.9
47	CAL-IS	scheelite	L/V	30.0	-40.0	-4.9	239.7	7.7
48	CAL-IS	scheelite	L/V	12.5	-37.0	-4.3	224.0	6.9
49	CAL-IS	scheelite	L/V	20.0		-4.2	229.6	6.7
50	CAL-IS	scheelite	L/V	17.5		-4.6	231.3	7.3
51	CAL-IS	scheelite	L/V	16.0	-37.1	-4.9	228.8	7.7
52	CAL-IS	scheelite	L/V	12.5	-44.2	-2.6	200.5	4.3
53	CAL-IS	scheelite	L/V	17.5	-33.9	-2.1	205.4	3.5
54	CAL-IS	scheelite	L/V	20.0	-33.4	-1.3	201.8	2.2
55	CAL-IS	scheelite	L/V	15.0	-31.5	-1.7		2.9
56	CAL-IS	scheelite	L/V	21.5	-40.5	-2.0	242.6	3.4
57	CAL-IS	scheelite	L/V	22.5	-45.4	-4.5	247.8	7.2
58	CAL-IS	scheelite	L/V	22.5	-38.2	-4.8	264.3	7.6
59	CAL-IS	scheelite	L/V	15.0	-47.3	-3.8	243.4	6.1
60	CAL-IS	scheelite	L/V	22.5	-38.3	-4.2		6.7
61	CAL-IS	scheelite	L/V	32.5	-32.6	-4.6		7.3
62	CAL-IS	scheelite	L/V	17.5	-39.8	-5.0	248.9	7.9
63	CAL-IS	scheelite	L/V	12.5	-37.0	-4.8	231.2	7.6
64	CAL-IS	scheelite	L/V	15.0	-38.4	-4.3	224.4	6.9
1	7304-1B	quartz	L/V	15.0		-4.8	209.2	7.6
2	7304-1B	quartz	L/V	19.0	-45.2	-4.8	264.0	7.6
3	7304-1B	quartz	L/V	10.0	-44.8	-4.3	242.0	6.9
4	7304-1B	quartz	L/V	27.0	-45.6	-4.5	233.4	7.2
5	7304-1B	quartz	L/V	16.0	-45.6	-4.6	237.0	7.3
6	7304-1B	quartz	L/V	25.0	-42.6	-4.9	245.0	7.7
7	7304-1B	quartz	L/V	10.0	-46.0	-4.2	220.0	6.7
8	7304-1B	quartz	L/V	12.0	-45.0	-4.7	244.0	7.4
9	7304-1B	quartz	L/V	15.0	-45.5	-4.6	254.0	7.3
10	7304-1B	quartz	L/V	11.0	-45.8	-4.2	209.0	6.7
11	7304-1B	quartz	L/V	18.0	-45.2	-4.8	233.0	7.6
12	7304-1B	quartz	L/V	13.0	-45.6	-4.3		6.9
1	CAL-IS	garnet	L/V	20.0	-37.0	-2.8	255.4	4.6
2	CAL-IS	garnet	L/V	39.0	-37.0	-2.5		4.2
3	CAL-IS	garnet	L/V	10.0	-32.5	-3.0	258.0	4.9

Table XIII. Fluid inclusion data (cont'd).

No.	Sample	Mineral	Type	Size (μm)	T(f°C)	T(m°C)	T(h°C)	Salinity wt%NaCl eq.
4	CAL-IS	garnet	L/V	12.0	-40.0		256.0	
5	CAL-IS	garnet	L/V	17.0	-37.5		264.3	
6	GF-2A	garnet	L/V	37.0	-34.6	-1.6	251.1	2.7
7	GF-2A	garnet	L/V	11.5	-36.0	-2.0	253.0	3.4
8	GF-2A	garnet	L/V	30.0	-36.6	-1.4	250.0	2.4
9	GF-2A	garnet	L/V	19.5	-39.0	-2.3	260.6	3.9
10	GF-2A	garnet	L/V	17.5	-35.2	-2.0	258.4	3.4
11	GF-2A	garnet	L/V	50.0	-33.9	-1.8	263.9	3.1
12	GF-2A	garnet	L/V	48.0	-37.9	-1.6	261.2	2.7
13	GF-2A	garnet	L/V	17.0	-37.4	-1.9	254.4	3.2
14	GF-2A	garnet	L/V	17.5	-35.4	-2.1	267.8	3.5
15	GF-2A	garnet	L/V	42.0	-38.0	-1.7	259.4	2.9
16	GF-2A	garnet	L/V	15.0	-37.2	-2.2	257.0	3.7
17	GF-2A	garnet	L/V	30.0	-38.6	-1.8	261.4	3.1
18	GF-2A	garnet	L/V	22.5	-38.6	-1.8	265.8	3.1
19	GF-2A	garnet	L/V	21.0	-38.7		257.6	
20	GF-2A	garnet	L/V	26.0	-36.5	-2.1	249.7	3.5
21	GF-2A	garnet	L/V	17.0	-38.0		267.3	
22	GF-2A	garnet	L/V	18.0	-37.8		248.8	

Table XIV. Modal compositions of the intrusive rocks at Calvert. Modal percentages were estimated from thin sections and are approximate. Data was not obtained by point-count method, but rather by careful petrographic analysis.

	Foolhen Mountain Tonalite			BC Granite
Sample	KTD1	KTD2	KTL1	KTL2
Quartz	32.0	30.2	31.0	32.8
K-Feldspar	1.0	1.0	1.0	37.0
Plagioclase	53.0	57.5	65.0	27.0
Muscovite	0.5	0.5	0.5	0.5
Biotite	10.5	8.0	1.0	0.5
Hornblende	1.5	1.0	0.5	0.5
Accessories	1.5	1.8	1.0	1.7
Zircon				
Magnetite				
Epidote				
Hematite				
Sphene				
Apatite				
Chlorite				
Recalculated Percentages				
Quartz	37.2	34.0	32.0	33.9
K-Feldspar	1.2	1.1	1.0	38.2
Plagioclase	61.6	64.9	67.0	27.9

Appendix B: Sample Photographs

These samples were taken from exposed outcrop and float. The scale is in inches.

JMCA1: prograde gr+ep+cal+qtz+sch-skarn

GS-JMF: prograde gr+ep+cal+sch-skarn

JMCA2: prograde gr+ep+cal+qtz+sch-skarn

JMCA3: moderate alteration of prograde skarn

JMCA4: moderate alteration of prograde skarn

JMHF10A: prograde gr+ep+cal+sch-skarn

M32b: fo+di+phl-marble

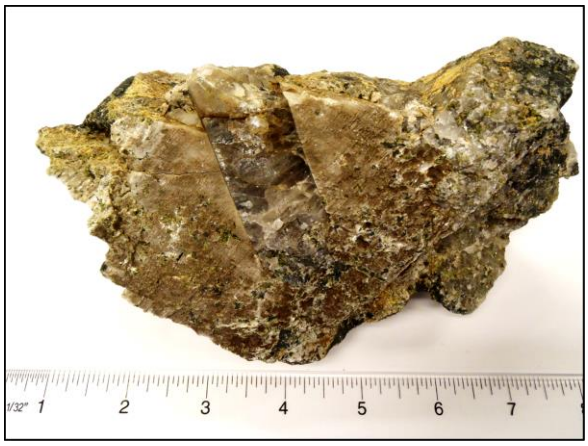

JMCA5: retrograde cal+qtz+act-skarn

S1-JMF-1H: alteration of ep+sch-skarn to actinolite and calcite retrograde assemblage

JH-FM-1C: highly altered gr+ep+cal+sch-skarn

JMCA6: moderately altered prograde skarn

S12-JMF: retrograde skarn

JMCA7: retrograde ep+cal-skarn

JMCA8: act+cal+qtz-skarn

4XIS: retrograde skarn

6492 (AMC): altered prograde skarn with magnet to indicate the presence of magnetite

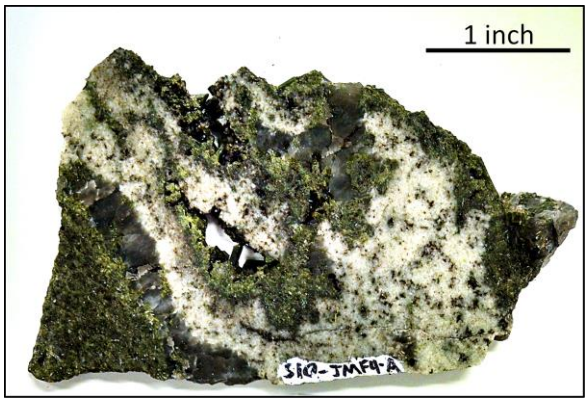

S10-JMF4-A: epidote-quartz endoskarn in tonalite

Core from CAL-IS

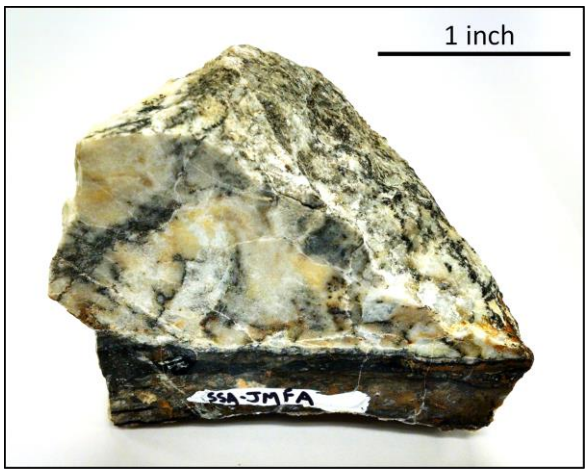

SSA-JMFA: altered marble

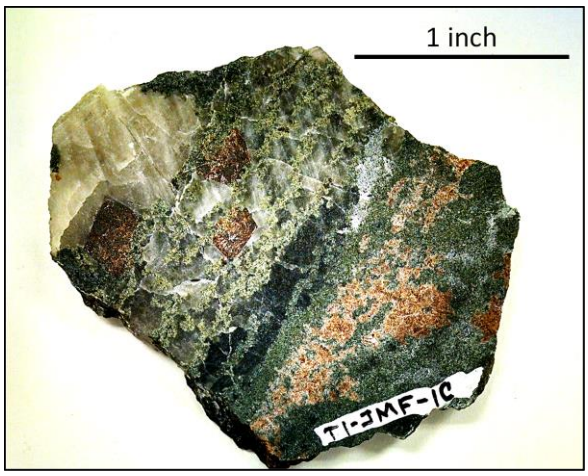

T1-JMF-1C

SS-JM-2F4

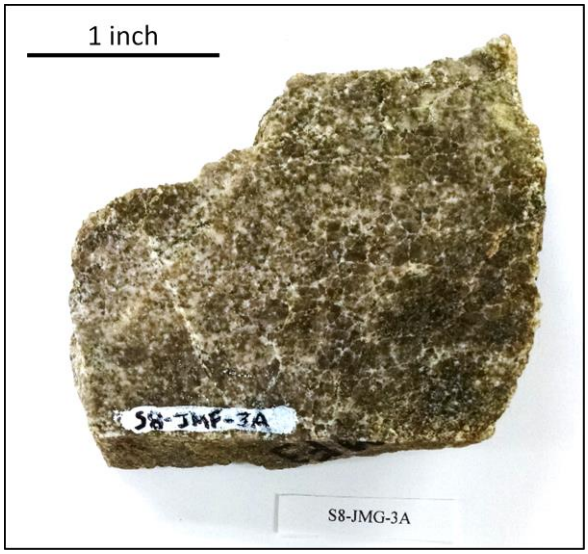

S8-JMF-3A: aplite

SIGNATURE PAGE

This is to certify that the thesis prepared by Joshua Messenger entitled "Paragenesis and Geochemistry of the Calvert Tungsten Skarn Deposit, Pioneer Mountains, Montana" has been examined and approved for acceptance by the Department of Geological Engineering, Montana Tech of The University of Montana, on the nineteenth day of April 2016.

Dr. Christopher Gammons, Professor
Department of Geological Engineering
Chair, Examination Committee

Dr. Diane Wolfgram, Professor
Department of Geological Engineering
Member, Examination Committee

Stanley Korzeb, Economic Geologist & Research Professor
Montana Bureau of Mines and Geology
Member, Examination Committee